General Framework of Multirate Sampling Control and Applications to Motion Control Systems

(マルチレートサンプリング制御の一般的枠組と
モーションコントロール系への応用)

by

Hiroshi Fujimoto

(藤本　博志)

Dissertation Submitted to

The Department of Electrical Engineering

for the Degree of

Doctor of Philosophy

at

The University of Tokyo

December 2000

Supervisor :

Professor Yoichi Hori

邦文概要

General Framework of Multirate Sampling Control and Applications to Motion Control Systems

(マルチレートサンプリング制御の一般的枠組と モーションコントロール系への応用)

藤本　博志

ロボット・モータ・ハードディスク装置などのメカトロ機器の高速・高精度制御系においては、コンピュータを用いて制御を行うディジタル制御が重要な役割を果たしている。これらの制御のサンプリング周期と制御周期は、計算機やセンサ・アクチュエータ、AD/DA 変換器の性能によって決定されるが、従来型の制御方式では、サンプリング周期と制御周期を同期させるシングルレート方式が使用されてきた。これに対して、本論文では入出力の周期を敢えて多重化するマルチレートサンプリング制御方式の提案を行った。

本論文は前半部では、1) マルチレートフィードフォワード制御を用いた完全追従制御 (Perfect Tracking Control: PTC)、2) マルチレートフィードバック制御を用いた完全外乱抑圧制御 (Perfect Disturbance Rejection: PDR)、3) マルチレートサンプリング制御を用いた完全状態一致制御 (Perfect State Matching: PSM) による制御器の離散化法というマルチレート制御系の新しい理論的枠組を構築した。後半部では、これらの核となる制御理論を、ロボット・サーボモータ・ハードディスク装置・2 慣性系・ビジュアルサーボ系などの実システムに応用し、計算機シミュレーション及び実機実験により、その有効性を明らにした。

本論文の内容及び構成は、以下のようになっている。

第 1 章では、従来のマルチレートサンプリング制御の研究を振り返り、その問題点を明らかにし、本研究の位置付けを行なった。従来からマルチレートサンプリング制御に関しては、零点配置・強安定化・同時安定化など様々な理論的研究が行なわれてきたが、制御入力が振動的になるなどの問題点が指摘され、これまでにこれらの研究が実システムに応用されたケースは数少ない。また、低精度エンコーダを用いたサーボモータの速度制御系や、ハードディスク装置に対して、マルチレート制御を適用する試みもなされてきた

が、各アプリケーションに対して固有の理論に留まっており、統一的な制御理論を構築する段階には到達していない。このような従来の研究を踏まえ、本論文ではマルチレート制御の統一的な理論体系を構築し、さらに実システムに応用し、実用的な制御方式に発展させた。

目標軌道に対して追従を行なう追従制御系において、従来のディジタル制御方式であるシングルレート制御系では、離散時間制御対象が必ず不安定零点を持つことから、安定な逆系を構成することが不可能となり、その結果大きな追従誤差を生じる問題点があった。これに対して、本論文の第 2 章ではマルチレートフィードフォワード制御という新しい制御手法を導入して、誤差なく目標軌道に追従する完全追従制御 (PTC) を提案した。さらに、この手法をハードウェアの制約によりサンプラやホールダの機構に制限がある系や、むだ時間を持つ系や多変数系に対しても対応できるよう理論の拡張を行なった。また提案する制御器が、伝達関数に基づく簡単な計算により容易に設計できることや、その構造が非常に見通しが良いことを明らかにした。

モーションコントロールにおいては、制御出力のサンプリング周期が制御入力の周期よりも長いという制限を持つ制御系が数多く存在する。例えば、ハードディスクのヘッドの位置決め制御系では、ディスク上に離散的に書かれたサーボシグナルが検出されたときのみ位置信号が検出されるが、最近の高速なプロセッサを使用すれば、制御周期を信号検出の周期よりも 4 倍程度は高速に設定することが可能である。また、ロボットのビジュアルサーボ系においては、視覚信号は 33[ms] 程度のビデオレートでしか検出できないが、制御入力となるジョイントサーボ系の制御周期は 1[ms] 以下と非常に高速である。さらに、低精度エンコーダを用いたサーボモータの速度制御系においては、速度信号の検出周期を短くすると、低速時に量子化誤差の影響が非常に大きくなることから、サンプリング周期を十分に大きく設定することが不可能である。また、近年プロセッサを搭載し、信号処理と通信の機能を追加した高性能なエンコーダが開発されつつあるが、これを使用したモーション制御系においては、位置信号の検出周期は通信の周期に固定化される。

このようなサンプリング周期が相対的に大きい系においては、従来のシングルレート制御方式では、ホールダによる大きな位相遅れにより安定性が損なわれる問題点や、ある程度高い周波数領域において、外乱抑圧特性が劣化するという問題点があった。これに対して第 3 章では、サンプル点間オブザーバとマルチレートフィードバック制御という新しい制御手法を提案し、これにより安定余裕が大幅に改善される手法と、定常状態においてサンプル点間に複数回、外乱を完全に抑圧する制御手法 (完全外乱抑圧制御:PDR) を提案した。さらに、開ループオブザーバとスイッチ機能を持つフィードフォワード制御器を導入すれば、ロバスト安定性を犠牲にすることなく、外乱を効果的に抑圧する制御系が構成できることを明らかにした。

ディジタル制御系の設計においては、従来は連続時間領域で設計した望ましい補償器を離散近似するという手法が適用されていた。しかしながら、制御性能の向上のために

は、制御帯域を限界まで広げる必要がある。このような場合には、サンプリング周波数が十分に高いという仮定が成立しなくなり、従来型の近似的に離散化した制御器では、望ましい性能が得られる保証がなく、制御系が不安定になってしまうことすらある。このような現状に対して、第 4 章はマルチレートサンプリング制御を導入して閉ループ特性を保存する新しい制御器の離散化の手法を提案した。その特徴は、ディジタル制御系の状態変数の閉ループ時間応答が、連続時間領域で設計した望ましい応答に完全に一致 (完全状態一致:PSM) するというものである。さらに、サンプリング周期が制御周期よりも長いという制限を持つ系にも対応できるよう理論的拡張を行なった。

本論文の後半では、前半部で構築した理論を、実際のモーションコントロール系へ適用した。第 5 章では、まず最初に第 2 章で提案したマルチレートフィードフォワード制御による完全追従制御 (PTC) を、DD ロボットのサーボモータの位置制御系に対して実験及びシミュレーションを行ない、従来型の手法に比べて、追従性能が格段に優れていることを実証した。次に、ハードディスク装置のヘッドの高速移動制御に適用して、その有効性を確認した。その成果は、最も重要とされているショートスパンシーク動作を、ハードウェアの大きな改良をすることなく、従来手法よりも飛躍的に高速化できるというものであった。

第 6 章では、第 3 章で提案したマルチレートフィードバック制御による完全外乱抑圧制御 (PDR) をハードディスク装置の高精度位置決め制御、及びロボットのビジュアルサーボ系に適用した。まず、ハードディスク装置に対して、提案するサンプル点間オブザーバを用れば、ホールダによって生じる大きな位相遅れが回復でき、安定余裕が大きく向上することを明らかにした。さらに完全外乱抑圧制御により、従来手法では不可能とされていたナイキスト周波数に近い高周波領域においても、効果的に Repeatable Runout と呼ばれる周期的な外乱が抑圧できることを示した。さらに、ビジュアルサーボ系に対して、作業空間コントローラと非線形写像を導入することにより線形化を行ない、提案するマルチレートフィードバック制御系を適用した。これにより、周期的な運動を繰り返す目標物体に対して、誤差なくロボットを追従させることが可能となることを示した。

第 7 章では、第 4 章で提案した完全状態一致制御 (PSM) による制御器の離散化手法をモーションコントロールに適用した。まず最初に、外乱オブザーバを用いたサーボモータのロバスト位置決め制御系に対して提案手法を適用し、従来手法よりも限界に近い高性能な設計が可能となることを明らかにした。次にハードディスク装置の振動抑制制御系に対して、本手法を適用すれば、従来は不可能とされていたナイキスト周波数周辺の振動抑制制御がマルチレート制御により可能となることを明らかにした。

第 8 章では、本論文のまとめとして、提案した完全追従制御・完全外乱抑圧制御・完全状態一致制御の理論を振り返り、フィードフォワード、フィードバックの両面性や、ハードウェアによるサンプリング機構の制限に関する視点や、応用可能なシステムに基づく観点から、提案した手法のそれぞれの関連性を見通し、本論文がマルチレート制御の統一的

な枠組を確立することに成功したと結論づけた。本論文は制御理論的な新規性も重要であるが、コンピュータの性能を限界まで利用する、実用的な制御法であるという観点からも、その工学的重要性は計り知れない。本論文の後半で述べた適用例は、従来の制御手法の性能を遥かに凌駕し、実際の製品にも適用され、実用化されている。この事実からも本研究が制御工学に新たなブレークスルーを与え、従来のモーションコントロールが超えられなかった壁を打破することに成功したと言うことができる。

なお、本文は英語により記述されていることを付記する。

General Framework of Multirate Sampling Control and Applications to Motion Control Systems

by

Hiroshi Fujimoto

Dissertation Submitted to

The Department of Electrical Engineering

for the Degree of

Doctor of Philosophy

at

The University of Tokyo

December 2000

Supervisor :

Professor Yoichi Hori

Acknowledgments

First of all, I would like to express my gratitude to my supervisor Professor Yoichi Hori for giving me valuable advice on this work and influencing my way of thinking. He taught me many things not only on my research but also how engineering and a researcher should be. His instructive advice always stimulated me to construct general and practical framework of multirate control systems. He also gave me opportunity to take part in academic committees and conferences, and to discuss with many academical and industrial researchers. I can never imagine that I could accomplish this work without his kind help. I am very proud of belonging his laboratory from 1998 to 2001, and these three years will be my precious treasure through my life.

I would like to thank Professor Atsuo Kawamura of Yokohama National University, who was my previous supervisor when I was in master course from 1996 to 1998. A part of the basic concepts of this dissertation was motivated by him. He also encouraged me to go on to the doctoral course in the University of Tokyo. I wish to thank Professor Masayoshi Tomizuka of University of California at Berkeley for many helpful discussions. His comments stimulated me to focus on the smooth transient response both of plant state and control input in practical motion control systems.

I appreciate all members of the committees for multi-dimensional motion control (MDMC) and mass storage system (MSS) of IEE Japan, where I served as a member and an observer. They gave me many comments about this work from the point of view both in the motion control theory and practical industries.

I am deeply indebted to Dr. Takashi Yamaguchi, Mr. Shinsuke Nakagawa and their colleagues of Hitachi, Ltd. for cooperation of the experiments of hard disk drive (HDD) and many helpful discussions, where I visited for about one month. After my work on the seeking control for HDD, they have improved and implemented the proposed method to the latest products. This success encouaged me very much.

I wish to express my gratitude to Professors Hidenori Kimura, Ichiro Nakatani, Katsushi Ikeuchi, Akihiko Yokoyama, Hideki Hashimoto, and Takefumi Koseki of the University of Tokyo, who are members of the judging committee of my doctoral degree with

Professor Yoichi Hori. Their constructive comments in the preliminary judging meeting helped me to modify this dissertation.

I am greatly thankful to the previous and current members of my laboratory. Mr. Uchida, technical staff, helped me both in the technical and official work to let me concentrate on this research. Discussion with my colleagues, Dr. Shin-ichiro Sakai, Fumiyasu Suzuki, Hichirosai Oyobe, Sehoon Oh, Hirokazu Seki and all members of my laboratory, always stimulated me. They sometimes helped me to prepare the experimental setups and to take care of our computer systems. I appreciate Ms. Takayo Usami and Ms. Mariko Kimura, Professor Hori's secretaries, for their sincere work.

This dissertation cannot have finished without financial support by Japan society for the promotion of science (JSPS), where I am supported as a research fellow. A part of this research was carried out with a subsidy of the Scientific Research Fund of the Ministry of Education, Science, Sports and Culture of Japan.

Finally, I would like to thank all my family members and good friends for their encouragement and support.

Hiroshi Fujimoto
The University of Tokyo
December 2000

Contents

List of Figures

List of Tables

Notation

$\triangleq$	defined as
$\boldsymbol{A}$	matrix
$\boldsymbol{x}$	row or column vector
$\boldsymbol{I}$	identity matrix
$\boldsymbol{O}$	zero matrix
$\boldsymbol{A}^T$	transpose of $\boldsymbol{A}$
$\boldsymbol{A}^{-1}$	inverse of $\boldsymbol{A}$
$G(s)$	continuous-time system
$G[z]$	discrete-time system
$x(t)$	continuous-time signal
$x[i]$	discrete-time signal
$\left[\begin{array}{c\|c} \boldsymbol{A} & \boldsymbol{B} \\ \hline \boldsymbol{C} & \boldsymbol{D} \end{array}\right]$	$\triangleq \boldsymbol{C}(z\boldsymbol{I}-\boldsymbol{A})^{-1}\boldsymbol{B}+\boldsymbol{D}$: shorthand for state space realization
$\boldsymbol{R}^n$	the set of real n-dimensional vectors
$\boldsymbol{R}^{n\times m}$	the set of $n \times m$ real matrices
$\boldsymbol{RH}_\infty$	the set of proper and stable rational functions
$\|\cdot\|$	norm of vector or matrix
$\|\boldsymbol{x}\|_2$	$\triangleq \sqrt{\sum_{i=1}^n \|x_i\|^2}$: the 2-norm of vector $\boldsymbol{x}$
$\|\boldsymbol{A}\|_F$	$\triangleq \sqrt{\sum_{i=1}^n \sum_{j=1}^m \|a_{ij}\|^2}$: the Frobenius norm of matrix $\boldsymbol{A}$
$Z[\cdot]$	$z-$transformation

Chapter 1

Introduction

1.1 Background of the Research

Owing to recent developments of the computer and interface hardware, digital controllers are utilized for controlling almost all mechanical systems such as robots, motors, machine tools, and hard disk drives, because of cost, reliability, flexibility, compactness, etc.

A generalized digital control system is shown in Fig. 1.1, where $P_c(s)$ is a continuous-time plant to be controlled, $\boldsymbol{C}[z]$ is a discrete-time controller implemented in digital computer. $d(t)$ and $n(t)$ are disturbance and measurement noise, respectively. Because the discrete-time controller has to deal with continuous-time signals in the digital control systems, it needs to have two samplers $\mathcal{S}$ for the reference signal $r(t)$ and the output $y(t)$, and one holder $\mathcal{H}$ on the input $u(t)$[1]. Therefore, there exist three time periods T_r, T_y, and

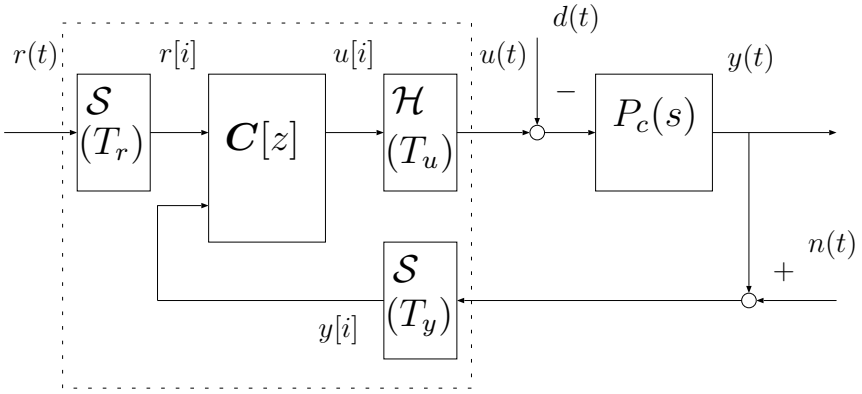

Figure 1.1: Digital control system.

[1]The reference signal is often given as a discrete-time signal $r[i]$. However, in this dissertation, it is assumed to be a continuous-time signal $r(t)$, and a sampler of the reference input is introduced in order to construct general framework of multirate sampling control and to consider the intersample response

T_u which represent the periods of $r(t), y(t)$, and $u(t)$, respectively. The input period T_u is generally decided by the speed of the actuator, D/A converter, or the calculation on the CPU. Moreover, the output period T_y is also determined by the speed of the sensor or the A/D converter.

Actual control systems usually hold hardware restrictions on these periods (T_u and/or T_y). Moreover, in case of multivariable systems, there exist many time periods. However, the conventional digital control systems make all periods equal to the longest period for simplification. On the other hand, the multirate sampling control systems have been studied from the point of view both of control theories and practical applications.

1.1.1 Theoretical Background

The range of theoretical research on digital controllers is very wide especially in the last several decades. But, as to the subjects related to this dissertation, recent theoretical advances are as follows [1].

1. Non-conventional digital controllers: general holds, general samplers, multirate control, time varying control, and periodically time varying control

2. Advanced sampled-data control theory: consideration of intersample response, lifting, fast sample and fast hold approximation, and sampled-data H_2 and H_∞ problems.

Non-conventional digital controllers

Recently, non conventional digital controllers have been studied not only for multirate controller but also for general hold circuits, general samplers, and time varying controllers by many control theorists. Historically, the generalized hold is firstly introduced in [2]. Thus, this work should be reviewed here before multirate control theory is discussed.

As shown in Fig. 1.2, in the generalized hold approach, the control input is generated by

$$u(t) = \sum_{i=0}^{\infty} h(t - iT_f)u[i], \tag{1.1}$$

where $h(t)$ is an arbitrary hold function and T_f is a frame period. This function is also called the Chammas-Leondes' generalized hold [1]. Utilizing the hold function as a design parameter, it is possible to assign all poles only by the gain output feedback without the state observer. This approach was extended to feedforward control in [3],

of $y(t)$.

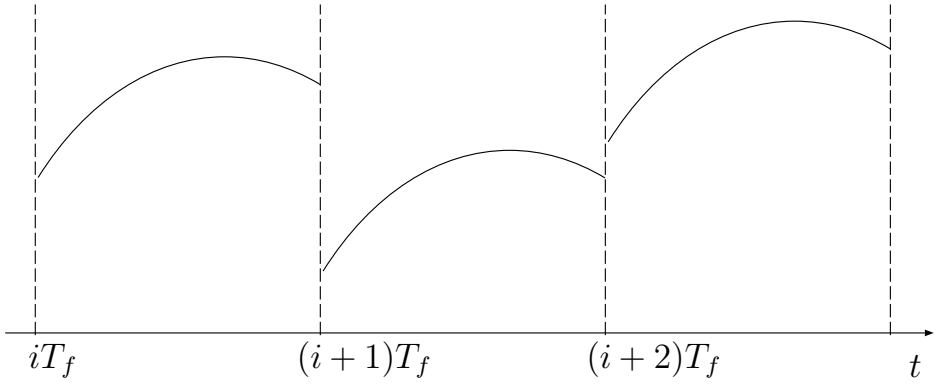

Figure 1.2: Generalized hold.

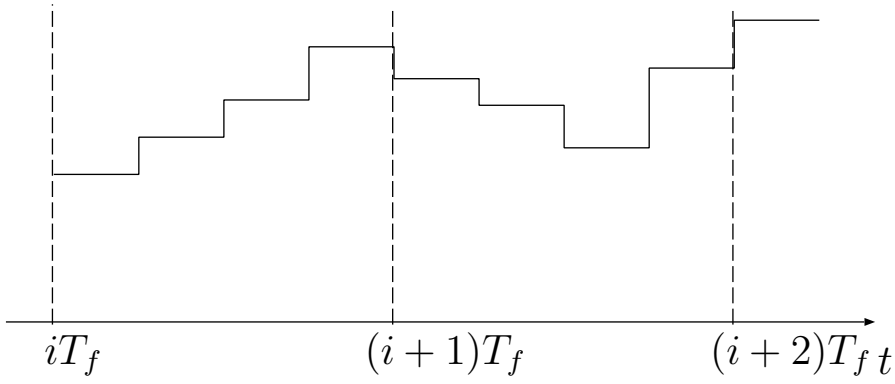

Figure 1.3: Multirate hold.

where simultaneous pole assignment, exact model matching, decoupling, and optimal noise rejection are successfully realized.

However, in this method, an arbitrary waveform is assumed to be generated as the hold function $h(t)$. In practice, it is very difficult to make arbitrary hold function because $h(t)$ is generally composed of exponential and sinusoidal functions. Thus, in [4], [5] and [6], the pole assignment method was modified to the multirate hold, in which the control input is piecewise constant, as shown in Fig. 1.3. Because this scheme is easily implemented by ordinary D/A converters, the multirate hold is a practical solution of the generalized hold.

Moreover, it is possible to assign not only poles but also zeros by the generalized holds [3] and multirate holds [7, 8]. These results have brought great advantages because the discrete-time plant usually has unstable zeros in the conventional single-rate digital control system [9] and it is impossible to allocate zeros by feedback control.

On the other hand, the generalized samplers and multirate samplers have been developed in [1, 8, 10, 11], as dual schemes of generalized holds and multirate holds. In [10], an

equivalent state feedback with loop transfer recovery (LTR) property is proposed based on the multirate output control, in which the plant output is detected several times during one control period. Next, in [8], multirate output control is proposed, which diminishes all finite zeros and constructs stable inverse systems and output feedback controllers with LTR property.

Other than the above work, many non-conventional digital controllers including multirate sampling control have been developed from the point of view of the various concepts, such as strong stabilization [12, 13, 14], simultaneous stabilization and simultaneous pole assignment [12, 15], decentralized stabilization [16], adaptive control [17, 18], arbitrarily-large gain-margin [12, 19], parameterization of stabilizing multirate controllers [20, 21], and feedback linearization for nonlinear system [22]. These results are well surveyed in [1] which has more than 100 references.

To sum up, the non-conventional digital controllers including multirate controllers can have the clear advantages, over the conventional single-rate controllers and sometimes even over the linear time invariant continuous-time controllers [1]. However, [12, 23, 24, 25] have indicated the theoretical negative aspects of the multirate sampling control. First, [12, 23] have proved that the feedback characteristics such as disturbance rejection performance and stability robustness against unstructured uncertainty can never be improved by multirate control in cases without hardware restriction on sampling scheme ($T_y = T_u$). Second, [24] shows that the zero assign methods sometimes have disadvantages of large overshoot and oscillation in the inter-sample points because the control input changes back and forth very quickly. Third, the multirate control system often has very poor performance against detection noise and modeling error [1, 25]. As a result, the previous multirate sampling control theories did not have many applications even though the theoretical advantages were very interesting.

Advanced sampled-data control theory

After the non-conventional digital control theory was eagerly researched mainly in 1980s, advanced sampled-data control theory has been focused on and developed very rapidly [26, 27]. Especially from 1990, a lot of important work about this topic has been done, which has been stimulated by Chen and Francis [28, 29]. The advantage of this theory is that the intersample behavior can be directly considered and designed.

The problem setup of this framework is shown in Fig. 1.4, where $\boldsymbol{G}(s)$ is a continuous-time generalized plant with weighting function, $\boldsymbol{C}[z]$ is a discrete-time controller, $\mathcal{H}$ is a zero-order hold, and $\mathcal{S}$ is an ideal sampler. The exogenous input $\boldsymbol{w}$ contains disturbances and reference signals, and the controlled output $\boldsymbol{z}$ is the signal which should be made

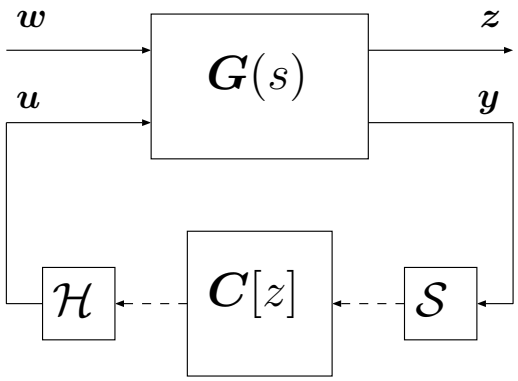

Figure 1.4: Generalized plant for sampled-data system.

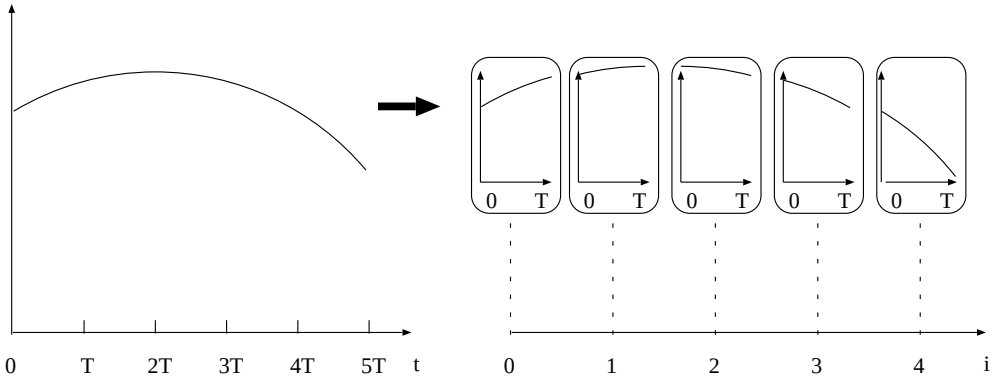

Figure 1.5: Continuous-time lifting.

small or zero. The control input $\boldsymbol{u}$ is generated by the discrete-time controller, and the measured output $\boldsymbol{y}$ is an input variable of the digital controller. This arrangement is called the hybrid system because it has both continuous-time and discrete-time signals.

The formulation of the advanced sampled-data theory is to find the digital controller $C[z]$ to minimize typically H_2 or H_∞ norm from $\boldsymbol{w}$ to $\boldsymbol{z}$ [30, 31, 32, 33, 34]. One of the most important mathematical methods in this framework is so-called "lifting" technique which is introduced to deal with the difficulty of the hybrid system [35, 36]. In the lifting technique, the continuous-time signal is chopped at the sampling points $t = 0, T, 2T, \cdots$, and regarded as a sequence of functional segments, as shown in Fig. 1.5. By using this idea, the hybrid system can be transformed to the equivalent discrete-time system which preserves the norm.

Moreover, advanced sampled-data theory has been able to define the frequency response, which can take into account the intersample behavior [37, 38]. Because the calculation sometimes has numerical difficulty, [39] introduced the fast sample and fast hold (FSFH) approximation. In the FSFH method, the continuous-time signals $\boldsymbol{z}$ is sampled

at every T/N, and $\boldsymbol{w}$ is held during T/N [40]. Thus, the original hybrid system can be converted to the equivalent discrete-time system. The frequency response of FSFH system has been proved to converge to that of the original hybrid system when $N \to \infty$. This approximation is a practical and useful approach because it is applicable not only to the analysis of the frequency response but also to the H_2 and H_∞ synthesis.

Moreover, this advanced sample-data theory is extended to the multirate control problem in [41, 42, 43]. Thus, we can say that advanced sampled-data theory is complete from the theoretical point of view.

However, in the present situation, this theory has solved only H_2 and H_∞ control problems, although many advanced topics are still been studied [26]. Thus, it is not always applicable to all problems, since H_2 and H_∞ synthesis is not always effective and it makes several assumptions in obtaining the solutions.

Moreover, because it is based on the small gain theorem to assure the stability robustness, the phase information of the uncertainty Δ is neglected, while the gain is assumed to be bounded $\|\Delta\|_\infty \leq 1$. Thus, the conservative controller is generally obtained. Because of this problem, in highly competitive industries such as the motion control systems of hard disk drives, the conservativeness of the small gain theorem is sometimes too restrictive [44], and conventional analysis remains based on the Nyquist diagram. Especially in the advanced sampled-data theory, analysis and synthesis based on the small gain theorem can be more conservative [45]. Thus, it is not always suitable to practical systems with highly demanding specifications such as very high speed and very high precision motion control systems.

Although this theory has been applied to several practical systems such as a pneumatic cylinder system [46] and hard disk drives [47, 48], more practical improvements such as in [49] will be desired in the future.

1.1.2 Practical Background

On the other hand, many applications have included the multirate sampling control. For example, in the head positioning system of hard disk drives, the head position is detected by the servo signal embedded in disks discretely, as shown in Fig. 1.6. Thus, the sampling frequency is restricted because it is determined by the rotational frequency and number of the servo signals. On the other hand, the control frequency of the actuator (voice coil motor) can be set faster than the sampling frequency of the head position. Therefore, multirate estimation and control have been applied to hard disk drives in [50, 51, 52, 53, 54, 55].

Another example is the visual servo system of robot manipulators. Although the

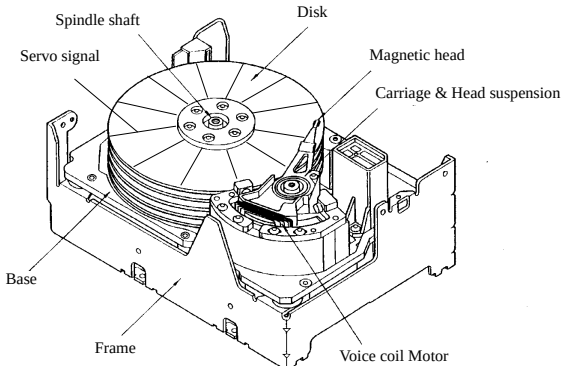

Figure 1.6: Hard disk drive.

sampling period of the vision sensor such as a CCD camera is comparatively slow (over 33 [ms]), the control period of the joint servo is very fast (less than 1 [ms]). Therefore, multirate controllers have been developed and implemented in the visual servo systems [56, 57, 58].

The third example is the velocity or position control of industrial motors with low precision encoders. In these systems, the sampling period cannot be set too short, because the velocity information cannot be detected due to the low resolution of the encoder. Therefore, the instantaneous speed observer has been developed in [59], which estimates the inter-sample velocity with use of the discrete-time observer.

Next, the industrial control systems of servomotors have utilized multi-loop multirate sampling controllers, because the time constants of the current, velocity and position loops are quite different. Thus, it is a smart solution to set sampling periods of each control loop independently [60].

Moreover, multirate filter bank is one of the hot research topics in the field of signal processing. Recently, sampled-data control theory is applied to design of the filter banks based on the continuous-time signal [61, 62].

In recent years, high performance and high precision intelligent encoders are being developed which have signal possessors and communication equipment. If these encoders are implemented to the motion control systems, the sampling frequency is fixed to the communication speed. Thus, the multirate sampling control will play a more important role in the future practical motion control systems.

1.2 Motivations of the Dissertation

As mentioned above, multirate control systems have been very important in various areas of control engineering. However, these topics have been developed separately both in theory and application. The objective of this dissertation is to construct an integrated theory of multirate sampling control and to further develop it into practical control methods.

In the first part of this dissertation, generalized theoretical framework for multirate sampling control is constructed, which is based on novel control strategies of 1) perfect tracking control (PTC) by multirate feedforward control, 2) perfect disturbance rejection (PDR) control by multirate feedback control, and 3) perfect state matching (PSM) control by multirate sampling control. In the second part, the proposed theory is applied to the practical motion control systems such as servomotors of robot manipulators, hard disk drives, two-mass systems, and visual servo systems.

The proposed method makes use of the extra degree-of-freedom of control input provided by multirate control, in the same way as previous theoretical papers [4, 5, 6, 10]. But, the significant feature of the proposed framework is that all the plant states are directly controlled at every period by using the increased degree-of-freedom of the control input. Because of this novel methodology, the transient time response of the plant state becomes very smooth and ripple-free, and the control input is prevented from oscillating. From the knowledge of the deadbeat control [63], it is easily understood that plant state becomes ripple-free by controlling state variable. But, this dissertation makes a first attempt to apply it to the multirate control.

This concept of controlling state variables is very important from the practical point of view. In many practical problems, the transient response characteristics is sometimes much more important than optimizing a performance index [64], while recent control theory is focused on the optimization problem. Especially in motion control systems, the plant state includes the variables of position and velocity, and the control input generally corresponds to the force command. Thus, it is physically reasonable to control the plant state and control input to obtain desirable transient waveforms.

While recent control theories tend to depend on the numerical optimization by Riccati equation or linear matrix inequality (LMI), this dissertation tries to obtain not numerical solutions but analytical solutions if it is possible. Moreover, it takes up the challenge to construct simple and clear control schemes, which are intuitively understandable and easily applicable to practical motion control systems, because a complex and difficult control theory does not always obtain the best results in the real world [65].

As mentioned in section 1.1.1, the theory for multirate control systems has been studied

by many researchers, and many important results have already been obtained. However, this previous work has never paid attention to the hardware restriction on the sampling scheme. On the other hand, this dissertation makes first attempt to construct general framework for systems with hardware restrictions in the sampling scheme.

This dissertation also focuses on the intersample response and sometimes utilizes the fast sampling technique, following the advanced sampled-data theory. As mentioned in section 1.1.1, advanced sampled-data theory is applicable to the multirate system [41, 42, 43]. But, the solution does not let us know the physical advantage of the multirate sampling scheme, although it gives the mathematical optimization. However, by using the proposed method, we find that the essential and intuitive advantages of multirate control are 1) to compensate large phase delay generated by the zero-order hold, 2) to reject disturbance at intersample points, 3) to improve tracking performance without unstable zero problem, and 4) to control plant state directly at every period. As will be demonstrated in chapter 6, improvements introduced by multirate control are superior to those of optimizing intersample response. Thus, it can be said that this dissertation gives a breakthrough in control engineering.

The most important progress of recent control engineering is the robustness against plant uncertainty. This dissertation also takes care of this problem. But, in motion control systems, it has become possible to design robust servo system by simple ways such as the disturbance observer [66, 67]. Thus, these simple and practical methods are utilized in this dissertation.

1.3 Outline of the Dissertation

The outline of this dissertation is illustrated in Fig. 1.7. This dissertation consists of two parts: theory and applications. All chapters on theory are independent from each other, except for several equations referred from other chapters. The chapters on applications correspond to the respective chapters on theory.

The details of each chapter are as follows.

In chapter 2, a novel perfect tracking control (PTC) method is proposed based on multirate feedforward control. The features of PTC are 1) the controller can be designed without considering the unstable zero problem of discrete-time plants, 2) the plant state matches the desired trajectories at every sampling point of reference input, and 3) high robust performance is assured by the robust feedback controller because the proposed controller is completely independent of the feedback characteristics. Moreover, by generalizing the relationship between the sampling period of plant output and the control

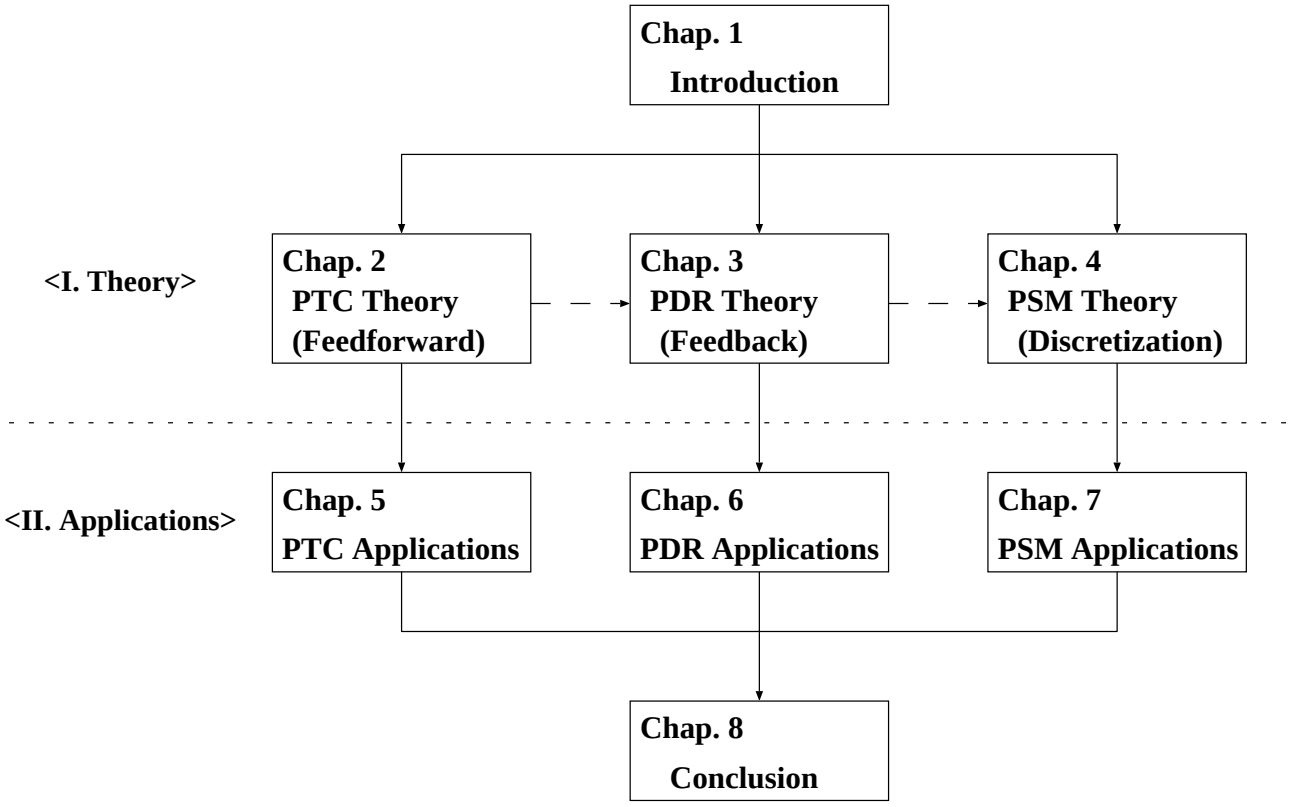

Figure 1.7: Outline of this dissertation

period of plant input, the proposed method can be applied to various systems with hardware restriction in the sampling scheme, leading to higher performance. Next, it is shown that the structure of the proposed perfect tracking controller is very simple and clear.

In chapter 3, novel multirate feedback controllers are proposed for digital control systems, where there is a restriction that the speed of the A/D converters is slower than that of the D/A converters. The proposed feedback controller assures perfect disturbance rejection (PDR) at M intersample points in the steady state. The proposed method is also extended to systems with time delay. Moreover, an intersample observer is developed in order to reduce phase delay caused by zero-order hold and to increase the stability margin by estimation and compensation of the intersample response. Next, the PDR is applied to the periodic disturbance rejection problem. The novel scheme of repetitive control is proposed based on the open-loop estimation and switching function, which enables rejection of periodical disturbance without any sacrifice of the closed-loop characteristics. Finally, intersample disturbance rejection performance is optimized by the fast sampling approach.

In chapter 4, a novel discretization method for continuous-time controllers is proposed based on perfect state matching (PSM) control by which the states in the continuous-

time systems are completely reserved in the obtained sampled-data system. The features of the proposed method are 1) multirate input control is employed, 2) the states of the discretized sampled-data system completely match those of the original continuous-time closed-loop system at every sampling period, and 3) the proposed method is applicable to a static state-feedback and/or a dynamic controller. Next, discretization method of observer is proposed based on multirate output control. Finally, the proposed method is extended to systems with relatively long sampling periods.

In chapter 5, the perfect tracking control (PTC) proposed in chapter 2 is applied to several motion control systems. First, the position control system of servomotor for robot manipulators is considered as an example without special hardware restriction ($T_u = T_y$). Combining the proposed feedforward controller with H_∞ robust feedback controller, perfect tracking performance is achieved with robustness. Second, the proposed method is applied to track-seeking control of hard disk drive which is as an example with time delay and long sampling period relative to the control input ($T_u < T_y$). For this system, it is shown that the proposed controller enables higher speed movement when compared with the conventional single-rate controller. Simulations and experiments both of servomotors and hard disk drives are performed, and advantages of this approach are demonstrated.

In chapter 6, the perfect disturbance rejection (PDR) control developed in chapter 3 is applied to motion control systems, where the sampling period of the sensor is shorter than the control period of the actuator. As examples, track-following mode of hard disk drive (HDD) and visual servo systems of robot manipulators are considered. First, the perfect disturbance rejection controller is applied to first-order disturbance mode of repeatable runout in HDD based on multirate feedback control. Second, the problem of the feedback approach for higher disturbance mode is explained, and the open-loop observer with switching function is implemented in order to overcome the problem. Moreover, the intersample observer compensates the large delay generated by the hold and improves the stability margin of the closed-loop system. Finally, the proposed method is applied to visual servo systems by introducing the workspace controller and perspective transformation.

In chapter 7, the perfect state matching (PSM) control developed in chapter 4 is applied to the motion control systems based on multirate sampling control. First, the position control system for a dc servomotor with disturbance observer is utilized as an example without hardware restriction in the sampling scheme. Simulations and experiments are performed, and advantages of this approach are demonstrated. Because the proposed method assures response matching independent of the sampling period, it enables to bring out the maximum performance of a control system. Second, vibration suppression control

is proposed based on multirate input control for a system in which the Nyquist frequency is relatively closed to the mechanical resonance mode and the sampling period is longer than the control period. For a two-mass system model of the hard disk drive, simulations demonstrate the possibility of controlling the critical resonance mode.

In chapter 8, the proposed three control schemes of PTC, PDR, and PSM are reviewed, and the obtained results are classified by the hardware restriction of their sampling schemes and according to the feedforward and feedback approaches. The constructed framework is summarized, and the conclusion of this dissertation is stated.

Part I

Theory

Chapter 2

Perfect Tracking Control Based on Multirate Feedforward Control

2.1 Abstract

In this chapter, a novel perfect tracking control method based on multirate feedforward control is proposed. The advantages of the proposed method are 1) the proposed multirate feedforward controller eliminates the notorious unstable zero problem in designing the discrete-time inverse system, 2) the states of the plant match the desired trajectories at every sampling point of reference input, and 3) the feedback characteristics are completely independent of the proposed controller. Thus, highly robust performance is assured by the robust feedback controller. Moreover, by generalizing the relationship between the sampling period of plant output and the control period of plant input, the proposed method can be applied to various systems with hardware restrictions in the sampling scheme, leading to higher performance. Next, it is shown that the structure of the proposed perfect tracking controller is very simple and clear. The proposed method is applied to position control systems of servomotors and hard disk drives in chapter 5.

2.2 Introduction

In digital motion control systems, tracking controllers are often employed for high-speed and high-precision servo systems because the controlled plant follows a smoothed desired trajectory. The best tracking controller is ideally the perfect tracking controller (PTC) which controls the object with zero tracking error [68]. Perfect tracking control can be achieved using d-step preview action and a feedforward controller $C_1[z]$ which is realized

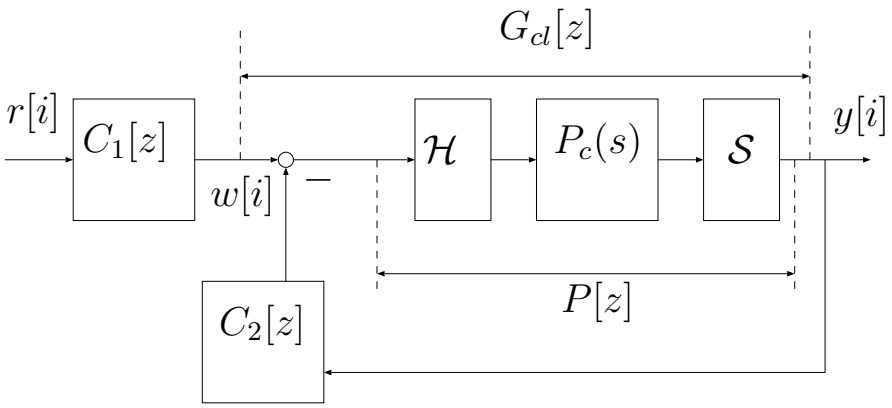

Figure 2.1: Conventional perfect tracking control system.

by an inverse of the closed-loop system $G_{cl}[z]$, as shown in Fig. 2.1.

$$C_1[z] = \frac{1}{z^d G_{cl}[z]} = \frac{1 + P[z]C_2[z]}{z^d P[z]} \tag{2.1}$$

$$r[i] = y_d[i + d] \tag{2.2}$$

Here, d is the relative degree of $G_{cl}[z]$ and $y_d[i]$ is the desired trajectory.

However, the discrete-time plant $P[z]$ discretized by the zero-order hold usually has unstable zeros [9]. Thus, $C_1[z]$ becomes unstable because $G_{cl}[z]$ has unstable zeros. Therefore, in conventional digital control systems utilizing zero-order holds, the perfect tracking control is usually impossible.

From this viewpoint, two feedforward control methods have been proposed for the discrete-time plant with unstable zeros [68]. First, the stable pole zero canceling (SPZC) controller cancels all poles and stable zeros of the closed-loop system, which has both phase and gain errors caused by the uncancellable unstable zeros. Second, the zero phase error tracking controller (ZPETC) adds the factors which cancel the phase error, to SPZC. However, the gain error caused by the unstable zeros remains. There have also been attempts to compensate for the gain error of ZPETC [69, 70, 71]. However, those efforts were not able to realize perfect tracking control because zero-order holds were employed.

In this chapter, a novel perfect tracking control method is proposed by using multirate feedforward control. In the proposed scheme, the tracking error of plant state becomes completely zero at every sampling period of reference input for a nominal plant without disturbance[1]. Moreover, by combining the proposed feedforward controller with a robust feedback controller such as disturbance observer or H_∞ controller, high tracking performance is preserved even if the plant has modeling error and disturbance.

[1]The word of "perfect tracking control" is originally defined in [68], which means the plant output perfectly tracks the desired trajectory with zero tracking error at every sampling point.

The unstable-zeros problem of the discrete-time plant has been resolved by zero assignment based on multirate control [3, 7, 8]. However, it has been shown that those methods sometimes have the disadvantages of large overshoot and oscillation in the intersample points because the control input changes back and forth very quickly [24]. On the other hand, the proposed method never has this problem because all of the plant states (e.g., position and velocity) are controlled along the smoothed desired trajectories.

Recently, modern sampled-data control theories have been developed, which can optimize the intersample response (e.g., [27, 26, 42]). However, the proposed method has the practical advantages that 1) the design method and structure of the controller are simple and clear, and 2) no complex calculations for optimization are required.

The contents of this chapter are as follows. In section 2.3, the perfect tracking controller is proposed in the simplest case for a single-input single-output (SISO) plant without hardware restrictions in the sampling scheme. Next, the proposed method is extended to applications in various systems with hardware restrictions by generalizing the sampling periods.

2.3 Perfect Tracking Control without Hardware Restrictions

A digital tracking control system usually has two samplers for the reference signal $r(t)$ and the output $y(t)$, and one holder on the input $u(t)$, as shown in Fig. 2.2. Therefore, as mentioned in chapter 1, there exist three time periods T_r, T_y, and T_u which represent the periods of $r(t), y(t)$, and $u(t)$, respectively. The input period T_u is generally decided by the speed of the actuator, the D/A converter, or the calculations on the CPU. On the other hand, the output period T_y is determined by the speed of the sensor or the A/D converter.

In this section, the perfect tracking control is proposed in the simplest case for a SISO plant without hardware restrictions on the sampler and holder ($T_y = T_u$) . Because actual control systems usually have restrictions on T_u and/or T_y, the proposed method is extended to general systems with these restrictions ($T_y \neq T_u$) in section 2.4.

In the proposed multirate feedforward control, the control input $u(t)$ is changed n times during one sampling period (T_r) of reference input $r(t)$, as shown in Fig. 2.3. Here n is the plant order. The advantage of the proposed method is that the tracking error of plant state becomes perfectly zero at every T_r.

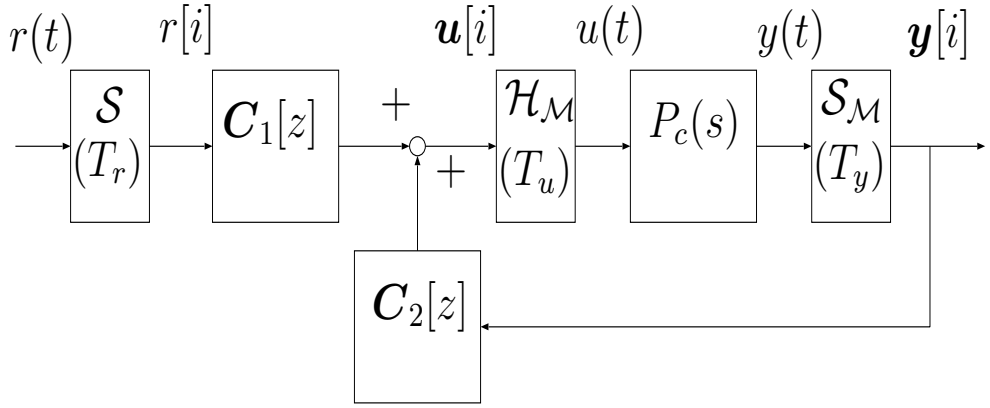

Figure 2.2: Two-degree-of-freedom control system.

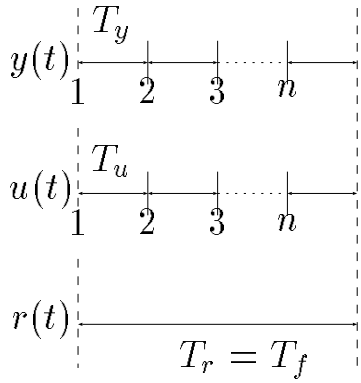

Figure 2.3: Multirate feedforward control.

2.3.1 Plant Discretization and Parameterization

Consider the continuous-time nth-order plant $P_c(s)$ described by

$$\dot{\boldsymbol{x}}(t) = \boldsymbol{A}_c\boldsymbol{x}(t) + \boldsymbol{b}_c u(t)\ , \quad y(t) = \boldsymbol{c}_c\boldsymbol{x}(t). \tag{2.3}$$

The discrete-time plant $P[z_s]$ discretized by the short sampling period T_y $(= T_u)$ of Fig. 2.4 becomes

$$\boldsymbol{x}[k+1] \;=\; \boldsymbol{A}_s\boldsymbol{x}[k] + \boldsymbol{b}_s u[k] \tag{2.4}$$

$$y[k] \;=\; \boldsymbol{c}_s\boldsymbol{x}[k], \tag{2.5}$$

where $\boldsymbol{x}[k] = \boldsymbol{x}(kT_y)$, $z_s \triangleq e^{sT_y}$, and

$$\boldsymbol{A}_s \triangleq e^{\boldsymbol{A}_c T_y}, \quad \boldsymbol{b}_s \triangleq \int_0^{T_y} e^{\boldsymbol{A}_c\tau}\boldsymbol{b}_c d\tau, \quad \boldsymbol{c}_s \triangleq \boldsymbol{c}_c. \tag{2.6}$$

Thus, the discrete-time plant $\boldsymbol{P}[z]$ discretized by the multirate sampling control of Fig. 2.4 can be represented by

$$\boldsymbol{x}[i+1] \;=\; \boldsymbol{A}\boldsymbol{x}[i] + \boldsymbol{B}\boldsymbol{u}[i] \tag{2.7}$$

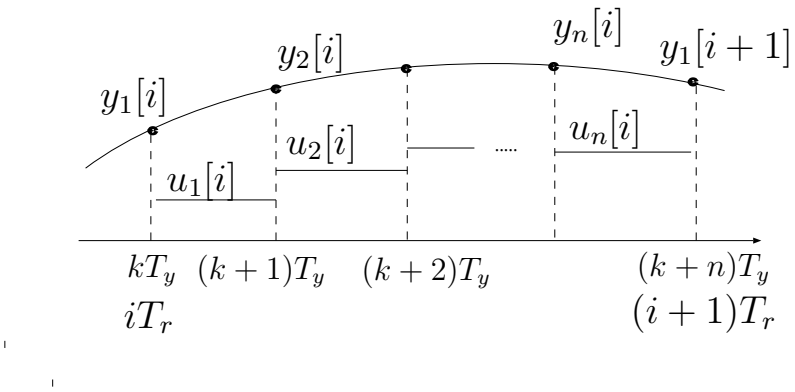

Figure 2.4: Multirate sampling control at same interval.

$$\boldsymbol{y}[i] \;=\; \boldsymbol{C}\boldsymbol{x}[i] + \boldsymbol{D}\boldsymbol{u}[i], \tag{2.8}$$

where $\boldsymbol{x}[i] = \boldsymbol{x}(iT_r), z \stackrel{\triangle}{=} e^{sT_r}$, and multirate input and output vectors $\boldsymbol{u}, \boldsymbol{y}$ are defined as [2]

$$\boldsymbol{u}[i] \;\stackrel{\triangle}{=}\; [u_1[i], \cdots, u_n[i]]^T = [u(kT_y), u((k+1)T_y), \cdots, u((k+n-1)T_y)]^T, \tag{2.9}$$

$$\boldsymbol{y}[i] \;\stackrel{\triangle}{=}\; [y_1[i], \cdots, y_n[i]]^T = [y(kT_y), y((k+1)T_y), \cdots, y((k+n-1)T_y)]^T, \tag{2.10}$$

and matrices $\boldsymbol{A}, \boldsymbol{B}, \boldsymbol{C}, \boldsymbol{D}$ are given by [3]

$$\left[\begin{array}{c|c} \boldsymbol{A} & \boldsymbol{B} \\ \hline \boldsymbol{C} & \boldsymbol{D} \end{array}\right] \stackrel{\triangle}{=} \left[\begin{array}{c|cccc} \boldsymbol{A}_s^n & \boldsymbol{A}_s^{n-1}\boldsymbol{b}_s & \boldsymbol{A}_s^{n-2}\boldsymbol{b}_s & \cdots & \boldsymbol{A}_s\boldsymbol{b}_s & \boldsymbol{b}_s \\ \hline \boldsymbol{c}_s & 0 & 0 & \cdots & 0 & 0 \\ \boldsymbol{c}_s\boldsymbol{A}_s & \boldsymbol{c}_s\boldsymbol{b}_s & 0 & \cdots & 0 & 0 \\ \vdots & \vdots & & & \vdots & \\ \boldsymbol{c}_s\boldsymbol{A}_s^{n-1} & \boldsymbol{c}_s\boldsymbol{A}_s^{n-2}\boldsymbol{b}_s & \boldsymbol{c}_s\boldsymbol{A}_s^{n-3}\boldsymbol{b}_s & \cdots & \boldsymbol{c}_s\boldsymbol{b}_s & 0 \end{array}\right]. \tag{2.11}$$

Concerning the matrices $\boldsymbol{B}$ and $\boldsymbol{C}$, the following theorems are obtained in [6, 10, 72].

[2] The operations of (2.9) and (2.10) are called "discrete-time lifting" in advanced sampled-data control theory [27] .

[3] For example, in case of $n = 2$, (2.11) is obtained as follows.

$$\begin{aligned}
\boldsymbol{x}[k+1] &= \boldsymbol{A}_s\boldsymbol{x}[k] + \boldsymbol{b}_s u[k] \\
\boldsymbol{x}[k+2] &= \boldsymbol{A}_s\boldsymbol{x}[k+1] + \boldsymbol{b}_s u[k+1] = \boldsymbol{A}_s(\boldsymbol{A}_s\boldsymbol{x}[k] + \boldsymbol{b}_s u[k]) + \boldsymbol{b}_s u[k+1] \\
&= \boldsymbol{A}_s^2\boldsymbol{x}[k] + \boldsymbol{A}_s\boldsymbol{b}_s u[k] + \boldsymbol{b}_s u[k+1] \\
y[k] &= \boldsymbol{c}_s\boldsymbol{x}[k] \\
y[k+1] &= \boldsymbol{c}_s\boldsymbol{x}[k+1] = \boldsymbol{c}_s(\boldsymbol{A}_s\boldsymbol{x}[k] + \boldsymbol{b}_s u[k])
\end{aligned}$$

$$\left(\begin{array}{c} \boldsymbol{x}[k+2] \\ \hline y[k] \\ y[k+1] \end{array}\right) = \left(\begin{array}{c|cc} \boldsymbol{A}_s^2 & \boldsymbol{A}_s\boldsymbol{b}_s & \boldsymbol{b}_s \\ \hline \boldsymbol{c}_s & 0 & 0 \\ \boldsymbol{c}_s\boldsymbol{A}_s & \boldsymbol{c}_s\boldsymbol{b}_s & 0 \end{array}\right) \left(\begin{array}{c} \boldsymbol{x}[k] \\ \hline u[k] \\ u[k+1] \end{array}\right).$$

Theorem 2.1 *If $(\boldsymbol{A}_c, \boldsymbol{b}_c)$ of the continuous system (2.3) is a controllable pair, the input matrix $\boldsymbol{B}$ of the multirate system (2.7) is nonsingular for almost every sampling period T_y.*

Theorem 2.2 *If $(\boldsymbol{A}_c, \boldsymbol{c}_c)$ of the continuous system (2.3) is an observable pair, the output matrix $\boldsymbol{C}$ of the multirate system (2.7) is nonsingular for almost every sampling period T_y.*

These theorems are easily proved in case of the SISO system. If the continuous system (2.3) is controllable and observable, the discrete-time system (2.4) becomes controllable and observable for almost every sampling period T_y [73]. Therefore, the matrices $\boldsymbol{B}$ and $\boldsymbol{C}$ of (2.11) become nonsingular because they are equal to the controllability and observability matrices of (2.4), respectively.

The proposed method employs the multirate-input control as a two-degree-of-freedom control, as shown in Fig. 2.2. In the figures, $\mathcal{H}_{\mathcal{M}}$ and $\mathcal{S}_{\mathcal{M}}$ represent the multirate hold and the multirate sampler, respectively. The functions of $\mathcal{H}_{\mathcal{M}}$ and $\mathcal{S}_{\mathcal{M}}$ are shown in Fig. 2.4, and defined in (2.9) and (2.10).

In the ideal tracking control system, the transfer characteristic (G_{yr}) from the command r to the output y is generally 1. In this chapter, the feedforward controller $\boldsymbol{C}_1[z]$ is considered so that the transfer characteristic from the desired state $\boldsymbol{x}_d$ to the plant state $\boldsymbol{x}$ can be $\boldsymbol{I}$.

2.3.2 Design of the Feedback Controller $\boldsymbol{C}_2[z]$

Before the perfect tracking controller $\boldsymbol{C}_1[z]$ is designed, the feedback controller $\boldsymbol{C}_2[z]$ must be determined. Here, $\boldsymbol{C}_2[z]$ must be a robust controller which renders the sensitivity function $\boldsymbol{S}[z] = (\boldsymbol{I} - \boldsymbol{P}[z]\boldsymbol{C}_2[z])^{-1}$ sufficiently small at the frequency of the desired trajectory. The reason is that the sensitivity function $\boldsymbol{S}[z]$ represents variation of the command response $\boldsymbol{G}_{yr}[z]$ under the variation of $\boldsymbol{P}[z]$ [74]. The feedback controller satisfying this specification can be designed easily by using a disturbance observer approach or H_∞ theory [66, 67, 75].

For systems without special hardware restrictions in which the feedback loop is single-rate ($T_y = T_u$), the feedback controller $C_2[z_s] = \{\boldsymbol{A}_{s2}, \boldsymbol{b}_{s2}, \boldsymbol{c}_{s2}, d_{s2}\}$ is designed for $P_c(s)$ with a single-rate sampling period T_y ($= T_u$), where $z_s = e^{sT_y}$. Subsequently, $C_2[z_s]$ is transferred to an n-input n-output system $\boldsymbol{C}_2[z]$ using (2.12), in order to realize $\boldsymbol{C}_1[z]$

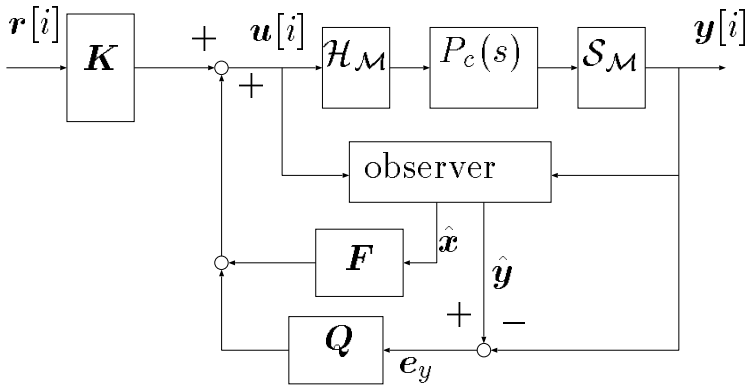

Figure 2.5: Basic structure of TDOF control.

and $\boldsymbol{C}_2[z]$ together, where $z = e^{sT_y} = z_s^n$.

$$\boldsymbol{C}_2[z] = \left[\begin{array}{c|cccc} \boldsymbol{A}_{s2}^n & \boldsymbol{A}_{s2}^{n-1}\boldsymbol{b}_{s2} & \boldsymbol{A}_{s2}^{n-2}\boldsymbol{b}_{s2} & \cdots & \boldsymbol{b}_{s2} \\ \hline \boldsymbol{c}_{s2} & d_{s2} & 0 & \cdots & 0 \\ \boldsymbol{c}_{s2}\boldsymbol{A}_{s2} & \boldsymbol{c}_{s2}\boldsymbol{b}_{s2} & d_{s2} & \cdots & 0 \\ \vdots & \vdots & & & \vdots \\ \boldsymbol{c}_{s2}\boldsymbol{A}_{s2}^{n-1} & \boldsymbol{c}_{s2}\boldsymbol{A}_{s2}^{n-2}\boldsymbol{b}_{s2} & \boldsymbol{c}_{s2}\boldsymbol{A}_{s2}^{n-3}\boldsymbol{b}_{s2} & \cdots & d_{s2} \end{array}\right] \tag{2.12}$$

Because the feedback characteristics such as disturbance rejection performance and stability robustness are never improved by the multirate control in the case where there is no hardware restriction in the sampling scheme ($T_y = T_u$) [12, 23], it is not necessary to design a n-input n-output multirate system as the feedback controller $\boldsymbol{C}_2[z]$. Therefore, a single-rate feedback controller $C_2[z_s]$ is adequate in the case of $T_y = T_u$.

2.3.3 Design of the Perfect Tracking Controller $\boldsymbol{C}_1[z]$ – State Space Approach

In this section, the multirate feedforward controller $\boldsymbol{C}_1[z]$ is designed using the state space approach. The proposed method can assure perfect tracking at every sampling point T_r.

From Fig. 2.2, the multirate control law of the proposed method is described by [4]

$$\boldsymbol{u}[i] = \boldsymbol{C}_1[z]\boldsymbol{r}[i] + \boldsymbol{C}_2[z]\boldsymbol{y}[i] \tag{2.13}$$

$$= \boldsymbol{F}\hat{\boldsymbol{x}}[i] + \boldsymbol{Q}[z]\boldsymbol{e}_y[i] + \boldsymbol{K}[z]\ \boldsymbol{r}[i], \tag{2.14}$$

where $\boldsymbol{K}[z], \boldsymbol{Q}[z] \in \boldsymbol{RH}_\infty$ are free parameters. Therefore, Fig. 2.2 can be transferred to Fig. 2.5 [76]. The details of the derivation are shown in Appendix A. In this chapter, $\boldsymbol{K}[z]$ is a constant matrix $\boldsymbol{K}$.

[4] Strictly speaking, (2.13) should be written as $\boldsymbol{U}[z] = \boldsymbol{C}_1[z]\boldsymbol{R}[z] + \boldsymbol{C}_2[z]\boldsymbol{Y}[z]$. In this thesis, however, signals are simply represented in time domain in the same way as [68].

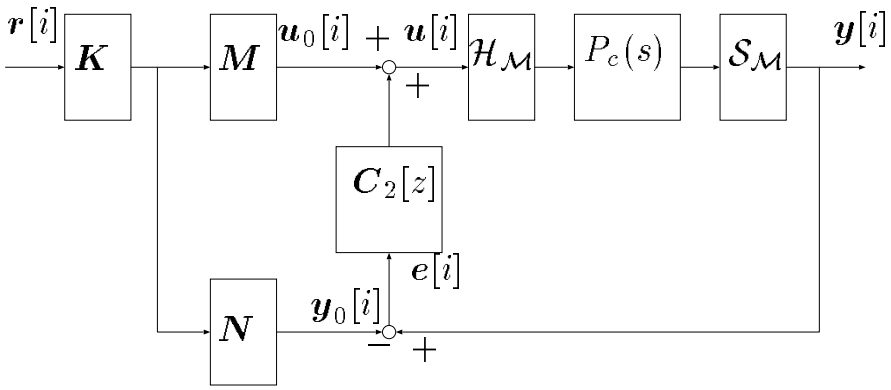

Figure 2.6: Implementation of the proposed controller.

Because the estimation errors of the observer become zero ($\hat{\boldsymbol{x}}[i] = \boldsymbol{x}[i], \boldsymbol{e}_y[i] = \hat{\boldsymbol{y}}[i] - \boldsymbol{y}[i] = 0$) for the nominal plant, the system (2.7) is represented from (2.14) by

$$\boldsymbol{x}[i+1] = (\boldsymbol{A} + \boldsymbol{BF})\boldsymbol{x}[i] + \boldsymbol{BK}\boldsymbol{r}[i]. \tag{2.15}$$

Because nonsingularity of matrix $\boldsymbol{B}$ is assured from theorem 2.1, the parameters $\boldsymbol{F}$ and $\boldsymbol{K}$ can be selected so that the following equations are satisfied.

$$\boldsymbol{A} + \boldsymbol{BF} = \boldsymbol{O}\ , \quad \boldsymbol{BK} = \boldsymbol{I}, \tag{2.16}$$

From (2.16), $\boldsymbol{F}$ and $\boldsymbol{K}$ are given by

$$\boldsymbol{F} = -\boldsymbol{B}^{-1}\boldsymbol{A}\ , \quad \boldsymbol{K} = \boldsymbol{B}^{-1}. \tag{2.17}$$

Therefore, (2.15) is described by

$$\boldsymbol{x}[i+1] = \boldsymbol{r}[i], \tag{2.18}$$

Utilizing the future desired state, let the reference input be

$$\boldsymbol{r}[i] = \boldsymbol{x}_d[i+1], \tag{2.19}$$

where $\boldsymbol{x}_d[i]$ is the desired state. This method of control, where the reference input is generated from the future desired trajectory, is known as preview control. From (2.18) and (2.19), we find that perfect tracking $\boldsymbol{x}[i] = \boldsymbol{x}_d[i]$ is achieved at every sampling point T_r.

Here, Fig. 2.2 can be represented by Fig. 2.6 because (2.13) is rewritten as (2.20) [74]. The derivation is shown in Appendix B. Therefore, the proposed controller is simply implemented by

$$\boldsymbol{u}[i] = (\boldsymbol{M}[z] - \boldsymbol{C}_2[z]\boldsymbol{N}[z])\boldsymbol{K}\boldsymbol{r}[i] + \boldsymbol{C}_2[z]\boldsymbol{y}[i] \tag{2.20}$$

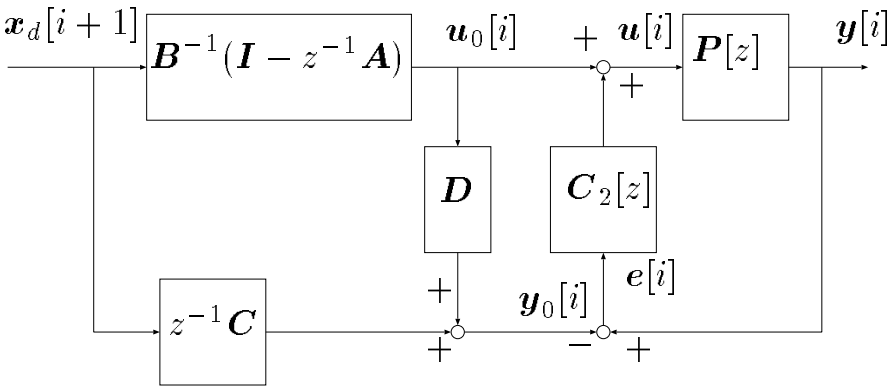

Figure 2.7: Perfect tracking controller by the transfer function approach.

$$\begin{bmatrix} \boldsymbol{M}[z] \\ \boldsymbol{N}[z] \end{bmatrix} = \left[\begin{array}{c|c} \boldsymbol{A}+\boldsymbol{B}\boldsymbol{F} & \boldsymbol{B} \\ \hline \boldsymbol{F} & \boldsymbol{I} \\ \boldsymbol{C}+\boldsymbol{D}\boldsymbol{F} & \boldsymbol{D} \end{array}\right] = \begin{bmatrix} \boldsymbol{I}+z^{-1}\boldsymbol{F}\boldsymbol{B} \\ \boldsymbol{D}+z^{-1}(\boldsymbol{C}+\boldsymbol{D}\boldsymbol{F})\boldsymbol{B} \end{bmatrix}, \tag{2.21}$$

where $\boldsymbol{M}[z]$ and $\boldsymbol{N}[z]$ are parameters of the coprime factorization of the plant $\boldsymbol{P}[z] = \boldsymbol{N}[z]\boldsymbol{M}[z]^{-1}$. The two-degree-of-freedom controller (2.20) should be realized with minimum order. Assuming the initial value of plant is known[5], the initial value of controller (2.20) should be set to be equal to that of the plant $\boldsymbol{x}[0]$.

From (2.16), the proposed controller has a similar structure to that of the robust deadbeat controller [77] because it is composed of the feedforward controller with deadbeat characteristics and a robust feedback controller. However, conventional deadbeat controllers deal with fixed desired trajectories such as step or ramp function and followed them within several sampling time. On the other hand, the proposed method deals with arbitrary desired trajectories and there is no tracking delay. Therefore, in this chapter, novel concepts are introduced such as the preview of the desired trajectory, the sampler of desired trajectory, desired state variable, and multirate feedforward.

2.3.4 Design of the Perfect Tracking Controller $\boldsymbol{C}_1[z]$ – Transfer Function Approach

In this section, the perfect tracking controller is designed using the transfer function approach, which can be understood more intuitively than the state space approach of section 2.3.3.

[5]In trajectory tracking control system, this assumption is generally satisfied because the initial velocity is usually zero. If the initial value of plant $\boldsymbol{x}[0]$ is unknown, it works as an impulse disturbance and the effect is rejected by the robust feedback controller $\boldsymbol{C}_2[z]$.

From (2.7) and (2.8), the transfer function from $\boldsymbol{x}[i+1]$ to $\boldsymbol{u}[i]$ and $\boldsymbol{y}[i]$ is described by

$$\begin{aligned}\boldsymbol{u}[i] &= \boldsymbol{B}^{-1}(\boldsymbol{x}[i+1]-\boldsymbol{A}\boldsymbol{x}[i]) = \boldsymbol{B}^{-1}(\boldsymbol{I}-z^{-1}\boldsymbol{A})\ \boldsymbol{x}[i+1] \\ &= \left[\begin{array}{c|c} \boldsymbol{O} & -\boldsymbol{A} \\ \hline \boldsymbol{B}^{-1} & \boldsymbol{B}^{-1} \end{array}\right] \boldsymbol{x}[i+1] \qquad (2.22) \\ \boldsymbol{y}[i] &= z^{-1}\boldsymbol{C}\ \boldsymbol{x}[i+1]+\boldsymbol{D}\ \boldsymbol{u}[i]. \qquad (2.23)\end{aligned}$$

In (2.22), the nonsingularity of matrix $\boldsymbol{B}$ is assured by theorem 2.1. Because all poles of the transfer function (2.22) are zero, it is found that (2.22) is a stable inverse system. Thus, if the control input is calculated by (2.24) as shown in Fig. 2.7, perfect tracking is guaranteed because (2.24) is an exact inverse plant.

$$\boldsymbol{u}_0[i] = \boldsymbol{B}^{-1}(\boldsymbol{I}-z^{-1}\boldsymbol{A})\ \boldsymbol{x}_d[i+1] \qquad (2.24)$$

The output of the nominal plant model can be calculated by

$$\boldsymbol{y}_0[i] = z^{-1}\boldsymbol{C}\boldsymbol{x}_d[i+1]+\boldsymbol{D}\boldsymbol{u}_0[i]. \qquad (2.25)$$

When the tracking error $\boldsymbol{e}$ is caused by disturbance or modeling error, it can be eliminated using the robust feedback controller $\boldsymbol{C}_2[z]$ by applying (2.26).

$$\boldsymbol{u}[i] = \boldsymbol{u}_0[i]+\boldsymbol{C}_2[z](\boldsymbol{y}[i]-\boldsymbol{y}_0[i]) \qquad (2.26)$$

Next, it is shown that the feedforward controller (2.20) obtained by the state space approach is identical with (2.25) and (2.26), which are designed in this transfer function approach. From (2.17) and (2.21), two feedforward paths $\boldsymbol{M}[z]\boldsymbol{K}$ and $\boldsymbol{N}[z]\boldsymbol{K}$ are represented by

$$\begin{aligned}\boldsymbol{u}_0[i] &= \boldsymbol{M}[z]\boldsymbol{K}\boldsymbol{x}_d[i+1] \\ &= (\boldsymbol{I}+z^{-1}\boldsymbol{F}\boldsymbol{B})\boldsymbol{K}\boldsymbol{x}_d[i+1] \\ &= (\boldsymbol{I}-z^{-1}\boldsymbol{B}^{-1}\boldsymbol{A}\boldsymbol{B})\boldsymbol{B}^{-1}\boldsymbol{x}_d[i+1] \\ &= \boldsymbol{B}^{-1}(\boldsymbol{I}-z^{-1}\boldsymbol{A})\boldsymbol{x}_d[i+1], \qquad (2.27)\end{aligned}$$

$$\begin{aligned}\boldsymbol{y}_0[i] &= \boldsymbol{N}[z]\boldsymbol{K}\boldsymbol{x}_d[i+1] \\ &= (\boldsymbol{D}+z^{-1}(\boldsymbol{C}+\boldsymbol{D}\boldsymbol{F})\boldsymbol{B})\boldsymbol{K}\boldsymbol{x}_d[i+1] \\ &= (\boldsymbol{D}+z^{-1}(\boldsymbol{C}-\boldsymbol{D}\boldsymbol{B}^{-1}\boldsymbol{A})\boldsymbol{B})\boldsymbol{B}^{-1}\boldsymbol{x}_d[i+1] \\ &= z^{-1}\boldsymbol{C}\boldsymbol{x}_d[i+1]+\boldsymbol{D}\boldsymbol{B}^{-1}(\boldsymbol{I}-z^{-1}\boldsymbol{A})\boldsymbol{x}_d[i+1] \\ &= z^{-1}\boldsymbol{C}\boldsymbol{x}_d[i+1]+\boldsymbol{D}\boldsymbol{u}_0[i]. \qquad (2.28)\end{aligned}$$

From the above equations, it is found that the controllers obtained by the two different approaches are equivalent and the structure of the proposed controller is very simple and clear as shown in Fig. 2.7.

2.4 Perfect Tracking Control with Generalized Sampling Periods

In section 2.4, perfect tracking control was proposed for a plant without hardware restrictions on the sampler and holder ($T_y = T_u$) . On the other hand, many industrial systems often have hardware restrictions on both the sampling periods for detecting plant output and the control periods for generating plant input. For example, in head-positioning control of hard disk drives and visual servo systems, the sampling periods of plant output would be long, because the detection period of servo signals and video signals are shorter than the period of control input. In contrast, systems with low-speed D/A converters or CPUs have the restriction that the period of plant input is shorter than the sampling period of plant output.

In this section, perfect tracking control is extended to applications in various systems with the above hardware restrictions, by generalizing the output sampling period. Next, it is shown that the structure of the proposed controller is very simple and clear. Finally, two examples are presented to demonstrate the advantages of this approach through simulations and experiments of position control using a dc servomotor. The first example shows that the proposed multirate feedforward control has better performance than the single-rate controller even in the usual servo system without the special hardware restrictions, in which the sampling period of plant output is equal to the control period of plant input. The second example indicates that the proposed method is applicable to a system with special hardware restrictions, in which the output sampling period is longer than the input period. For this system, the proposed method improves the intersample response.

2.4.1 Generalizations of the Sampling Periods

As mentioned in section 2.3, digital control system generally has three time periods T_r, T_y, and T_u, as shown in Fig. 2.8. Actual control systems usually have restrictions on T_u and/or T_y because the speed of actuators, sensors, CPU calculations, or A/D–D/A converters is limited. In conventional digital control systems, these three periods are made equal to the longer of the two periods T_u and T_y for simplification both of theory and algorithm.

On the other hand, the authors have shown that perfect tracking control can be achieved on every sampling point T_r by setting $T_r = nT_u$, where n is the plant order , as shown in section 2.3 [78]. In the following discussions, $T_r = nT_u$ is regarded as the condition for the perfect tracking control. We should consider the following two cases, which are very common in the industry. In the first case, T_u is decided in advance by the

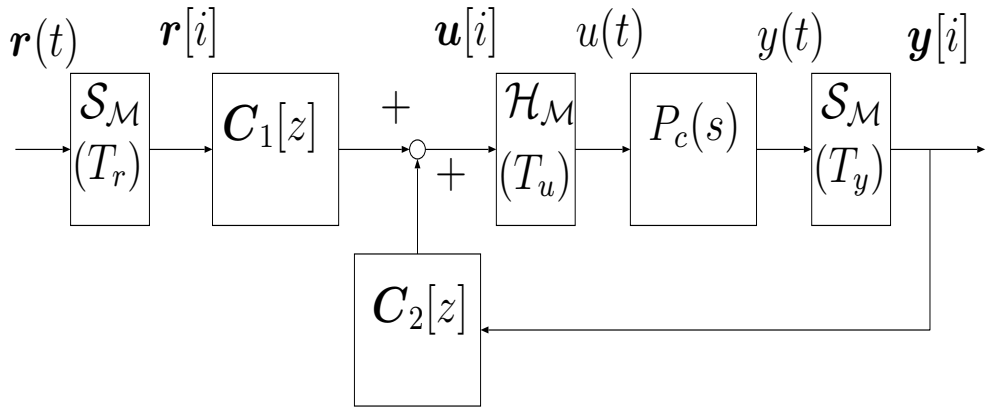

Figure 2.8: Two-degree-of-freedom control system.

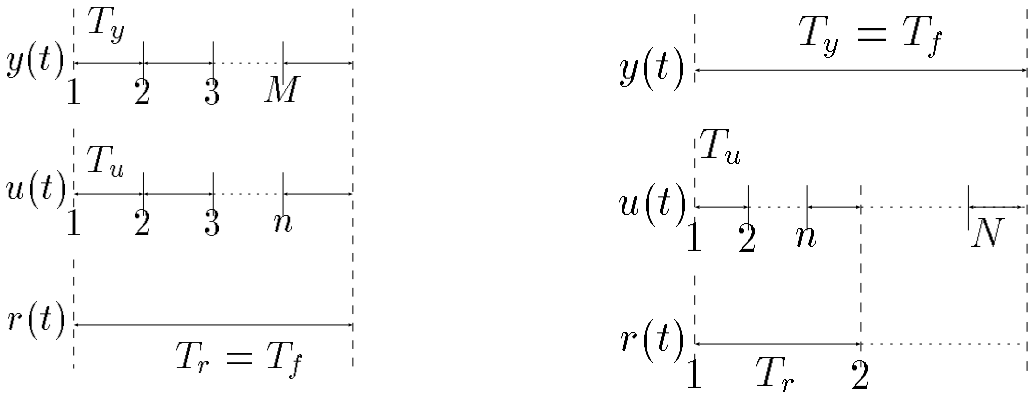

(a) Case 1 ($T_y \leq T_u$)

(b) Case 2 ($T_y > T_u$)

Figure 2.9: Multirate sampling control.

hardware restrictions, however, the plant output can be detected at the same or faster period ($T_y \geq T_u$), as shown in Fig. 2.9(a). This case is referred to as case 1 in this chapter, and includes the usual servo systems of $T_y = T_u$ without special hardware restrictions. In the second case, T_y is decided in advance, however, the plant input can be changed N times during T_y, as shown in Fig. 2.9(b). This case is referred to as case 2, and includes systems with special hardware restrictions such as hard disk drives [79, 80], visual servo systems [81], and servo systems with low precision encoders [59], as mentioned in section 1.1.2. In this case, the perfect tracking control can be assured at L ($\triangleq N/n$) intersample points during T_y.

For the above multiperiod systems, the longer period between T_r and T_y is defined as the frame period T_f [1], and the z-operator is defined as $z \triangleq e^{sT_f}$. By using these definitions, cases 1 and 2 can be dealt with together in the following discussions.

Fig. 2.10 shows the proposed multirate control scheme, in which the plant input is

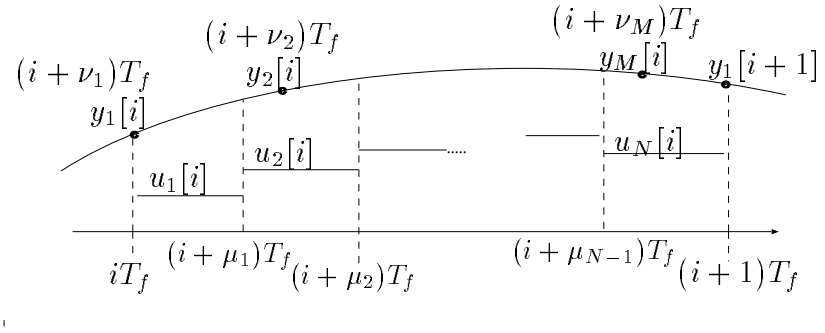

Figure 2.10: Generalized multirate sampling control.

changed N times during one frame period T_f, and the plant output is also detected M times during T_f. The positive integers M and N indicate input and output multiplicities, respectively.

In case 1, the frame period and the input multiplicity are set to $T_f = T_r$ and $N = n$, as shown in Fig. 2.9(a). The output multiplicity M is determined by the hardware restriction.

In case 2, the frame period and the output multiplicity are set to $T_f = T_y$ and $M = 1$, as shown in Fig. 2.9(b). The input multiplicity is decided by the hardware restriction. However, it is necessary that N/n $(= L)$ be an integer in the proposed method.

In Fig. 2.10, $\mu_j (j = 0, 1, \cdots, N)$ and $\nu_k (k = 1, \cdots, M)$ are the parameters for the timing of input change and output detection, which satisfy conditions (2.29) and (2.30).

$$0 = \mu_0 < \mu_1 < \mu_2 < ... < \mu_N = 1 \tag{2.29}$$

$$0 \leq \nu_1 < \nu_2 < ... < \nu_M < 1 \tag{2.30}$$

If T_f is divided into equal intervals as shown in Fig. 2.4, these parameters are set to $\mu_j = j/N$ and $\nu_k = (k-1)/M$.

2.4.2 Designs of the Proposed Controller

In this section, the proposed perfect tracking control method is presented. For simplification, the plant is assumed to be a SISO system. The proposed method, however, will be extended to deal with the MIMO system in section 2.5.2.

Plant Discretization and Parameterization

Consider the continuous-time nth-order plant $P_c(s)$ described by

$$\dot{\boldsymbol{x}}(t) = \boldsymbol{A}_c \boldsymbol{x}(t) + \boldsymbol{b}_c u(t) \ , \quad y(t) = \boldsymbol{c}_c \boldsymbol{x}(t). \tag{2.31}$$

The discrete-time plant $\boldsymbol{P}[z]$ discretized by generalized multirate sampling control (Fig. 2.10) becomes

$$\boldsymbol{x}[i+1] = \boldsymbol{A}\boldsymbol{x}[i] + \boldsymbol{B}\boldsymbol{u}[i] \tag{2.32}$$

$$\boldsymbol{y}[i] = \boldsymbol{C}\boldsymbol{x}[i] + \boldsymbol{D}\boldsymbol{u}[i], \tag{2.33}$$

where $\boldsymbol{x}[i] = \boldsymbol{x}(iT_f)$, and matrices $\boldsymbol{A}, \boldsymbol{B}, \boldsymbol{C}, \boldsymbol{D}$ and vectors $\boldsymbol{u}[i], \boldsymbol{y}[i]$ are given by

$$\left[\begin{array}{c|c} \boldsymbol{A} & \boldsymbol{B} \\ \hline \boldsymbol{C} & \boldsymbol{D} \end{array}\right] \triangleq \left[\begin{array}{c|ccc} e^{\boldsymbol{A}_c T_f} & \boldsymbol{b}_1 & \cdots & \boldsymbol{b}_N \\ \hline \boldsymbol{c}_1 & d_{11} & \cdots & d_{1N} \\ \vdots & \vdots & & \vdots \\ \boldsymbol{c}_M & d_{M1} & \cdots & d_{MN} \end{array}\right] \tag{2.34}$$

$$\boldsymbol{u}[i] \triangleq [u_1[i], \cdots, u_N[i]]^T, \ \boldsymbol{y}[i] \triangleq [y_1[i], \cdots, y_M[i]]^T \tag{2.35}$$

$$\boldsymbol{b}_j \triangleq \int_{(1-\mu_j)T_f}^{(1-\mu_{(j-1)})T_f} e^{\boldsymbol{A}_c \tau} \boldsymbol{b}_c d\tau \ , \ \boldsymbol{c}_k \triangleq \boldsymbol{c}_c e^{\boldsymbol{A}_c \nu_k T_f} \tag{2.36}$$

$$d_{kj} \triangleq \begin{cases} \mu_j < \nu_k : & \boldsymbol{c}_c \int_{(\nu_k - \mu_j)T_f}^{(\nu_k - \mu_{(j-1)})T_f} e^{\boldsymbol{A}_c \tau} \boldsymbol{b}_c d\tau \\ \mu_{(j-1)} < \nu_k \leq \mu_j : & \boldsymbol{c}_c \int_0^{(\nu_k - \mu_{(j-1)})T_f} e^{\boldsymbol{A}_c \tau} \boldsymbol{b}_c d\tau \\ \nu_k \leq \mu_{(j-1)} : & 0 \end{cases} . \tag{2.37}$$

Design of the Feedback Controller $\boldsymbol{C}_2[z]$

Before the perfect tracking controller $\boldsymbol{C}_1[z]$ is designed, the robust feedback controller $\boldsymbol{C}_2[z]$ must be determined in order to make the sensitivity of the closed-loop system sufficiently small.

Because systems with special hardware restrictions are considered in this section, the feedback loop also may become multirate ($T_y < T_u$ or $T_y > T_u$). Multirate feedback controllers with these restrictions are proposed in chapter 3 and [41, 42, 43]. These multirate controllers may improve the feedback characteristics. However, perfect tracking control can be achieved, even if the single-rate feedback controller is simply designed with a longer period between T_y and T_u, and transferred to an M-input N-output controller $\boldsymbol{C}_2[z]$ on T_f. For example, the feedback controller in case 2 ($T_y > T_u$) can be transferred to a 1-input N-output system by

$$\boldsymbol{C}_2[z] = \left[\begin{array}{c|c} \boldsymbol{A}_s & \boldsymbol{b}_s \\ \hline \boldsymbol{c}_s & d_s \\ \vdots & \vdots \\ \boldsymbol{c}_s & d_s \end{array}\right], \tag{2.38}$$

where $\{\boldsymbol{A}_s, \boldsymbol{b}_s, \boldsymbol{c}_s, d_s\}$ is a single-rate controller designed with T_y.

Design of Perfect Tracking Controller $\boldsymbol{C}_1[z]$

In this section, the multirate feedforward controller $\boldsymbol{C}_1[z]$ is designed using the state space approach in the same way as in section 2.3.3. In the proposed method, perfect tracking control can be assured at every sampling point of reference input T_r. For simplification, the parameters of multirate control are assumed to be selected as $\mu_j = j/N, \nu_k = (k-1)/M$. However, this assumption can be removed easily in the same way as in chapter 3.

The system of (2.32) is represented with the frame period T_f, and rewritten with the reference period $T_r = T_f/L$ as [6]

$$\tilde{\boldsymbol{x}}[i+1] = \tilde{\boldsymbol{A}}\boldsymbol{x}[i] + \tilde{\boldsymbol{B}}\boldsymbol{u}[i], \tag{2.39}$$

where $q \triangleq 1/L = n/N$, and where matrices $\tilde{\boldsymbol{A}}, \tilde{\boldsymbol{B}}$ and vectors $\tilde{\boldsymbol{x}}$ are given by

$$\tilde{\boldsymbol{x}}[i+1] \triangleq \begin{bmatrix} \boldsymbol{x}[i+q] \\ \vdots \\ \boldsymbol{x}[i+lq] \\ \vdots \\ \boldsymbol{x}[i+Lq] \end{bmatrix}, \quad \tilde{\boldsymbol{A}} \triangleq \begin{bmatrix} e^{\boldsymbol{A}_c T_r} \\ \vdots \\ e^{\boldsymbol{A}_c l T_r} \\ \vdots \\ e^{\boldsymbol{A}_c L T_r} \end{bmatrix} \tag{2.40}$$

$$\tilde{\boldsymbol{B}} \triangleq \begin{bmatrix} \boldsymbol{B}_L & \boldsymbol{O} & \cdots & \cdots & \cdots & \boldsymbol{O} \\ \vdots & \ddots & & & & \boldsymbol{O} \\ \boldsymbol{B}_{L-l} & \cdots & \boldsymbol{B}_L & \boldsymbol{O} & \cdots & \boldsymbol{O} \\ \vdots & & & \ddots & & \boldsymbol{O} \\ \boldsymbol{B}_1 & \boldsymbol{B}_2 & \cdots & \cdots & \cdots & \boldsymbol{B}_L \end{bmatrix} \tag{2.41}$$

$$\boldsymbol{B}_l = [\boldsymbol{b}_{(l-1)n+1}, \cdots, \boldsymbol{b}_{ln}] \quad (l = 1, \cdots, L). \tag{2.42}$$

As shown in (2.13), the two-degree-of-freedom control law is described by

$$\boldsymbol{u}[i] = \boldsymbol{F}\hat{\boldsymbol{x}}[i] + \boldsymbol{Q}[z]\boldsymbol{e}_y[i] + \boldsymbol{K}\boldsymbol{r}[i]. \tag{2.43}$$

Because the estimation errors of the observer become zero ($\hat{\boldsymbol{x}} = \boldsymbol{x}, \boldsymbol{e}_y = \hat{\boldsymbol{y}} - \boldsymbol{y} = 0$) for the nominal plant, from (2.39) and (2.43), this system is represented by

$$\tilde{\boldsymbol{x}}[i+1] = (\tilde{\boldsymbol{A}} + \tilde{\boldsymbol{B}}\boldsymbol{F})\boldsymbol{x}[i] + \tilde{\boldsymbol{B}}\boldsymbol{K}\boldsymbol{r}[i]. \tag{2.44}$$

And as nonsingularity of matrix $\boldsymbol{B}_l$ can be assured by theorem 2.1, $\tilde{\boldsymbol{B}}$ of (2.41) also becomes nonsingular. Therefore, the parameters $\boldsymbol{F}$ and $\boldsymbol{K}$ can be selected such that the following equations are satisfied.

$$\tilde{\boldsymbol{A}} + \tilde{\boldsymbol{B}}\boldsymbol{F} = \boldsymbol{O}\ , \quad \tilde{\boldsymbol{B}}\boldsymbol{K} = \boldsymbol{I}, \tag{2.45}$$

[6] In case 1, (2.39) is equal to (2.32) ($\boldsymbol{x}[i+1] = \boldsymbol{A}\boldsymbol{x}[i] + \boldsymbol{B}\boldsymbol{u}[i]$) because $L = 1$.

From (2.45), $\boldsymbol{F}$ and $\boldsymbol{K}$ are given by

$$\boldsymbol{F} = -\tilde{\boldsymbol{B}}^{-1}\tilde{\boldsymbol{A}}\ , \quad \boldsymbol{K} = \tilde{\boldsymbol{B}}^{-1}. \tag{2.46}$$

Therefore, (2.44) is described by

$$\tilde{\boldsymbol{x}}[i+1] = \boldsymbol{r}[i], \tag{2.47}$$

Utilizing the future desired state, let the reference input be

$$\boldsymbol{r}[i] = \tilde{\boldsymbol{x}}_d[i+1] = \begin{bmatrix} \boldsymbol{x}_d[i+q] \\ \vdots \\ \boldsymbol{x}_d[i+Lq] \end{bmatrix}, \tag{2.48}$$

where $\tilde{\boldsymbol{x}}_d[i]$ is the desired state. From (2.47) and (2.48), we find that perfect tracking $\tilde{\boldsymbol{x}}[i] = \tilde{\boldsymbol{x}}_d[i]$ is achieved at every sampling point T_r. Using (2.46), the proposed controller can be implemented by (2.20), as shown in Fig. 2.6.

Structure of Perfect Tracking Controller $\boldsymbol{C}_1[z]$

In this section, it is shown that the structure of the perfect tracking controller is very simple and clear. For system without hardware restrictions, that was shown in section 2.3.4. In this section, the results of section 2.3.4 are extended to system with hardware restrictions ($T_y \neq T_u$). From (2.46) and (2.21), the two elements $\boldsymbol{M}[z]\boldsymbol{K}$ and $\boldsymbol{N}[z]\boldsymbol{K}$ in Fig. 2.6 are represented by

$$\boldsymbol{M}[z]\boldsymbol{K} = (\boldsymbol{I} - z^{-1}\tilde{\boldsymbol{B}}^{-1}\tilde{\boldsymbol{A}}\boldsymbol{B})\tilde{\boldsymbol{B}}^{-1}, \tag{2.49}$$

$$\boldsymbol{N}[z]\boldsymbol{K} = z^{-1}\boldsymbol{C}\boldsymbol{B}\tilde{\boldsymbol{B}}^{-1} + \boldsymbol{D}(\boldsymbol{I} - z^{-1}\tilde{\boldsymbol{B}}^{-1}\tilde{\boldsymbol{A}}\boldsymbol{B})\tilde{\boldsymbol{B}}^{-1}. \tag{2.50}$$

On the other hand, from (2.32) and (2.39), the transfer function from $\boldsymbol{u}[i]$ to $\tilde{\boldsymbol{x}}[i+1]$ is described by

$$\tilde{\boldsymbol{x}}[i+1] = \left[\begin{array}{c|c} \boldsymbol{A} & \boldsymbol{B} \\ \hline \tilde{\boldsymbol{A}} & \tilde{\boldsymbol{B}} \end{array}\right] \boldsymbol{u}[i]. \tag{2.51}$$

The inverse system of (2.51) is given by

$$\boldsymbol{u}[i] = \left[\begin{array}{c|c} \boldsymbol{A} - \boldsymbol{B}\tilde{\boldsymbol{B}}^{-1}\tilde{\boldsymbol{A}} & \boldsymbol{B}\tilde{\boldsymbol{B}}^{-1} \\ \hline -\tilde{\boldsymbol{B}}^{-1}\tilde{\boldsymbol{A}} & \tilde{\boldsymbol{B}}^{-1} \end{array}\right] \tilde{\boldsymbol{x}}[i+1]. \tag{2.52}$$

Based on the definitions of $\tilde{\boldsymbol{A}}$ and $\tilde{\boldsymbol{B}}$ in (2.40) and (2.41), the following equations are obtained.

$$\boldsymbol{A} = [\overbrace{\boldsymbol{O}, \cdots, \boldsymbol{O}}^{L-1}, \boldsymbol{I}]\tilde{\boldsymbol{A}}, \tag{2.53}$$

$$\boldsymbol{B} = [\boldsymbol{O}, \cdots, \boldsymbol{O}, \boldsymbol{I}]\tilde{\boldsymbol{B}} \tag{2.54}$$

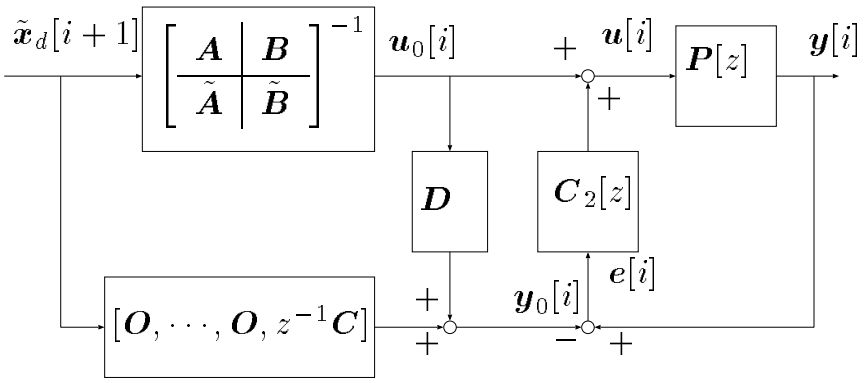

Figure 2.11: Structure of the proposed controller.

Thus, the $(1,1)$ element of matrix (2.52) becomes

$$\boldsymbol{A} - \boldsymbol{B}\tilde{\boldsymbol{B}}^{-1}\tilde{\boldsymbol{A}} = \boldsymbol{A} - [\boldsymbol{O}, \cdots, \boldsymbol{O}, \boldsymbol{I}]\tilde{\boldsymbol{A}} = \boldsymbol{O}. \tag{2.55}$$

Therefore, (2.52) is given by [7]

$$\boldsymbol{u}[i] = \left[\begin{array}{c|c} \boldsymbol{O} & \boldsymbol{B}\tilde{\boldsymbol{B}}^{-1} \\ \hline -\tilde{\boldsymbol{B}}^{-1}\tilde{\boldsymbol{A}} & \tilde{\boldsymbol{B}}^{-1} \end{array}\right] \tilde{\boldsymbol{x}}[i+1]. \tag{2.56}$$

Based on (2.49) and (2.56), it is found that $\boldsymbol{M}[z]\boldsymbol{K}$ is equal to the transfer function from $\tilde{\boldsymbol{x}}[i+1]$ to $\boldsymbol{u}[i]$, which represents the stable inverse system. This point is one of the advantages of multirate control because the inverse system becomes unstable in single-rate systems. Moreover, (2.33) is described using (2.56) as [8]

$$\begin{aligned} \boldsymbol{y}[i] &= z^{-1}\boldsymbol{C}\boldsymbol{x}[i+1] + \boldsymbol{D}\boldsymbol{u}[i] \\ &= z^{-1}\boldsymbol{C}[\boldsymbol{O}, \cdots, \boldsymbol{O}, \boldsymbol{I}]\tilde{\boldsymbol{x}}[i+1] \\ &\quad + \boldsymbol{D}(\boldsymbol{I} - z^{-1}\tilde{\boldsymbol{B}}^{-1}\tilde{\boldsymbol{A}}\boldsymbol{B})\tilde{\boldsymbol{B}}^{-1}\tilde{\boldsymbol{x}}[i+1]. \end{aligned} \tag{2.57}$$

Based on (2.50) and (2.57), it is shown that $\boldsymbol{N}[z]\boldsymbol{K}$ represents the transfer function from $\tilde{\boldsymbol{x}}[i+1]$ to $\boldsymbol{y}[i]$.

The structure of the proposed controller is shown in Fig. 2.11. The plant $\boldsymbol{P}[z]$ is driven by the stable inverse system, in the same way as the case without hardware restriction. When the tracking error $\boldsymbol{e}$ is generated by disturbance or modeling error, the robust feedback controller $\boldsymbol{C}_2[z]$ acts to eliminate $\boldsymbol{e}$.

[7] In case 1, (2.56) becomes $\boldsymbol{u}[i] = \boldsymbol{B}^{-1}(\boldsymbol{I} - z^{-1}\boldsymbol{A})\ \boldsymbol{x}[i+1]$, which is obtained directly from $\boldsymbol{x}[i+1] = \boldsymbol{A}\boldsymbol{x}[i] + \boldsymbol{B}\boldsymbol{u}[i]$ of (2.32), because $\tilde{\boldsymbol{B}} = \boldsymbol{B}$.

[8] In case 1, (2.57) becomes $\boldsymbol{y}[i] = z^{-1}\boldsymbol{C}\boldsymbol{x}[i+1]$, because $\boldsymbol{D} = \boldsymbol{O}$.

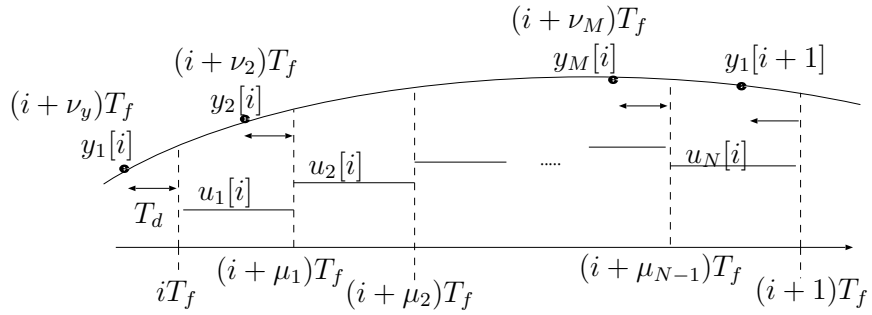

Figure 2.12: Generalized multirate sampling control with time delay.

2.5 Extension to Time Delay and Multivariable System

2.5.1 Extension to System with Time Delay

In this section, the proposed perfect tracking control is extended to plants with time delay. As shown in Fig. 2.12, the time delay can be considered to exist on the plant output. The continuous-time plant with time delay T_d is described by

$$\dot{\boldsymbol{x}}(t) = \boldsymbol{A}_c\boldsymbol{x}(t) + \boldsymbol{b}_c u(t) \tag{2.58}$$

$$y(t) = \boldsymbol{c}_c\boldsymbol{x}(t - T_d). \tag{2.59}$$

The time delay can also be considered to exist on the plant input, and expressed by [82]

$$\dot{\boldsymbol{x}}(t) = \boldsymbol{A}_c\boldsymbol{x}(t) + \boldsymbol{b}_c u(t - T_d) \tag{2.60}$$

$$y(t) = \boldsymbol{c}_c\boldsymbol{x}(t). \tag{2.61}$$

This section adopts (2.59) because it can make this extension more simple theoretically. Moreover, the time delay is assumed to be $T_d \leq T_f$ for simplification. The proposed methods, however, can be extended to the time delay of $T_d > T_f$ by the same way as [82].

Consider the discrete-time plant discretized by the multirate sampling control with time delay. Because (2.58) is not related to the time delay, the discrete-time state equation becomes

$$\boldsymbol{x}[i+1] = \boldsymbol{A}\boldsymbol{x}[i] + \boldsymbol{B}\boldsymbol{u}[i], \tag{2.62}$$

where $\boldsymbol{A}$ and $\boldsymbol{B}$ are given by (2.34). From (2.39), the intersample plant state can be represented by

$$\tilde{\boldsymbol{x}}[i+1] = \tilde{\boldsymbol{A}}\boldsymbol{x}[i] + \tilde{\boldsymbol{B}}\boldsymbol{u}[i]. \tag{2.63}$$

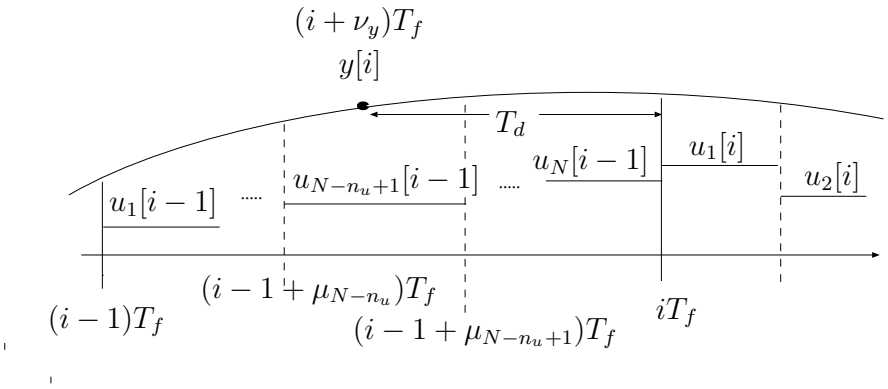

Figure 2.13: Time chart of the time delay.

Considering the output equation, some output ($y_1[i]$ in case of Fig. 2.12) is detected at the time before $t = iT_f$, and the other output ($y_2[i], \cdots y_M[i]$) is detected from $t = iT_f$ to $t = (i+1)T_f$. The latter output can be easily calculated from (2.33) by selecting the parameters ν_k appropriately.

On the other hand, the former output depends on the previous control input $\boldsymbol{u}[i-1]$, as shown in Fig. 2.13. Thus, the output is given by

$$y[i] = \boldsymbol{c}\boldsymbol{x}[i] + \boldsymbol{g}\boldsymbol{u}[i-1], \tag{2.64}$$

$$\boldsymbol{c} \triangleq \boldsymbol{c}_c e^{\boldsymbol{A}_c \nu_y T_f}, \boldsymbol{g} \triangleq [g_1, \cdots, g_N], \nu_y \triangleq -\frac{T_d}{T_f} \tag{2.65}$$

$$g_j \triangleq \begin{cases} \nu_y \le -1 + \mu_{(j-1)} & : \; -\boldsymbol{c}_c e^{\boldsymbol{A}_c \nu_y T_f} \int_{(1-\mu_j)T_f}^{(1-\mu_{(j-1)})T_f} e^{\boldsymbol{A}_c \tau} \boldsymbol{b}_c d\tau \\ -1 + \mu_{(j-1)} \le \nu_y < -1 + \mu_j & : \; -\boldsymbol{c}_c e^{\boldsymbol{A}_c \nu_y T_f} \int_{(1-\mu_j)T_f}^{-\nu_y T_f} e^{\boldsymbol{A}_c \tau} \boldsymbol{b}_c d\tau \\ -1 + \mu_j \le \nu_y < 0 & : \; 0 \end{cases}, \tag{2.66}$$

where n_u is the number of the of $\boldsymbol{u}[i-1]$ elements during T_d as shown in Fig. 2.13.

Collecting all output, the multirate output vector $\boldsymbol{y}[i] = [y_1[i], \cdots, y_M[i]]^T$ can be represented by

$$\boldsymbol{y}[i] = \boldsymbol{C}_\delta \boldsymbol{x}[i] + \boldsymbol{D}_\delta \boldsymbol{u}[i] + \boldsymbol{G}_\delta \boldsymbol{u}[i-1], \tag{2.67}$$

where $\boldsymbol{C}_\delta, \boldsymbol{D}_\delta$ and $\boldsymbol{G}_\delta$ are calculated by (2.36), (2.37), and (2.64).

Therefore, by the same discussion as section 2.3.4 and 2.4.2, the perfect tracking controller can be designed by

$$\boldsymbol{u}[i] = \boldsymbol{u}_0[i] + \boldsymbol{C}_2[z](\boldsymbol{y}[i] - \boldsymbol{y}_0[i]), \tag{2.68}$$

where $\boldsymbol{u}_0[i]$ and $\boldsymbol{y}_0[i]$ are obtained by

$$\boldsymbol{u}_0[i] \;=\; \left[\begin{array}{c|c} \boldsymbol{A} & \boldsymbol{B} \\ \hline \tilde{\boldsymbol{A}} & \tilde{\boldsymbol{B}} \end{array}\right]^{-1} \tilde{\boldsymbol{x}}_d[i+1], \tag{2.69}$$

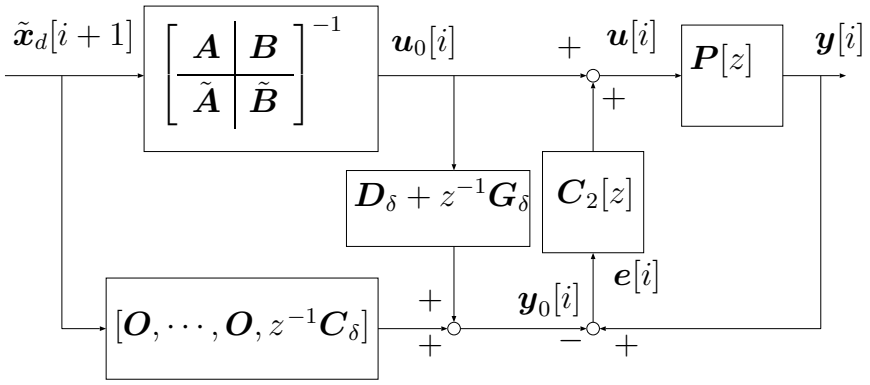

Figure 2.14: Perfect tracking controller with time delay.

$$\boldsymbol{y}_0[i] = z^{-1}\boldsymbol{C}_\delta \boldsymbol{x}_d[i+1] + (\boldsymbol{D}_\delta + z^{-1}\boldsymbol{G}_\delta)\boldsymbol{u}_0[i] \tag{2.70}$$

$$= [\boldsymbol{O}, \cdots, \boldsymbol{O}, z^{-1}\boldsymbol{C}_\delta]\tilde{\boldsymbol{x}}_d[i+1] + (\boldsymbol{D}_\delta + z^{-1}\boldsymbol{G}_\delta)\boldsymbol{u}_0[i]. \tag{2.71}$$

The block diagram of this controller is shown in Fig. 2.14.

2.5.2 Extension to Multivariable System

In the above discussion, the plant was assumed to be a single-input single-output (SISO) system. In this section, the proposed perfect tracking control method is extended to multi-input multi-output (MIMO) systems.

Consider the continuous-time plant described by

$$\dot{\boldsymbol{x}}(t) = \boldsymbol{A}_c\boldsymbol{x}(t) + \boldsymbol{B}_c\boldsymbol{u}(t) \tag{2.72}$$

$$\boldsymbol{y}(t) = \boldsymbol{C}_c\boldsymbol{x}(t), \tag{2.73}$$

$$\boldsymbol{B}_c = [\boldsymbol{b}_{c1}, \cdots, \boldsymbol{b}_{cm}], \boldsymbol{C}_c = \begin{bmatrix} \boldsymbol{c}_{c1} \\ \vdots \\ \boldsymbol{c}_{cp} \end{bmatrix} \tag{2.74}$$

where the plant state $\boldsymbol{x} \in \boldsymbol{R}^n$, the plant input $\boldsymbol{u} \in \boldsymbol{R}^m$, and the plant output $\boldsymbol{y} \in \boldsymbol{R}^p$.

For this plant, multirate input and multirate output controls are employed. In these schemes, the lth ($l = 1, 2, \cdots, m$) plant input is changed N_l times during one frame period T_f, as shown in Fig. 2.15. On the other hand, the qth ($q = 1, 2, \cdots, p$) plant output is detected M_q times during one frame period, as shown in Fig. 2.16. The discrete-time transfer function from the lth input to the $q$the output is given by

$$\boldsymbol{y}_q[i] = \left[\begin{array}{c|c} \boldsymbol{A} & \boldsymbol{B}_l \\ \hline \boldsymbol{C}_q & \boldsymbol{D}_{ql} \end{array}\right] \boldsymbol{u}_l[i] \tag{2.75}$$

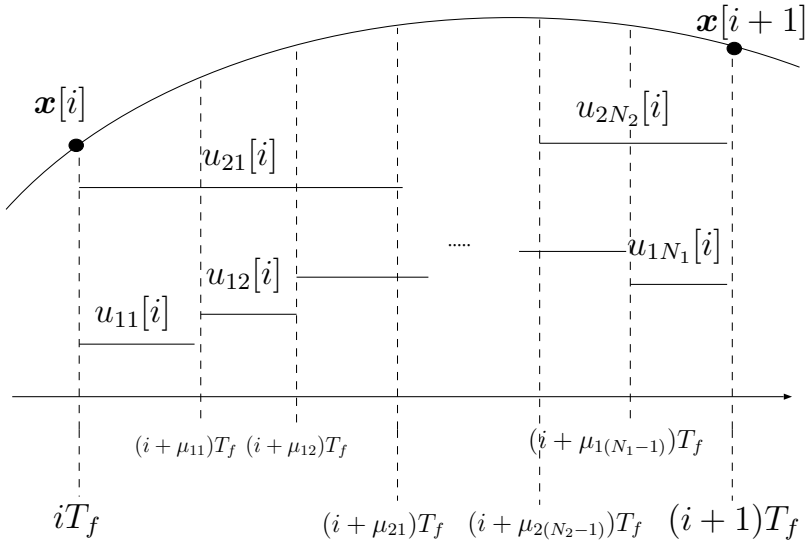

Figure 2.15: Multirate input control.

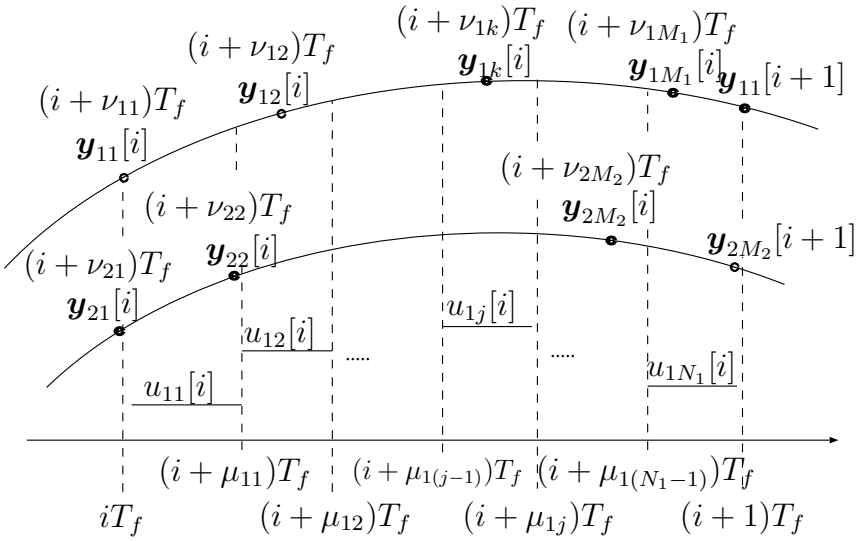

Figure 2.16: Multirate output control.

$$\boldsymbol{y}_q[i] \triangleq [y_{q1}[i], \cdots, y_{qM_q}[i]]^T, \quad \boldsymbol{u}_l[i] \triangleq [u_{l1}[i], \cdots, u_{lN_l}[i]]^T, \tag{2.76}$$

The coefficient matrices of (2.75) are obtained from (2.34) by substituting $\boldsymbol{b}_{cl}$ and $\boldsymbol{c}_{cq}$ for $\boldsymbol{b}_c$ and $\boldsymbol{c}_c$, respectively.

From (2.75), the multivariable multirate system is formulated by

$$\boldsymbol{x}[i+1] = \boldsymbol{A}\boldsymbol{x}[i] + \boldsymbol{B}\boldsymbol{u}[i] \tag{2.77}$$

$$\boldsymbol{y}[i] = \boldsymbol{C}\boldsymbol{x}[i] + \boldsymbol{D}\boldsymbol{u}[i], \tag{2.78}$$

where $\boldsymbol{x}[i] = \boldsymbol{x}(iT_f)$, and input and output vectors $\boldsymbol{u}[i], \boldsymbol{y}[i]$ are defined as

$$\boldsymbol{u}[i] \triangleq [\boldsymbol{u}_1[i], \cdots, \boldsymbol{u}_m[i]]^T = [u_{11}[i], \cdots, u_{1N_1}[i], u_{21}[i], \cdots, u_{mN_m}[i]]^T, \tag{2.79}$$

$$\boldsymbol{y}[i] \triangleq [\boldsymbol{y}_1[i], \cdots, \boldsymbol{y}_p[i]]^T = [y_{11}[i], \cdots, y_{1M_1}[i], y_{21}[i], \cdots, y_{pM_p}[i]]^T, \tag{2.80}$$

and matrices $\boldsymbol{A}, \boldsymbol{B}, \boldsymbol{C}$, and $\boldsymbol{D}$ are given by

$$\left[\begin{array}{c|c} \boldsymbol{A} & \boldsymbol{B} \\ \hline \boldsymbol{C} & \boldsymbol{D} \end{array}\right] \triangleq \left[\begin{array}{c|ccc} e^{\boldsymbol{A}_c T_f} & \boldsymbol{B}_1 & \cdots & \boldsymbol{B}_m \\ \hline \boldsymbol{C}_1 & \boldsymbol{D}_{11} & \cdots & \boldsymbol{D}_{1m} \\ \vdots & \vdots & & \vdots \\ \boldsymbol{C}_p & \boldsymbol{D}_{p1} & \cdots & \boldsymbol{D}_{pm} \end{array}\right]. \tag{2.81}$$

Because discrete-time representation is obtained, the perfect tracking controller can be designed in the same way as section 2.3. The conditions for perfect tracking are given by

$$\boldsymbol{A} + \boldsymbol{B}\boldsymbol{F} = \boldsymbol{O}\ , \quad \boldsymbol{B}\boldsymbol{K} = \boldsymbol{I}, \tag{2.82}$$

as in (2.16). Thus, the input multiplicities N_l $(l = 1, 2, .., m_p)$ should be selected such that the matrix $\boldsymbol{B}$ can have full row rank. The output multiplicities M_q $(q = 1, 2, \cdots, p)$ are determined by the hardware restriction.

The selections of the N_l are made by the following condition.

$$N_l \geq \sigma_l \tag{2.83}$$

where $(\sigma_1, ..., \sigma_m)$ is a set of generalized controllability indices of $(\boldsymbol{A}_c, \boldsymbol{B}_c)$ which are introduced by author [72, 83, 84], and which are defined as follows.

Definition 2.1 *Generalized controllability indices of* $(\boldsymbol{A}_c, \boldsymbol{B}_c)$ *are defined as follows for* $\boldsymbol{A}_c \in \boldsymbol{R}^{n\times n}$ *and* $\boldsymbol{B}_c \in \boldsymbol{R}^{n\times m}$. *If* $(\boldsymbol{A}_c, \boldsymbol{B}_c)$ *is a controllable pair, n linearly independent vectors can be selected from*

$$\{\boldsymbol{b}_{c1}, .., \boldsymbol{b}_{cm}, \boldsymbol{A}_c\boldsymbol{b}_{c1}, .., \boldsymbol{A}_c\boldsymbol{b}_{cm}, .., \boldsymbol{A}_c^{n-1}\boldsymbol{b}_{cm}\}$$

where $\boldsymbol{B}_c = [\boldsymbol{b}_{c1}, .., \boldsymbol{b}_{cm}]$. *Letting* φ *be a set of these n vectors,* σ_l *are defined by*

$$\sigma_l = number\{k | \boldsymbol{A}_c^{k-1}\boldsymbol{b}_{cl} \in \varphi\} \tag{2.84}$$

$$\sum_{l=1}^{m} \sigma_l = n. \tag{2.85}$$

In case of the single input plant ($m = 1$), this index is simply the same number as the plant order ($\sigma_1 = n$). The above definition includes that of Kronecker invariants or controllability indices defined in [6].

Concerning the matrix $\boldsymbol{B}$, the next theorem is proved by the author in [72] for the generalized controllability index. In the case of the controllability index, it is also proved in [6].

Theorem 2.3 *Let $(\boldsymbol{A}_c, \boldsymbol{B}_c)$ be a controllable pair. If the input multiplicities satisfy $N_l \geq \sigma_l$ for $(l = 1, 2, .., m)$, for almost all $\mu_{lj}(l = 1, 2, .., m, j = 1, .., N_l - 1)$ and almost all T, the matrix $\boldsymbol{B}$ has full row rank, i.e.*

$$rank\boldsymbol{B} = n. \tag{2.86}$$

Because the full rank of the matrix $\boldsymbol{B}$ is guaranteed by this theorem, the solution of (2.82) is exactly obtained by

$$\boldsymbol{F} = -\boldsymbol{B}^{-}\boldsymbol{A}\ , \quad \boldsymbol{K} = \boldsymbol{B}^{-}, \tag{2.87}$$

where $\boldsymbol{B}^{-}$ is generalized inverse of matrix $\boldsymbol{B}$ [85][9]. By using these parameters $\boldsymbol{F}$ and $\boldsymbol{K}$, the perfect tracking controller is given by (2.20), as shown in Fig. 2.6.

2.6 Summary

A novel perfect tracking control method using multirate feedforward control was proposed. The proposed method was extended to various systems with hardware restrictions on both the sampling and control periods. Moreover, it was shown that the structure of the proposed perfect tracking controller is very simple and clear. Next, the proposed method was extended to systems with time delay and multivariable systems.

The advantage of this method is that the feedforward controller could be designed without considering the unstable zero problem. Moreover, by combining the proposed feedforward controller with a robust feedback controller, high robust tracking performance is obtained.

[9] If the input multiplicities are selected to minimum number ($N_l = \sigma_l$), the matrix $\boldsymbol{B}$ becomes square and $\boldsymbol{B}^{-} = \boldsymbol{B}^{-1}$

Chapter 3

Perfect Disturbance Rejection Control Based on Multirate Feedback Control

3.1 Abstract

In this chapter, novel multirate feedback controllers are proposed for digital control systems, where the speed of the A/D converters is restricted to be slower than that of the D/A converters. The proposed feedback controller assures perfect disturbance rejection (PDR) at M intersample points in the steady state. Next, the proposed method is extended to systems with time delay. Moreover, the intersample observer is developed in order to reduce the phase delay caused by zero-order hold and to increase the stability margin by estimation and compensation of the intersample response.

In section 3.4, the PDR is applied to the periodic disturbance rejection problem. The novel scheme of repetitive control is proposed based on the open-loop estimation and switching function, which enables the rejection of periodical disturbance without any sacrifice of the closed-loop characteristics. Finally, the intersample disturbance rejection performance is optimized using the fast sampling approach.

The proposed controllers are applied to the track-following modes of hard disk drives and the visual servo system of robot manipulators in chapter 6.

3.2 Introduction

In chapter 2, a novel multirate feedforward controller has been proposed. Next, in this chapter, a multirate feedback controller will be considered. Historically, many multirate

feedback control theories have been developed as reviewed in chapter 1. These theoretical approaches have reached the negative result that feedback characteristics such as disturbance rejection performance and stability robustness are never improved by the multirate control [12, 23].

However, this theoretical result is limited to the case where there is no hardware restriction on the sampling scheme ($T_y = T_u$). On the other hand, many industrial systems have hardware restrictions in their sampling mechanisms. Thus, in this chapter, digital control systems where the sampling periods of plant output are longer than the control periods ($T_u < T_y$) are considered. For these systems, novel multirate feedback controllers are proposed which improve disturbance rejection performance and stability margin.

The restriction of $T_u < T_y$ may be general because D/A converters are usually faster than the A/D converters. In particular, head-positioning systems of the hard disk drive (HDD) and visual servo systems of robot manipulators belong to this category, because the sampling rates of the measurement are relatively slow, as mentioned in section 1.1.2.

The structure of this chapter is as follows. In section 3.3, a novel multirate feedback controller is proposed, which achieves perfect disturbance rejection (PDR) at M intersample points. Next, an intersample observer is designed, which enables estimation of intersample plant state and increases stability margin. In the repetitive control system [86, 87], conventional single-rate controllers do not have sufficient intersample performance to reject disturbance in the semi-Nyquist frequency region [88]. In section 3.4, the proposed perfect disturbance rejection controller is modified for repetitive control, and applied to reject high order repeatable runout of hard disk drives.

Repetitive feedback controllers based on the internal model principle have the disadvantages that closed-loop characteristics worsen and it becomes difficult to assure stability robustness [88]. Therefore, in section 3.4.2, a novel control scheme that never has these problems is proposed based on open-loop estimation with switching function and disturbance rejection by feedforward approach.

3.3 Perfect Disturbance Rejection Control and Intersample Observer

3.3.1 Plant Discretization by Multirate Sampling

For the restriction of $T_u < T_y$, the frame period T_f is defined as $T_f = T_y$, and the dynamics of the controller is described by T_f. For simplification, the continuous-time

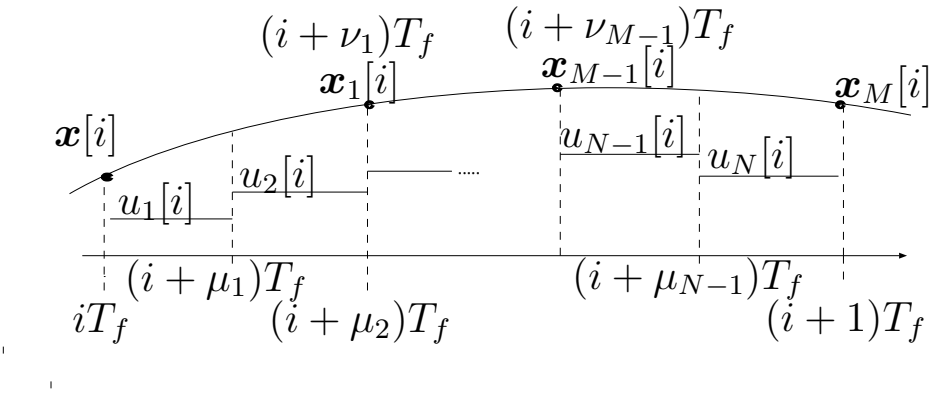

Figure 3.1: Multirate sampling control.

plant is assumed to be a SISO system in this chapter. The proposed methods, however, can be extended to deal with the MIMO system in the same way as section 2.5.2.

In the proposed multirate scheme considered in this chapter, the plant input is changed N times during T_f and the plant state is evaluated M times in this interval, as shown in Fig. 3.1. The positive integers M and N are referred to as input and state multiplicities, respectively. N is determined by the hardware restriction. In this section, the state multiplicity is defined as $M = N/n$, where n is the plant order.

In Fig. 3.1, $\mu_j (j = 0, 1, \cdots, N)$ and $\nu_k (k = 1, \cdots, M)$ are parameters for the timing of input changing and state evaluation, which satisfy the conditions (3.1) and (3.2).

$$0 = \mu_0 < \mu_1 < \mu_2 < ... < \mu_N = 1 \tag{3.1}$$

$$0 < \nu_1 < \nu_2 < ... < \nu_M = 1 \tag{3.2}$$

If T_y is divided at equal intervals, the parameters are set to $\mu_j = j/N$ and $\nu_k = k/M$.

Consider the continuous-time plant described by

$$\dot{\boldsymbol{x}}(t) = \boldsymbol{A}_c \boldsymbol{x}(t) + \boldsymbol{b}_c u(t) \ , \quad y(t) = \boldsymbol{c}_c \boldsymbol{x}(t). \tag{3.3}$$

The discrete-time plant discretized by the multirate sampling control of Fig. 3.1 becomes

$$\boldsymbol{x}[i+1] = \boldsymbol{A}\boldsymbol{x}[i] + \boldsymbol{B}\boldsymbol{u}[i] \ , \quad y[i] = \boldsymbol{C}\boldsymbol{x}[i], \tag{3.4}$$

where $\boldsymbol{x}[i] = \boldsymbol{x}(iT)$, and where matrices $\boldsymbol{A}, \boldsymbol{B}, \boldsymbol{C}$, and vector $\boldsymbol{u}[i]$ are given by

$$\left[\begin{array}{c|c} \boldsymbol{A} & \boldsymbol{B} \\ \hline \boldsymbol{C} & \boldsymbol{O} \end{array}\right] \triangleq \left[\begin{array}{c|ccc} e^{\boldsymbol{A}_c T_f} & \boldsymbol{b}_1 & \cdots & \boldsymbol{b}_N \\ \hline \boldsymbol{c}_c & 0 & \cdots & 0 \end{array}\right], \tag{3.5}$$

$$\boldsymbol{b}_j \triangleq \int_{(1-\mu_j)T_f}^{(1-\mu_{(j-1)})T_f} e^{\boldsymbol{A}_c \tau} \boldsymbol{b}_c d\tau \ , \ \boldsymbol{u}[i] \triangleq [u_1[i], \cdots, u_N[i]]^T. \tag{3.6}$$

The intersample plant state at $t = (i + \nu_k)T_f$ is represented by

$$\tilde{\boldsymbol{x}}[i] = \tilde{\boldsymbol{A}}\boldsymbol{x}[i] + \tilde{\boldsymbol{B}}\boldsymbol{u}[i], \tag{3.7}$$

where $\tilde{\boldsymbol{x}}[i]$ is a vector composed of the intersample plant state $\boldsymbol{x}_k[i] \triangleq \boldsymbol{x}((i + \nu_k)T_f)$ of Fig. 3.1.

$$\begin{aligned} \tilde{\boldsymbol{x}}[i] &\triangleq [\boldsymbol{x}_1^T[i], \boldsymbol{x}_2^T[i], \cdots, \boldsymbol{x}_M^T[i]]^T \\ &= [\boldsymbol{x}_1^T((i+\nu_1)T_f), \boldsymbol{x}_2^T((i+\nu_2)T_f), \cdots, \boldsymbol{x}_M^T((i+1)T_f)]^T \end{aligned} \tag{3.8}$$

The coefficient matrices of (3.7) are given by

$$\left[\begin{array}{c|ccc} \tilde{\boldsymbol{A}} & \tilde{\boldsymbol{B}} & & \end{array}\right] \triangleq \left[\begin{array}{c|ccc} \tilde{\boldsymbol{A}}_1 & \tilde{\boldsymbol{b}}_{11} & \cdots & \tilde{\boldsymbol{b}}_{1N} \\ \vdots & \vdots & & \vdots \\ \tilde{\boldsymbol{A}}_M & \tilde{\boldsymbol{b}}_{M1} & \cdots & \tilde{\boldsymbol{b}}_{MN} \end{array}\right], \tag{3.9}$$

$$\tilde{\boldsymbol{A}}_k \triangleq e^{\boldsymbol{A}_c \nu_k T_f},\ \tilde{\boldsymbol{b}}_{kj} \triangleq \begin{cases} \mu_j < \nu_k : & \int_{(\nu_k - \mu_j)T_f}^{(\nu_k - \mu_{(j-1)})T_f} e^{\boldsymbol{A}_c \tau}\boldsymbol{b}_c d\tau \\ \mu_{(j-1)} < \nu_k \le \mu_j : & \int_0^{(\nu_k - \mu_{(j-1)})T_f} e^{\boldsymbol{A}_c \tau}\boldsymbol{b}_c d\tau \\ \nu_k \le \mu_{(j-1)} : & 0 \end{cases}.$$

3.3.2 Design of Perfect Disturbance Rejection Controller

In this section, a new multirate feedback controller is proposed based on the state-space design method of the disturbance observer.

Consider the continuous-time plant model described by

$$\dot{\boldsymbol{x}}_p(t) = \boldsymbol{A}_{cp}\boldsymbol{x}_p(t) + \boldsymbol{b}_{cp}(u(t) - d(t)) \tag{3.10}$$

$$y(t) = \boldsymbol{c}_{cp}\boldsymbol{x}_p(t), \tag{3.11}$$

where $d(t)$ is the disturbance input. Let the disturbance model be

$$\dot{\boldsymbol{x}}_d(t) = \boldsymbol{A}_{cd}\boldsymbol{x}_d(t)\ ,\ d(t) = \boldsymbol{c}_{cd}\boldsymbol{x}_d(t). \tag{3.12}$$

For example, step type disturbance can be modeled by

$$\boldsymbol{A}_{cd} = 0\ \ ,\ \ \boldsymbol{c}_{cd} = 1, \tag{3.13}$$

and sinusoidal type disturbance with frequency ω_d can be modeled by

$$\boldsymbol{A}_{cd} = \begin{bmatrix} 0 & 1 \\ -\omega_d^2 & 0 \end{bmatrix}\ \ ,\ \ \boldsymbol{c}_{cd} = [1, 0]. \tag{3.14}$$

The continuous-time augmented system consisting of (3.10) and (3.12) is represented by

$$\dot{\boldsymbol{x}}(t) = \boldsymbol{A}_c\boldsymbol{x}(t) + \boldsymbol{b}_c u(t) \tag{3.15}$$

$$y(t) = \boldsymbol{c}_c\boldsymbol{x}(t) \tag{3.16}$$

$$\boldsymbol{A}_c \triangleq \begin{bmatrix} \boldsymbol{A}_{cp} & -\boldsymbol{b}_{cp}\boldsymbol{c}_{cd} \\ \boldsymbol{O} & \boldsymbol{A}_{cd} \end{bmatrix}, \boldsymbol{b}_c \triangleq \begin{bmatrix} \boldsymbol{b}_{cp} \\ \boldsymbol{0} \end{bmatrix}, \boldsymbol{x} \triangleq \begin{bmatrix} \boldsymbol{x}_p \\ \boldsymbol{x}_d \end{bmatrix}$$

$$\boldsymbol{c}_c \triangleq [\boldsymbol{c}_{cp}, \boldsymbol{0}].$$

Discretizing (3.15) using multirate sampling control, the intersample plant state at $t = (i + \nu_k)T_f$ can be calculated from the kth row of (3.7) by

$$\boldsymbol{x}[i + \nu_k] = \tilde{\boldsymbol{A}}_k\boldsymbol{x}[i] + \tilde{\boldsymbol{B}}_k\boldsymbol{u}[i] \tag{3.17}$$

$$\tilde{\boldsymbol{A}}_k = \begin{bmatrix} \tilde{\boldsymbol{A}}_{pk} & \tilde{\boldsymbol{A}}_{pdk} \\ \boldsymbol{O} & \tilde{\boldsymbol{A}}_{dk} \end{bmatrix}, \tilde{\boldsymbol{B}}_k = \begin{bmatrix} \tilde{\boldsymbol{B}}_{pk} \\ \boldsymbol{O} \end{bmatrix}.$$

For the plant (3.15) discretized by (3.4), the discrete-time observer at the sampling points is obtained from Gopinath's method by

$$\hat{\boldsymbol{v}}[i + 1] = \hat{\boldsymbol{A}}\hat{\boldsymbol{v}}[i] + \hat{\boldsymbol{b}}y[i] + \hat{\boldsymbol{J}}\boldsymbol{u}[i] \tag{3.18}$$

$$\hat{\boldsymbol{x}}[i] = \hat{\boldsymbol{C}}\hat{\boldsymbol{v}}[i] + \hat{\boldsymbol{d}}y[i]. \tag{3.19}$$

As shown in Fig. 3.2, let the feedback control law be

$$\boldsymbol{u}[i] = \boldsymbol{u}_p[i] + \boldsymbol{u}_d[i] = \boldsymbol{F}_p\hat{\boldsymbol{x}}_p[i] + \boldsymbol{F}_d\hat{\boldsymbol{x}}_d[i] = \boldsymbol{F}\hat{\boldsymbol{x}}[i], \tag{3.20}$$

where $\boldsymbol{F} \triangleq [\boldsymbol{F}_p, \boldsymbol{F}_d]$. Letting $\boldsymbol{e}_v[i]$ be the estimation error of the observer ($\boldsymbol{e}_v[i] = \hat{\boldsymbol{v}}[i] - \boldsymbol{v}[i]$), the following equation is obtained.

$$\hat{\boldsymbol{x}}[i] = \boldsymbol{x}[i] + \hat{\boldsymbol{C}}\boldsymbol{e}_v[i]. \tag{3.21}$$

From (3.17) to (3.21), the closed-loop system is represented by

$$\begin{bmatrix} \boldsymbol{x}_p[i + \nu_k] \\ \boldsymbol{x}_d[i + \nu_k] \\ \boldsymbol{e}_v[i + 1] \end{bmatrix} = \begin{bmatrix} \tilde{\boldsymbol{A}}_{pk} + \tilde{\boldsymbol{B}}_{pk}\boldsymbol{F}_p & \tilde{\boldsymbol{A}}_{pdk} + \tilde{\boldsymbol{B}}_{pk}\boldsymbol{F}_d & \tilde{\boldsymbol{B}}_{pk}\boldsymbol{F}\hat{\boldsymbol{C}} \\ \boldsymbol{O} & \tilde{\boldsymbol{A}}_{dk} & \boldsymbol{O} \\ \boldsymbol{O} & \boldsymbol{O} & \hat{\boldsymbol{A}} \end{bmatrix} \begin{bmatrix} \boldsymbol{x}_p[i] \\ \boldsymbol{x}_d[i] \\ \boldsymbol{e}_v[i] \end{bmatrix}. \tag{3.22}$$

Because full row rank of the matrix $\tilde{\boldsymbol{B}}_{pk}$ can be assured by theorem 2.3, $\boldsymbol{F}_d$ can be selected such that the (1,2) element of the above equation becomes zero for all $k = 1, \cdots, M$.

$$\tilde{\boldsymbol{A}}_{pdk} + \tilde{\boldsymbol{B}}_{pk}\boldsymbol{F}_d = \boldsymbol{O} \tag{3.23}$$

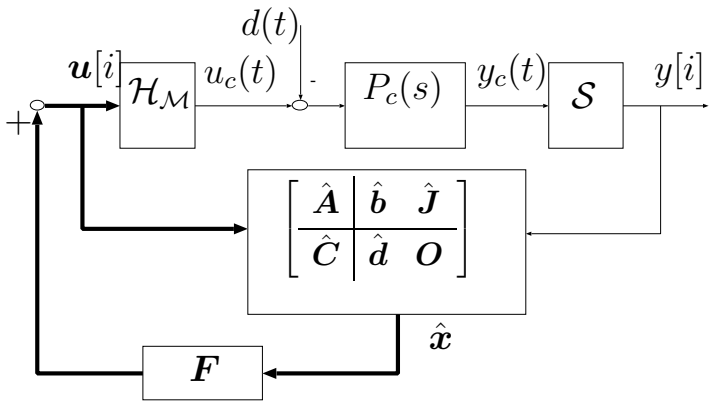

Figure 3.2: Multirate control with disturbance observer.

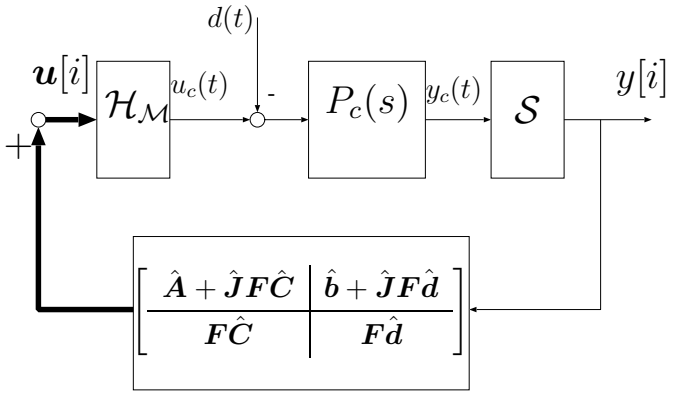

Figure 3.3: State space representation of $\boldsymbol{C}_2[z]$.

The simultaneous equation of (3.23) for all k becomes

$$\tilde{\boldsymbol{A}}_{pd} + \tilde{\boldsymbol{B}}_p \boldsymbol{F}_d = \boldsymbol{O}, \tag{3.24}$$

$$\left[\begin{array}{c|c} \tilde{\boldsymbol{A}}_{pd} & \tilde{\boldsymbol{B}}_p \end{array}\right] \triangleq \left[\begin{array}{c|c} \tilde{\boldsymbol{A}}_{pd1} & \tilde{\boldsymbol{B}}_{p1} \\ \vdots & \vdots \\ \tilde{\boldsymbol{A}}_{pdM} & \tilde{\boldsymbol{B}}_{pM} \end{array}\right]. \tag{3.25}$$

From (3.24), $\boldsymbol{F}_d$ is obtained by

$$\boldsymbol{F}_d = -\tilde{\boldsymbol{B}}_p^{-1} \tilde{\boldsymbol{A}}_{pd}. \tag{3.26}$$

In (3.22) and (3.23), the influence from disturbance $\boldsymbol{x}_d[i]$ to the intersample state $\boldsymbol{x}_p[i+\nu_k]$ at $t = (i+\nu_k)T_f$ can become zero. Moreover, $\boldsymbol{x}_p[i]$ and $\boldsymbol{e}_v[i]$ at the sampling point converge to zero at the rate of the eigenvalues of $\tilde{\boldsymbol{A}}_{pM} + \tilde{\boldsymbol{B}}_{pM}\boldsymbol{F}_p$ and $\hat{\boldsymbol{A}}$ (the poles of the regulator and observer). Therefore, perfect disturbance rejection is achieved ($\boldsymbol{x}_p[i+\nu_k] = 0$) in the steady state. The poles of the regulator and observer will be tuned by taking account of the tradeoff between the performance and stability robustness.

Substituting (3.18) for (3.20), the feedback type controller is obtained by

$$\begin{bmatrix} \hat{\boldsymbol{v}}[i+1] \\ \boldsymbol{u}[i] \end{bmatrix} = \begin{bmatrix} \hat{\boldsymbol{A}} + \hat{\boldsymbol{J}}\boldsymbol{F}\hat{\boldsymbol{C}} & \hat{\boldsymbol{b}} + \hat{\boldsymbol{J}}\boldsymbol{F}\hat{\boldsymbol{d}} \\ \boldsymbol{F}\hat{\boldsymbol{C}} & \boldsymbol{F}\hat{\boldsymbol{d}} \end{bmatrix} \begin{bmatrix} \hat{\boldsymbol{v}}[i] \\ y[i] \end{bmatrix}, \tag{3.27}$$

as shown in Fig. 3.3.

3.3.3 Design of Intersample Observer and Feedback Controller

Because the multirate system becomes a MISO system, the feedback gain $\boldsymbol{F}_p$ cannot be uniquely decided only by the pole assignment of $\tilde{\boldsymbol{A}}_{pM} + \tilde{\boldsymbol{B}}_{pM}\boldsymbol{F}_p$. A simple solution to eliminate this redundancy is to make the state-feedback control input $\boldsymbol{u}_p[i]$ hold a constant value during the sampling period, which is represented by

$$\boldsymbol{u}_p[i] = \begin{bmatrix} u_{p1}[i] \\ \vdots \\ u_{pN}[i] \end{bmatrix} = \begin{bmatrix} \boldsymbol{f}_y \\ \vdots \\ \boldsymbol{f}_y \end{bmatrix} \hat{\boldsymbol{x}}_p[i], \tag{3.28}$$

where $\boldsymbol{f}_y$ is the state-feedback gain designed for the sampling period T_y.

Because the above control law generates a large phase delay when using the zero-order hold, a novel observer which estimates the intersample response is introduced in this section. By using this observer, the state feedback gain $\boldsymbol{F}_p$ is calculated. From the estimated state (3.19) at the sampling points, the intersample plant state is estimated by[1]

$$\hat{\tilde{\boldsymbol{x}}}_p[i] = \tilde{\boldsymbol{A}}_p\hat{\boldsymbol{x}}_p[i] + \tilde{\boldsymbol{B}}_p\boldsymbol{u}[i], \tag{3.29}$$

where $\hat{\tilde{\boldsymbol{x}}}_p[i] = [\hat{\boldsymbol{x}}_p[i+\mu_0], \cdots, \hat{\boldsymbol{x}}_p[i+\mu_{N-1}]]^T$, and $\tilde{\boldsymbol{A}}_p$ and $\tilde{\boldsymbol{B}}_p$ are calculated by (3.7). Because the plant output cannot be measured during the sampling period, the intersample state is calculated based on open-loop sense using the mathematical model. Convergence of the estimation error can be assured at the sampling points.

Utilizing the intersample estimated state, let the state-feedback control input be

$$\boldsymbol{u}_p[i] = \begin{bmatrix} u_{p1}[i] \\ \vdots \\ u_{pN}[i] \end{bmatrix} = \begin{bmatrix} \boldsymbol{f}_u & & \boldsymbol{O} \\ & \ddots & \\ \boldsymbol{O} & & \boldsymbol{f}_u \end{bmatrix} \begin{bmatrix} \hat{\boldsymbol{x}}_p[i] \\ \vdots \\ \hat{\boldsymbol{x}}_p[i+\mu_{N-1}] \end{bmatrix} = \boldsymbol{F}_u\hat{\tilde{\boldsymbol{x}}}_p[i], \tag{3.30}$$

where $\boldsymbol{f}_u$ is the state-feedback gain designed for the control period T_u.

Assuming $\boldsymbol{u}[i] = \boldsymbol{u}_p[i]$ on (3.30), the control input of (3.29) is represented by

$$\boldsymbol{u}_p[i] = \boldsymbol{F}_u\hat{\tilde{\boldsymbol{x}}}_p[i] = \boldsymbol{F}_u(\tilde{\boldsymbol{A}}_p\hat{\boldsymbol{x}}_p[i] + \tilde{\boldsymbol{B}}_p\boldsymbol{u}_p[i]). \tag{3.31}$$

[1] In (3.29), $\hat{\cdot}$ and $\tilde{\cdot}$ represent the estimated and intersample variables, respectively.

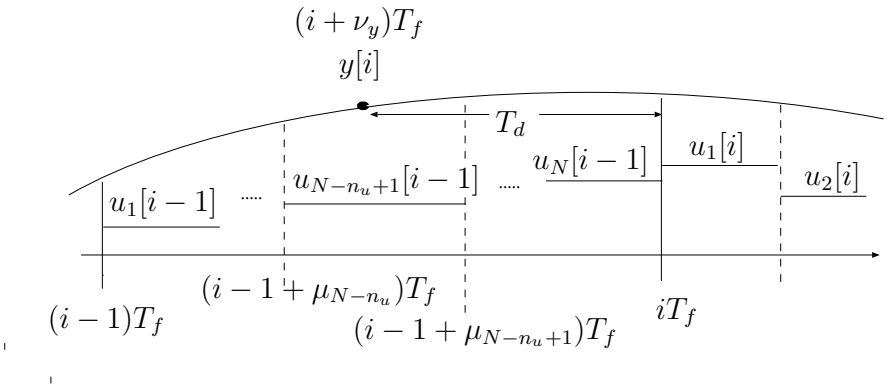

Figure 3.4: Time chart of the time delay (same figure as Fig. 2.13).

Solving (3.31) for $\boldsymbol{u}_p[i]$, the following equation is obtained.

$$\boldsymbol{u}_p[i] = (\boldsymbol{I} - \boldsymbol{F}_u\tilde{\boldsymbol{B}}_p)^{-1}\boldsymbol{F}_u\tilde{\boldsymbol{A}}_p\hat{\boldsymbol{x}}_p[i] \tag{3.32}$$

Thus, $\boldsymbol{F}_p$ is obtained by

$$\boldsymbol{F}_p = (\boldsymbol{I} - \boldsymbol{F}_u\tilde{\boldsymbol{B}}_p)^{-1}\boldsymbol{F}_u\tilde{\boldsymbol{A}}_p. \tag{3.33}$$

Because the proposed intersample observer can compensate for the large phase delay caused by zero-order hold, the stability margin of the closed-loop system is improved as will be shown in section 6.2. This approach is essentially equivalent to the instantaneous speed observer for servomotors [59] and the multirate estimation for hard disk drive [50, 51, 55, 89]. The advantages of the proposed intersample observer are 1) calculation resources can be saved because the feedback gain (3.33) is obtained by off-line calculation, 2) the proposed theory is generalized and not oriented to one application, and 3) it is applicable to systems with time delay.

3.3.4 Extension to systems with time delay

In this section, the proposed multirate feedback control is extended to plants with time delay in the same way as section 2.5.1. The continuous-time plant with time delay T_d is described by

$$\dot{\boldsymbol{x}}(t) = \boldsymbol{A}_c\boldsymbol{x}(t) + \boldsymbol{b}_c u(t) \tag{3.34}$$

$$y(t) = \boldsymbol{c}_c\boldsymbol{x}(t - T_d), \tag{3.35}$$

as shown in Fig. 3.4. Because the time delay is considered to be delay due to calculation, it is assumed to be shorter than the frame period ($T_d \leq T_f$) for simplification. However, longer time delay can also be considered in the same way as [82].

The discrete-time plant with multirate hold can be represented by

$$\bar{\boldsymbol{x}}[i+1] = \bar{\boldsymbol{A}}\bar{\boldsymbol{x}}[i] + \bar{\boldsymbol{B}}\boldsymbol{u}[i] \tag{3.36}$$

$$\bar{\boldsymbol{y}}[i] = \bar{\boldsymbol{C}}\bar{\boldsymbol{x}}[i] \tag{3.37}$$

$$\bar{\boldsymbol{A}} \triangleq \begin{bmatrix} \boldsymbol{A} & \boldsymbol{O} \\ \boldsymbol{O} & \boldsymbol{O} \end{bmatrix},\ \bar{\boldsymbol{B}} \triangleq \begin{bmatrix} \boldsymbol{B} \\ \boldsymbol{E} \end{bmatrix},\ \bar{\boldsymbol{C}} \triangleq \begin{bmatrix} \boldsymbol{c} & \boldsymbol{g} \\ \boldsymbol{O} & \boldsymbol{I}_{n_u} \end{bmatrix}, \tag{3.38}$$

$$\bar{\boldsymbol{x}} \triangleq \begin{bmatrix} \boldsymbol{x} \\ \boldsymbol{x}_u \end{bmatrix},\ \bar{\boldsymbol{y}} \triangleq \begin{bmatrix} y \\ \boldsymbol{x}_u \end{bmatrix} \tag{3.39}$$

$$\boldsymbol{c} \triangleq \boldsymbol{c}_c e^{\boldsymbol{A}_c \nu_y T_f}, \boldsymbol{g} \triangleq [g_{N-n_u+1}, \cdots, g_N], \tag{3.40}$$

$$\boldsymbol{E} \triangleq [\boldsymbol{O}, \boldsymbol{I}_{n_u}], \nu_y \triangleq -\frac{T_d}{T_f} \tag{3.41}$$

where g_j is defined in (2.66), n_u is a number of $\boldsymbol{u}[i-1]$ elements during T_d in Fig. 3.4, and $\boldsymbol{x}_u$ is a vector composed of this control input ($\boldsymbol{x}_u[i] = [u_{N-n_u+1}[i-1], \cdots, u_N[i-1]]^T$).

In (3.37), the measurement variable $\bar{\boldsymbol{y}}$ includes the past control input $\boldsymbol{x}_u$ in order to make the system observable[2].

For the plant with time delay represented by (3.36) and (3.37), the discrete-time observer at the sampling points is obtained from Gopinath's method by

$$\hat{\boldsymbol{v}}[i+1] = \hat{\boldsymbol{A}}\hat{\boldsymbol{v}}[i] + \hat{\boldsymbol{B}}\bar{\boldsymbol{y}}[i] + \hat{\boldsymbol{J}}\boldsymbol{u}[i] \tag{3.42}$$

$$\hat{\boldsymbol{x}}[i] = \hat{\boldsymbol{C}}\hat{\boldsymbol{v}}[i] + \hat{\boldsymbol{D}}\bar{\boldsymbol{y}}[i]. \tag{3.43}$$

Using the feedback gain designed in (3.26), let the control law be

$$\boldsymbol{u}[i] = \bar{\boldsymbol{F}}\bar{\boldsymbol{x}}[i], \quad \bar{\boldsymbol{F}} \triangleq [\boldsymbol{F}_d, \boldsymbol{O}]. \tag{3.44}$$

By the parallel discussion with section 3.3.2, perfect disturbance rejection performance is preserved by (3.44).

Substituting (3.44) for (3.42) and (3.43), the feedback type observer is obtained by

$$\begin{aligned} \begin{bmatrix} \hat{\boldsymbol{v}}[i+1] \\ \boldsymbol{u}[i] \end{bmatrix} &= \left[\begin{array}{c|c} \hat{\boldsymbol{A}} + \hat{\boldsymbol{J}}\boldsymbol{F}\hat{\boldsymbol{C}} & \hat{\boldsymbol{B}} + \hat{\boldsymbol{J}}\bar{\boldsymbol{F}}\hat{\boldsymbol{D}} \\ \hline \boldsymbol{F}\hat{\boldsymbol{C}} & \boldsymbol{F}\hat{\boldsymbol{D}} \end{array}\right] \begin{bmatrix} \hat{\boldsymbol{v}}[i] \\ \bar{\boldsymbol{y}}[i] \end{bmatrix} \\ &= \left[\begin{array}{c|cc} \boldsymbol{A}_c & \boldsymbol{b}_{c1} & \boldsymbol{B}_{c2} \\ \hline \boldsymbol{C}_c & \boldsymbol{d}_{c1} & \boldsymbol{D}_{c2} \end{array}\right] \begin{bmatrix} \hat{\boldsymbol{v}}[i] \\ y[i] \\ \boldsymbol{x}_u[i] \end{bmatrix}. \end{aligned} \tag{3.45}$$

[2]If $\boldsymbol{x}_u$ is not included in the measurement variable, the system becomes unobservable.

Using the definition of $\boldsymbol{x}_u[i+1] = \boldsymbol{E}\boldsymbol{u}[i]$, state space representation of $\boldsymbol{C}_2[z]$ is obtained by

$$\left[\begin{array}{c} \hat{\boldsymbol{v}}[i+1] \\ \hline \boldsymbol{x}_u[i+1] \\ \hline \boldsymbol{u}[i] \end{array}\right] = \left[\begin{array}{cc|c} \boldsymbol{A}_c & \boldsymbol{B}_{c2} & \boldsymbol{b}_{c1} \\ \hline \boldsymbol{E}\boldsymbol{C}_c & \boldsymbol{E}\boldsymbol{D}_{c2} & \boldsymbol{E}\boldsymbol{d}_{c1} \\ \hline \boldsymbol{C}_c & \boldsymbol{D}_{c2} & \boldsymbol{d}_{c1} \end{array}\right] \left[\begin{array}{c} \hat{\boldsymbol{v}}[i] \\ \boldsymbol{x}_u[i] \\ y[i] \end{array}\right]. \tag{3.46}$$

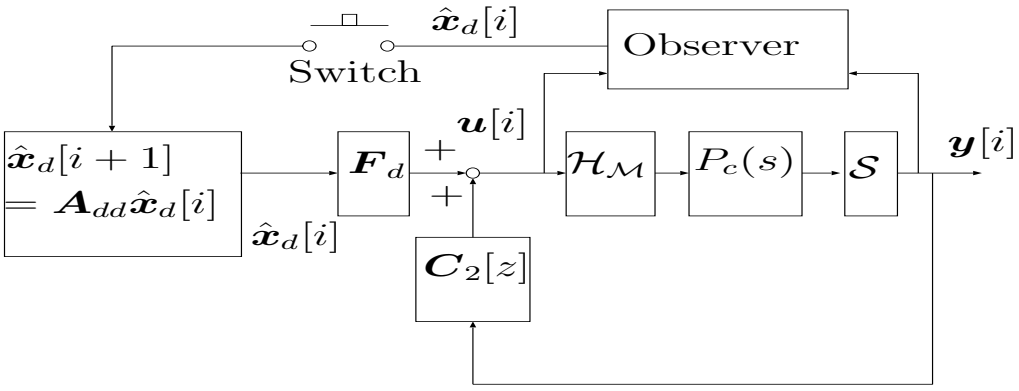

Figure 3.5: Feedforward repetitive control.

3.4 Periodic Disturbance Rejection Control

In this section, PDR is applied to periodic disturbance, and two multirate repetitive controllers are proposed, they are 1) feedback approach based on the internal model principle and 2) feedforward disturbance rejection approach based on open-loop estimation.

3.4.1 Feedback Repetitive Control

The disturbance with period $T_0 \triangleq 2\pi/\omega_0$ can be represented by the Fourier series as

$$d(t) = a_0 + \sum_{k=1}^{\infty} a_k \cos k\omega_0 t + b_k \sin k\omega_0 t. \tag{3.47}$$

where ω_0 is known and a_k, b_k are unknown parameters. Letting the disturbance model (3.12) be (3.47), the repetitive feedback controller is obtained by (3.27), having the internal model $s^2 + (k\omega_0)^2$ in discrete-time domain. Repetitive disturbance is perfectly rejected ($\boldsymbol{x}_p[i+\nu_k] = 0$) at M inter-sample points in the steady state.

3.4.2 Feedforward Repetitive Control

Repetitive feedback control based on the internal model principle has the disadvantages that closed-loop characteristics worsen and it becomes difficult to assure stability robustness [90]. Therefore, in this section, a novel repetitive controller based on open-loop estimation with switching function and feedforward disturbance rejection is proposed, as shown in Fig. 3.5

The repetitive disturbance is estimated by the open-loop disturbance observer. When the estimation converges to the steady state, the switch turns on at $t = t_0$. After that,

the switch turns off immediately. Repetitive disturbance is calculated by (3.48) from the initial value $\hat{\boldsymbol{x}}_d[t_0]$ which contains the amplitude and phase information of the disturbance.

$$\hat{\boldsymbol{x}}_d[i+1] = \boldsymbol{A}_{dd}\hat{\boldsymbol{x}}_d[i], \quad \boldsymbol{A}_{dd} = e^{\boldsymbol{A}_{cd}T_f} \tag{3.48}$$

Because the disturbance feedforward $\boldsymbol{F}_d$ is obtained by (3.26), perfect disturbance rejection is achieved at M inter-sample points. The advantage of this approach is that the feedback controller $\boldsymbol{C}_2[z]$ is completely independent of the repetitive controller. Thus, stability robustness is guaranteed by the feedback controller. With this scheme, it becomes possible to construct the repetitive controller without sacrifice of the feedback characteristics.

Moreover, by introducing the initial value compensation of the feedback controller $\boldsymbol{C}_2[z]$ at $t = t_0$, transient response can be improved after the switching action. If the initial state of the observer $\hat{\boldsymbol{v}}[t_0]$ is set by (3.49), the plant state $\boldsymbol{x}_p[i]$ of (3.22) converges to zero at the rate of the eigenvalues of $\tilde{\boldsymbol{A}}_{pM} + \tilde{\boldsymbol{B}}_{pM}\boldsymbol{F}_p$ at the sampled points. Thus, if the poles of the regulator are assigned appropriately, it is possible to prevent overshoot.

$$\hat{\boldsymbol{C}}\hat{\boldsymbol{v}}[t_0] = \boldsymbol{x}[t_0] - \hat{\boldsymbol{d}}y[t_0] \tag{3.49}$$

In (3.49), the plant state $\boldsymbol{x}[t_0]$ is obtained from the value estimated by the open-loop observer $\hat{\boldsymbol{x}}[t_0]$.

3.4.3 Optimization of the Inter-sample Disturbance Rejection Performance

In section 3.4.1 and section 3.4.2, the state multiplicity is defined as $M = N/n$ in order to reject the disturbance perfectly at M inter-sample points. In this section, M is selected to be more than N/n in order to optimize the inter-sample performance. This approach is referred to as the fast sampling technique in the advanced sampled-data control theory [27, 39, 40].

When M is selected to be more than N/n, it is impossible to satisfy (3.24) because the number of rows of $\tilde{\boldsymbol{B}}_p$ is larger than that of columns. Therefore, the inter-sample performance can be optimized by minimizing $\tilde{\boldsymbol{B}}_p$ for all $k(= 1, \cdots, M)$. Thus, the problem is formulated by

$$\min_{\boldsymbol{F}_d} \|\tilde{\boldsymbol{A}}_{pd} + \tilde{\boldsymbol{B}}_p\boldsymbol{F}_d\| \quad \text{s. t.} \quad \tilde{\boldsymbol{A}}_{pdM} + \tilde{\boldsymbol{B}}_{pM}\boldsymbol{F}_d = \boldsymbol{O}. \tag{3.50}$$

The above constraint is the condition that the controller includes the disturbance model, which assures the convergence of $\boldsymbol{x}_p[i]$ at the sampling points ($k = M$).

From Lagrange's undetermined multiplier method, the solution of (3.50) is obtained by

$$\boldsymbol{F}_d = \boldsymbol{Z}[\boldsymbol{Y}^T(\boldsymbol{Y}\boldsymbol{Z}\boldsymbol{Y}^T)^{-1}\boldsymbol{Y}\boldsymbol{Z}\boldsymbol{X}^T - \boldsymbol{X}^T, -\boldsymbol{Y}^T(\boldsymbol{Y}\boldsymbol{Z}\boldsymbol{Y}^T)^{-1}]\tilde{\boldsymbol{A}}_{pd}, \tag{3.51}$$

where $\boldsymbol{X} \triangleq [\tilde{\boldsymbol{B}}_{p1}^T, \cdots \tilde{\boldsymbol{B}}_{p(M-1)}^T]^T, \boldsymbol{Y} \triangleq \tilde{\boldsymbol{B}}_{pM}, \boldsymbol{Z} \triangleq (\boldsymbol{X}^T\boldsymbol{X})^{-1}$, and the Frobenius norm is adopted in (3.50). The proof is shown in Appendix C. M has to be selected more than N to assure the non-singularity of $\boldsymbol{Z}$.

3.5 Summary

In this chapter, digital control systems which have hardware restrictions of $T_u < T_y$ were assumed. In section 3.3, the multirate feedback controller was proposed, which guarantees perfect disturbance rejection at M intersample points in the steady state. Next, the intersample observer was proposed, which increases the stability margin by estimation and compensation of the intersample response. Moreover, the proposed method is extended to systems with time delay.

In section 3.4, two multirate repetitive controllers were proposed, they are 1) feedback approach based on internal model principle and 2) feedforward disturbance rejection approach based on the open-loop estimation and switching function. By using the latter approach, it becomes possible to prevent the closed characteristics from worsening when using the internal model.

Chapter 4

Controller Discretization Based on Perfect State Matching

4.1 Abstract

In this chapter, a novel discretization method for continuous-time controllers is proposed based on perfect state matching (PSM) control. In the PSM, the states in the continuous-time system are completely reserved in the obtained sampled-data system. The features of the proposed method are 1) multirate input control is employed, and the lth plant input is changed N_l times during one sampling period, 2) the states of the discretized sampled-data system completely match those of the original continuous-time closed-loop system at every sampling period, and 3) the proposed method is applicable to static state-feedback and/or dynamic controllers. Next, the continuous-time observer is discretized using the multirate output control. Moreover, the proposed method is extended to the systems with long sampling period relative to the control period.

The proposed perfect state matching control is applied to position control systems for servomotors and vibration suppression control for hard disk drives in chapter 7.

4.2 Introduction

In digital control systems, the controlled plant is a continuous-time system while the controller is a discrete-time system. Thus, the conversion from continuous-time system to discrete-time system is required in either the modeling or controller design stage, as shown in Fig. 4.1. Concerning the issue of when it should be discretized, it is possible to classify the design of digital controller into three methods [26, 73].

First, the "controller discretization" considered in this chapter is a technique by which

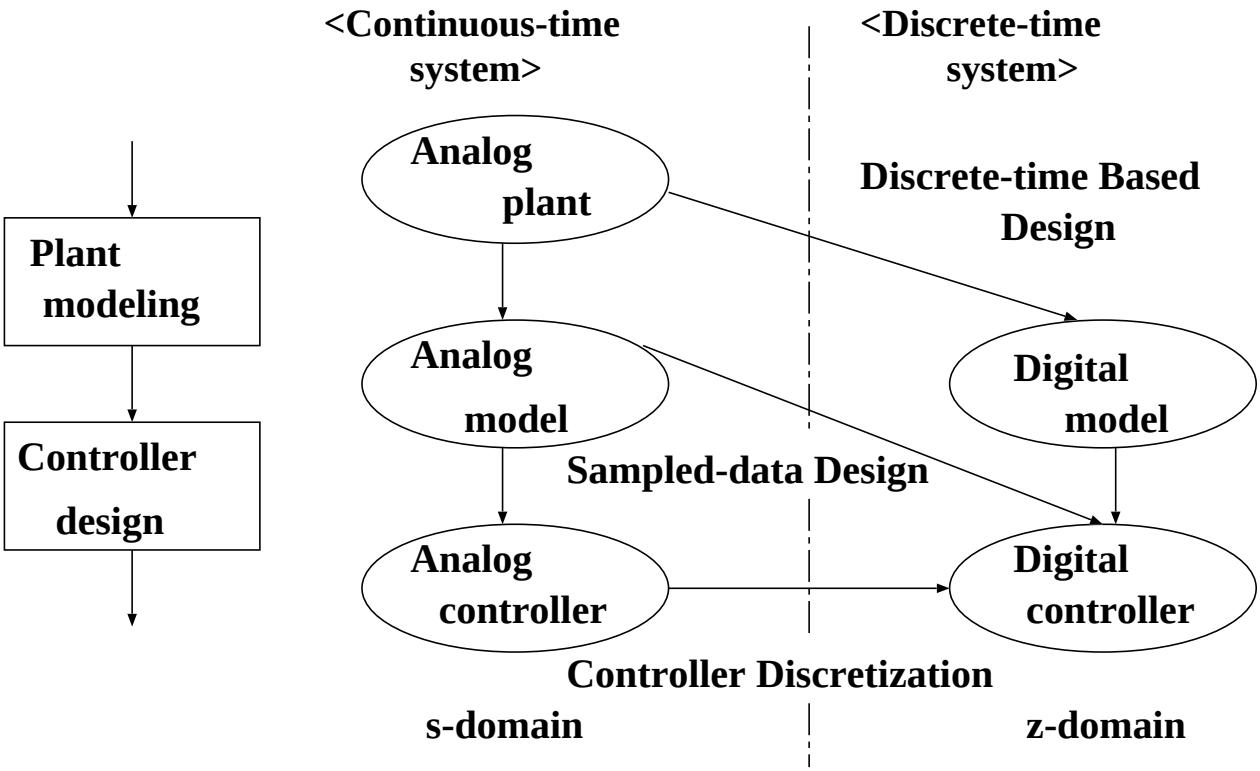

Figure 4.1: The procedure for the digital control system design

an ideal analog controller designed in continuous-time is converted to an equivalent digital controller. This approach is also referred as digital redesign [73, 91] or continuous-based synthesis [26]. In this approach, ideal closed-loop characteristics is preserved if the sampling period is short enough. However, because conventional discretization methods are based on approximations, they do not assure the ideal closed-loop characteristics and stability if the sampling period cannot be set short enough.

Second, in discrete-time based design, the plant is modeled in discrete-time, and the digital controller is designed based on discrete-time theory. This approach assures the stability of the closed-loop system and the performance at the sampled points. However, it does not consider the intersample response.

Third, in sampled-data design, the digital controller is obtained directly from the continuous-time plant considering the intersample response, as mentioned in section 1.1.1. However, in this approach, only the H_2 and H_∞ problems have been resolved. The advantage of this approach is that robust stability for the plant uncertainty can be assured. But, sometimes the approach is overly conservative. This approach is not always applicable, because H_2 and H_∞ theory generally have many assumptions.

Moreover, the sampling period has to be determined before the controller design stage

in the discrete-time based and the sampled-data approaches. In practice, however, the sampling period sometimes cannot be determined in the design stage, and is changed several times during the implementation to real systems.

Thus, in this chapter, a novel discretization method of controllers is developed considering the closed-loop system. The necessity and importance of controller discretization are as follows [73].

1. An existing analogue controller can be replaced. Thus, the tuning knowledge of conventional controllers such as PID controller is available.

2. The sampling period depends on the order of the controller and the capability of the processor and interface. In practice, it cannot be determined prior to implementation. Thus, the continuous controller is designed based on the continuous-time model, and it is replaced by the digital controller with the shortest sampling period. Introducing controller discretization, it is possible to greatly lighten the engineers' burden when the sampling period is changed.

3. Continuous-time theory has a longer history than discrete-time and sampled-data theory. Moreover, in continuous-time design, the controller can be designed without considering Nyquist frequency limitations.

Historically, one of the most popular discretization methods is the Tustin (or bilinear) transformation, in which an s-domain analog controller is transformed into a z-domain digital controller by

$$s = \frac{2(z-1)}{T(z+1)}. \tag{4.1}$$

This approach is straightforward, and the stable poles of the controller in s-domain are mapped inside the unit circle in z-domain. However, the closed-loop stability is not assured. Therefore, in this approach, the feedback system may become unstable if the sampling time is set too long.

In [91, 92, 93], discretization methods based on closed-loop characteristics were developed. However, these attempts do not assure closed-loop stability, because approximations were made to obtain solutions of the discretization (see chapter 4.3.1). In [94], the feedforward and feedback gains are altered at every sampling period, so that the states of the two systems match at the end of N sampling periods. The method in [94] is similar to the proposed method only in certain special cases. However, the number of times of gain alternation, N, is redundant compared to the proposed method in this chapter.

The method of [91] was further investigated in [95], and a different approximation was proposed for obtaining a solution of the discretization, in which the closed-loop stability

was maintained. However, the transition matrices of the original and approximately discretized systems are not same. Furthermore, the methods in [91, 92, 93, 94, 95] have a limitation that the original continuous-time controller must be of the static state-feedback type and that all of plant state variables must be directly detected.

The other discretization methods for dynamic controllers were developed in [96, 97, 40]. These methods tried to match closed-loop frequency response approximately. However, because of using these approximations, closed-loop stability could not be assured [96, 97], and the solution of the discretization could not be obtained in large sampling period [40].

Multirate digital controls have been proposed for applications in the pole/zero assignment problem, strong stabilization, simultaneous stabilization, adaptive control, and so on, as mentioned in chapter 1. However, this chapter makes the first attempt to apply multirate digital control to the controller discretization problem.

The purpose of the proposed method is to develop a new digital controller from the analog controller so that all of the states of the sampled-data closed-loop system completely match those of the original continuous-time closed-loop system at every sampling instance. This dissertation refers to the technique as perfect state matching (PSM) control. Thus, the stability of the closed-loop system is retained, and the transition matrices of the two systems become identical. In the proposed method, multirate-input digital control is employed, and the lth plant input is changed N_l times during one sampling period. [24] and [83] called this method N-Delay control after [8]. The digital controller can be automatically discretized by the following procedure. Moreover, discretization method for an observer is also presented, in which multirate-output digital control is employed. Therefore, the proposed method can deal with the system even if a part of the plant states are not directly detected, and it is applicable both to static state-feedback controllers and dynamic controllers.

4.3 Controller Discretization without Hardware Restriction

In this section, novel discretization methods of continuous-time controllers are proposed for systems without hardware restrictions in the sampling mechanism. After the problems of the conventional method are explained in section 4.3.1, a discretization method is proposed for two-degree-of-freedom state-feedback controllers with dynamics based on multirate input control in section 4.3.2. Next, the continuous-time observer is discretized based on multirate output control in section 4.3.3.

4.3.1 Problem of the Conventional Method

In this section, we consider the problem of matching the responses of an existing continuous-time system as shown in Fig. 4.2, with those of the discrete-time system shown in Fig. 4.3 for the same initial conditions. Consider the linear continuous-time system described by

$$\dot{\boldsymbol{x}}(t) = \boldsymbol{A}_c\boldsymbol{x}(t) + \boldsymbol{b}_c u(t). \tag{4.2}$$

Also, let the continuous-time state-feedback control law be

$$u(t) = \boldsymbol{f}_c\boldsymbol{x}(t). \tag{4.3}$$

The continuous-time closed-loop system becomes

$$\dot{\boldsymbol{x}}(t) = (\boldsymbol{A}_c + \boldsymbol{b}_c\boldsymbol{f}_c)\boldsymbol{x}(t) \tag{4.4}$$

and its sampled-data system with sampling period T is

$$\boldsymbol{x}((i+1)T) = e^{(\boldsymbol{A}_c+\boldsymbol{b}_c\boldsymbol{f}_c)T}\boldsymbol{x}(iT). \tag{4.5}$$

Consider the discrete-time system utilizing conventional zero-order hold described by

$$\boldsymbol{x}[i+1] = \boldsymbol{A}\boldsymbol{x}[i] + \boldsymbol{b}u[i] \tag{4.6}$$

where $\boldsymbol{x}[i] = \boldsymbol{x}(iT), \boldsymbol{A} \triangleq e^{\boldsymbol{A}_cT}$, and $\boldsymbol{b} \triangleq \int_0^T e^{\boldsymbol{A}_c\tau}d\tau\boldsymbol{b}_c$. Letting the discrete-time state-feedback control law be $u[i] = \boldsymbol{f}(T)\boldsymbol{x}[i]$, the discrete-time closed-loop system becomes

$$\boldsymbol{x}[i+1] = (\boldsymbol{A} + \boldsymbol{b}\boldsymbol{f}(T))\boldsymbol{x}[i]. \tag{4.7}$$

From (4.5) and (4.7), the discretization problem is to find the discrete-time gain $\boldsymbol{f}(T)$ from the continuous-time gain $\boldsymbol{f}_c$ so that the equation

$$\boldsymbol{A} + \boldsymbol{b}\boldsymbol{f}(T) = e^{(\boldsymbol{A}_c+\boldsymbol{b}_c\boldsymbol{f}_c)T} \tag{4.8}$$

is satisfied. If the above condition is satisfied, perfect state matching (PSM) control is achieved, in which the states of the digitally controlled system in (4.7) completely match those of the continuous-time system in (4.5) at every sampling point. The existence of $\boldsymbol{f}(T)$ in (4.8), however, is not always guaranteed because the dimension of the input is generally less than that of the state. Therefore, in [91, 92], (4.8) is approximately solved for $\boldsymbol{f}(T)$. But, because of the approximation, the stability of the obtained digital closed-loop system is not always assured, and the time response is different from that of the continuous-time feedback system.

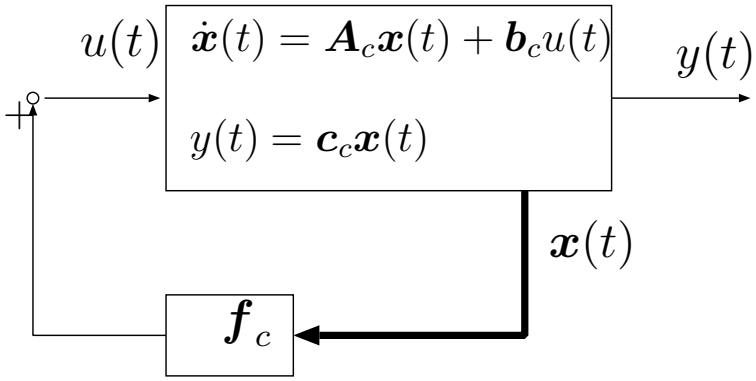

Figure 4.2: Continuous-time state-feedback control system.

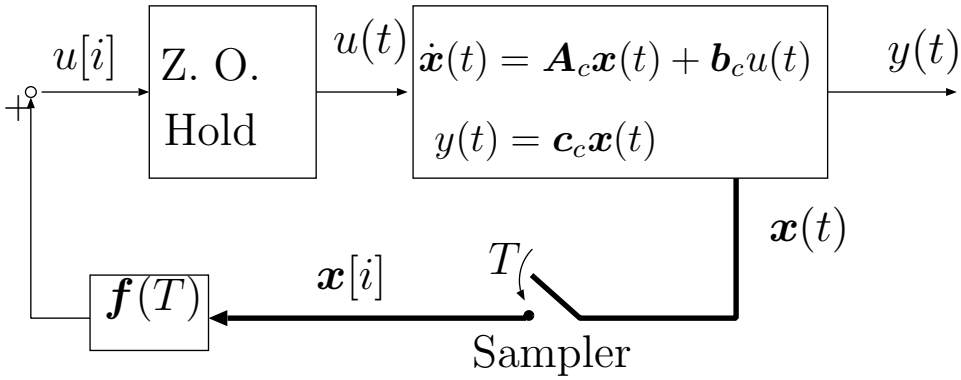

Figure 4.3: Discrete-time state-feedback control system.

4.3.2 Discretization of Controller by Multirate Input Control

In this section, a novel discretization method for continuous-time controllers is presented based on multirate input control, in which the lth plant input is changed N_l times during one sampling period. The introduction of multirate input control increases the input dimension, thus (4.8) can be solved without any approximation. Moreover, the proposed method is applicable both to continuous-time dynamic controllers ($u = K(s)y$) and static state-feedback controllers ($u = \boldsymbol{f}\boldsymbol{x}$). The proposed method succeeds in this generalization by the introduction of 1) the closed-loop augmented system consisting of the plant and the dynamic controller, and 2) multirate input control.

In this section, a two-degree-of-freedom controller with dynamics is considered as the original analogue controller. The plant is a linear multi-input multi-output (MIMO) system, and all of the plant states are assumed to be measurable. If a part of the plant states can not be detected directly, the discretized observer should be employed, as presented in section 4.3.3.

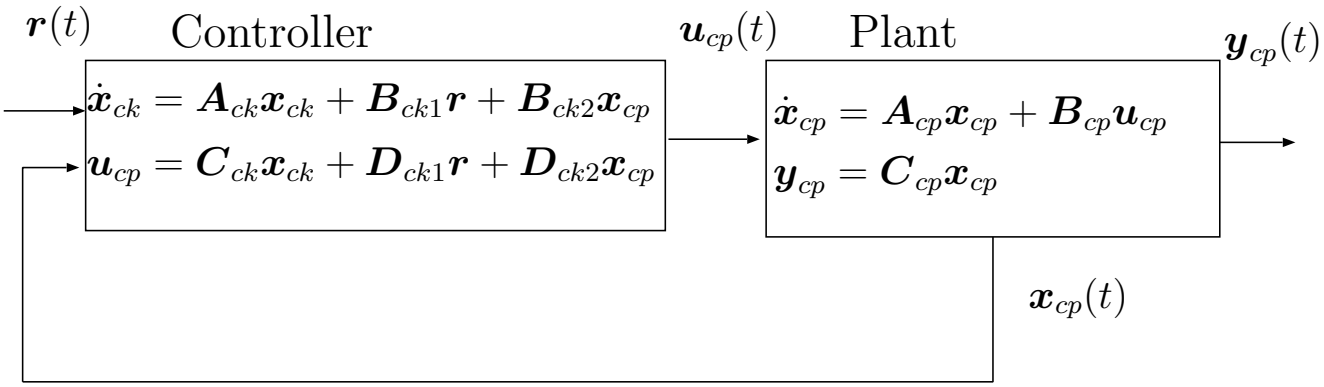

Figure 4.4: Continuous-time control system.

Consider the continuous-time plant described by

$$\dot{\boldsymbol{x}}_{cp}(t) = \boldsymbol{A}_{cp}\boldsymbol{x}_{cp}(t) + \boldsymbol{B}_{cp}\boldsymbol{u}_{cp}(t) \tag{4.9}$$

$$\boldsymbol{y}_{cp}(t) = \boldsymbol{C}_{cp}\boldsymbol{x}_{cp}(t) \tag{4.10}$$

where the plant state $\boldsymbol{x}_{cp} \in \boldsymbol{R}^{n_p}$, the plant input $\boldsymbol{u}_{cp} \in \boldsymbol{R}^{m_p}$, and the plant output $\boldsymbol{y}_{cp} \in \boldsymbol{R}^{p_p}$. As shown in Fig. 4.4, let the original continuous-time controller be

$$\dot{\boldsymbol{x}}_{ck}(t) = \boldsymbol{A}_{ck}\boldsymbol{x}_{ck}(t) + \boldsymbol{B}_{ck1}\boldsymbol{r}(t) + \boldsymbol{B}_{ck2}\boldsymbol{x}_{cp}(t) \tag{4.11}$$

$$\boldsymbol{u}_{cp}(t) = \boldsymbol{C}_{ck}\boldsymbol{x}_{ck}(t) + \boldsymbol{D}_{ck1}\boldsymbol{r}(t) + \boldsymbol{D}_{ck2}\boldsymbol{x}_{cp}(t), \tag{4.12}$$

where the controller state $\boldsymbol{x}_{ck} \in \boldsymbol{R}^{n_k}$ and the reference input $\boldsymbol{r} \in \boldsymbol{R}^{m_r}$. This representation includes a wide class of controllers such as static state feedback controller ($u(t) = \boldsymbol{f}_c\boldsymbol{x}(t)$), unity feedback controller with dynamics ($u(t) = K(s)(r(t) - y(t))$), and two-degree-of-freedom controller ($u(t) = \boldsymbol{C}_1(s)r(t) - \boldsymbol{C}_2(s)y(t)$).

From (4.9) $\sim$ (4.12), the continuous-time closed-loop augmented system consisting of the plant and the controller is represented by

$$\dot{\bar{\boldsymbol{x}}}_c(t) = \bar{\boldsymbol{A}}_c\bar{\boldsymbol{x}}_c(t) + \bar{\boldsymbol{B}}_c\boldsymbol{r}(t) \tag{4.13}$$

where

$$\bar{\boldsymbol{A}}_c \triangleq \begin{bmatrix} \boldsymbol{A}_{cp} + \boldsymbol{B}_{cp}\boldsymbol{D}_{ck2} & \boldsymbol{B}_{cp}\boldsymbol{C}_{ck} \\ \boldsymbol{B}_{ck2} & \boldsymbol{A}_{ck} \end{bmatrix}, \bar{\boldsymbol{B}}_c \triangleq \begin{bmatrix} \boldsymbol{B}_{cp}\boldsymbol{D}_{ck1} \\ \boldsymbol{B}_{ck1} \end{bmatrix}, \bar{\boldsymbol{x}}_c \triangleq \begin{bmatrix} \boldsymbol{x}_{cp} \\ \boldsymbol{x}_{ck} \end{bmatrix}. \tag{4.14}$$

Assuming the reference input $\boldsymbol{r}$ is piecewise-constant, i.e. $\boldsymbol{r}(t) = \boldsymbol{r}(iT)$ for $iT \le t < (i+1)T$, the sampled-data system for the sampling period T becomes

$$\bar{\boldsymbol{x}}_c((i+1)T) = \bar{\boldsymbol{A}}\bar{\boldsymbol{x}}_c(iT) + \bar{\boldsymbol{B}}\boldsymbol{r}(iT) \tag{4.15}$$

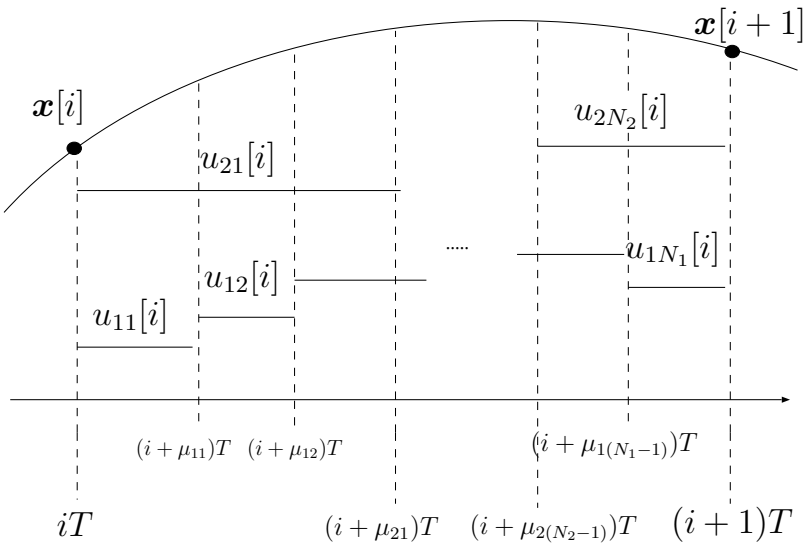

Figure 4.5: Multirate input control.

where

$$\bar{\boldsymbol{A}} \triangleq e^{\bar{\boldsymbol{A}}_c T} \triangleq \begin{matrix} \\ n_p \\ n_k \end{matrix} \begin{matrix} \begin{matrix} n_p & n_k \end{matrix} \\ \begin{pmatrix} \bar{\boldsymbol{A}}_{11} & \bar{\boldsymbol{A}}_{12} \\ \bar{\boldsymbol{A}}_{21} & \bar{\boldsymbol{A}}_{22} \end{pmatrix} \end{matrix}, \quad \bar{\boldsymbol{B}} \triangleq \int_0^T e^{\bar{\boldsymbol{A}}_c \tau} \bar{\boldsymbol{B}}_c d\tau \triangleq \begin{matrix} \\ n_p \\ n_k \end{matrix} \begin{matrix} \begin{matrix} m_r \end{matrix} \\ \begin{pmatrix} \bar{\boldsymbol{B}}_1 \\ \bar{\boldsymbol{B}}_2 \end{pmatrix} \end{matrix}. \tag{4.16}$$

Next, the discrete-time controller is obtained from the original continuous-time control system (4.15) using multirate input control. In this scheme, the lth ($l = 1, 2, \cdots, m_p$) plant input is changed N_l times during one sampling period as shown in Fig. 4.5. The selection of the N_l is made with reference to the following condition.

$$N_l \geq \sigma_l \tag{4.17}$$

where $(\sigma_1, ..., \sigma_{m_p})$ is a set of generalized controllability indices of $(\boldsymbol{A}_{cp}, \boldsymbol{B}_{cp})$ which are defined in section 2.5.2.

The discrete-time plant using multirate input control is given by

$$\boldsymbol{x}_{dp}[i+1] = \boldsymbol{A}\boldsymbol{x}_{dp}[i] + \boldsymbol{B}\boldsymbol{u}[i] \tag{4.18}$$

where $\boldsymbol{x}_{dp} \in \boldsymbol{R}^{n_p}$ is the plant state, the coefficient matrices $\boldsymbol{A}$ and $\boldsymbol{B}$ are calculated by (2.81), and $\boldsymbol{u}[i] \in \boldsymbol{R}^N (N \triangleq N_1 + N_2 + ... + N_{m_p} \geq n_p)$ is the multirate input vector defined by

$$\boldsymbol{u}[i] = [u_{11}[i], \cdots, u_{1N_1}[i], u_{21}[i], \cdots, u_{mN_m}[i]]^T, \tag{4.19}$$

where $u_{lj}[i] \in \boldsymbol{R}^1$ is the lth plant input for $(i+\mu_{l(j-1)})T \leq t < (i+\mu_{lj})T$ ($l = 1, .., m_p$, $j = 1, .., N_l$), as shown in Fig. 4.5.

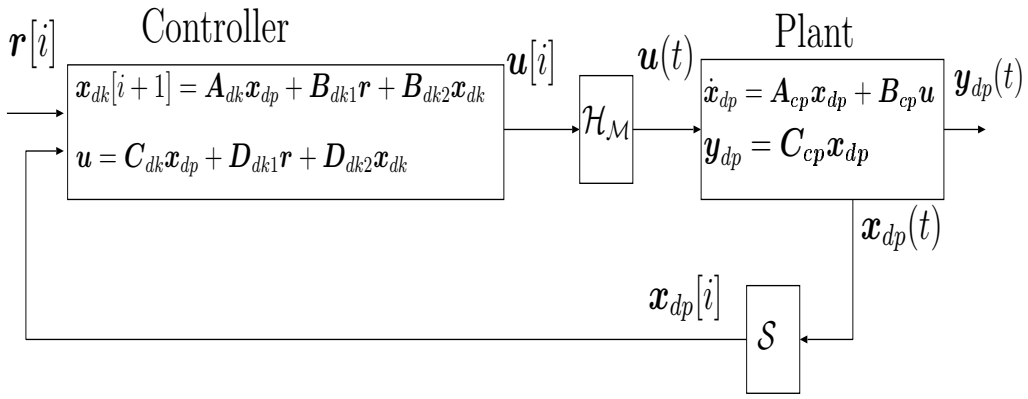

Figure 4.6: Discrete-time control system.

As shown in Fig. 4.6, let the discrete-time controller be

$$\boldsymbol{x}_{dk}[i+1] = \boldsymbol{A}_{dk}\boldsymbol{x}_{dp}[i] + \boldsymbol{B}_{dk1}\boldsymbol{r}[i] + \boldsymbol{B}_{dk2}\boldsymbol{x}_{dk}[i] \tag{4.20}$$

$$\boldsymbol{u}[i] = \boldsymbol{C}_{dk}\boldsymbol{x}_{dp}[i] + \boldsymbol{D}_{dk1}\boldsymbol{r}[i] + \boldsymbol{D}_{dk2}\boldsymbol{x}_{dk}[i]. \tag{4.21}$$

where the controller state $\boldsymbol{x}_{dk} \in \boldsymbol{R}^{n_k}$. From (4.18) $\sim$ (4.21), the discrete-time closed-loop augmented system is represented by

$$\bar{\boldsymbol{x}}_d[i+1] = \bar{\boldsymbol{A}}_d\bar{\boldsymbol{x}}_d[i] + \bar{\boldsymbol{B}}_d\boldsymbol{r}[i] \tag{4.22}$$

where

$$\bar{\boldsymbol{A}}_d \triangleq \begin{bmatrix} \boldsymbol{A} + \boldsymbol{B}\boldsymbol{D}_{dk2} & \boldsymbol{B}\boldsymbol{C}_{dk} \\ \boldsymbol{B}_{dk2} & \boldsymbol{A}_{dk} \end{bmatrix}, \quad \bar{\boldsymbol{B}}_d \triangleq \begin{bmatrix} \boldsymbol{B}\boldsymbol{D}_{dk1} \\ \boldsymbol{B}_{dk1} \end{bmatrix}, \quad \bar{\boldsymbol{x}}_d \triangleq \begin{bmatrix} \boldsymbol{x}_{dp} \\ \boldsymbol{x}_{dk} \end{bmatrix}. \tag{4.23}$$

Comparing (4.15) and (4.22), if the following conditions are satisfied, the states of the digitally controlled system ($\bar{\boldsymbol{x}}_d$) completely match the states of the continuous-time system ($\bar{\boldsymbol{x}}_c$) at every sampling period for any arbitrary initial state and piecewise-constant reference input.

$$\begin{bmatrix} \bar{\boldsymbol{A}}_{11} & \bar{\boldsymbol{A}}_{12} \\ \bar{\boldsymbol{A}}_{21} & \bar{\boldsymbol{A}}_{22} \end{bmatrix} = \begin{bmatrix} \boldsymbol{A} + \boldsymbol{B}\boldsymbol{D}_{dk2} & \boldsymbol{B}\boldsymbol{C}_{dk} \\ \boldsymbol{B}_{dk2} & \boldsymbol{A}_{dk} \end{bmatrix} \tag{4.24}$$

$$\begin{bmatrix} \bar{\boldsymbol{B}}_1 \\ \bar{\boldsymbol{B}}_2 \end{bmatrix} = \begin{bmatrix} \boldsymbol{B}\boldsymbol{D}_{dk1} \\ \boldsymbol{B}_{dk1} \end{bmatrix} \tag{4.25}$$

Here, the necessary and sufficient condition for the solution of the linear matrix equation ($\boldsymbol{A}\boldsymbol{x} = \boldsymbol{b}$) is

$$rank\boldsymbol{A} = rank[\boldsymbol{A}, b]. \tag{4.26}$$

Therefore, the necessary and sufficient conditions for the existence of $\boldsymbol{C}_{dk}, \boldsymbol{D}_{dk1}$, and $\boldsymbol{D}_{dk2}$ in (4.24) and (4.25) are given by

$$\begin{aligned} rank\boldsymbol{B} &= rank[\boldsymbol{B}, \bar{\boldsymbol{A}}_{11} - \boldsymbol{A}] \\ &= rank[\boldsymbol{B}, \bar{\boldsymbol{A}}_{12}] = rank[\boldsymbol{B}, \bar{\boldsymbol{B}}_1]. \end{aligned} \tag{4.27}$$

From theorem 2.3, the row rank of matrix $\boldsymbol{B}$ is full, thus, (4.27) is satisfied. As a result, the existence of the solution of (4.24) and (4.25) is assured. Solving (4.24) and (4.25), the parameters of the digital controller are given by

$$\begin{aligned} \boldsymbol{A}_{dk} = \bar{\boldsymbol{A}}_{22},\ \boldsymbol{B}_{dk1} = \bar{\boldsymbol{B}}_2,\ \boldsymbol{B}_{dk2} = \bar{\boldsymbol{A}}_{21},\ \boldsymbol{C}_{dk} = \boldsymbol{B}^{-}\bar{\boldsymbol{A}}_{12}, \\ \boldsymbol{D}_{dk1} = \boldsymbol{B}^{-}\bar{\boldsymbol{B}}_1,\ \boldsymbol{D}_{dk2} = \boldsymbol{B}^{-}(\bar{\boldsymbol{A}}_{11} - \boldsymbol{A}_{\boldsymbol{dp}}), \end{aligned} \tag{4.28}$$

where $\boldsymbol{B}^{-}$ is the generalized inverse of matrix $\boldsymbol{B}$ [85].

Comments 1) if $(\boldsymbol{A}_{cp}, \boldsymbol{B}_{cp})$ is a controllable pair, the proposed method is always applicable. 2) If the original continuous-time system is stably designed, the stability of the discretized system is assured because the two transition matrices (4.24) become identical. Moreover, (4.24) can guarantee the inter-sample stability [27]. 3) The states of the obtained sampled-data system completely match those of the original continuous-time closed-loop system at every sampling period, independent of sampling period. Therefore, the proposed method is superior to conventional methods [91, 92, 93, 94, 95, 96, 97, 40].

4.3.3 Discretization of Observer by Multirate Output Control

Because the digital controller obtained in 4.3.2 makes use of state-feedback control as shown in (4.20) and (4.21), all states need to be detected directly and instantaneously. However, in the general case, not all states are always detected directly, and the calculation time delay may not be negligible. Therefore, we should consider a discrete-time state observer to feedback the estimated plant state $\hat{\boldsymbol{x}}[i]$ instead of the plant state $\boldsymbol{x}[i]$.

In this section, the discretization method for a state observer is proposed using multirate-output control based on the duality of the discretization method for the controller. The advantage of the proposed method is that the discrete-time estimation errors completely match the continuous-time estimation errors at every frame period.

Consider the designed continuous-time observer of Fig. 4.7 for the continuous-time plant (4.9) described by

$$\dot{\hat{\boldsymbol{x}}}_{cp}(t) = \boldsymbol{A}_{cp}\hat{\boldsymbol{x}}_{cp}(t) + \boldsymbol{B}_{cp}\boldsymbol{u}_{cp}(t) + \boldsymbol{K}_{cp}(\boldsymbol{y}_{cp} - \boldsymbol{C}_{cp}\hat{\boldsymbol{x}}_{cp}(t)) \tag{4.29}$$

where $\hat{\boldsymbol{x}}_{cp}$ is the estimated plant state. The estimation error of the continuous-time state

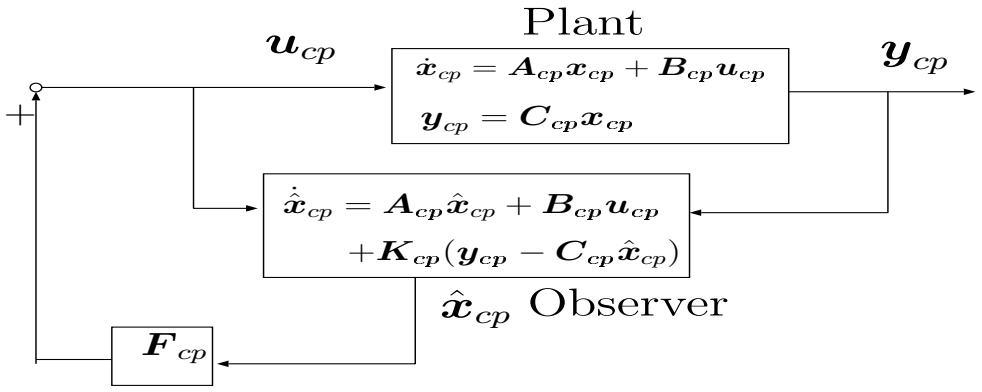

Figure 4.7: Continuous time observer.

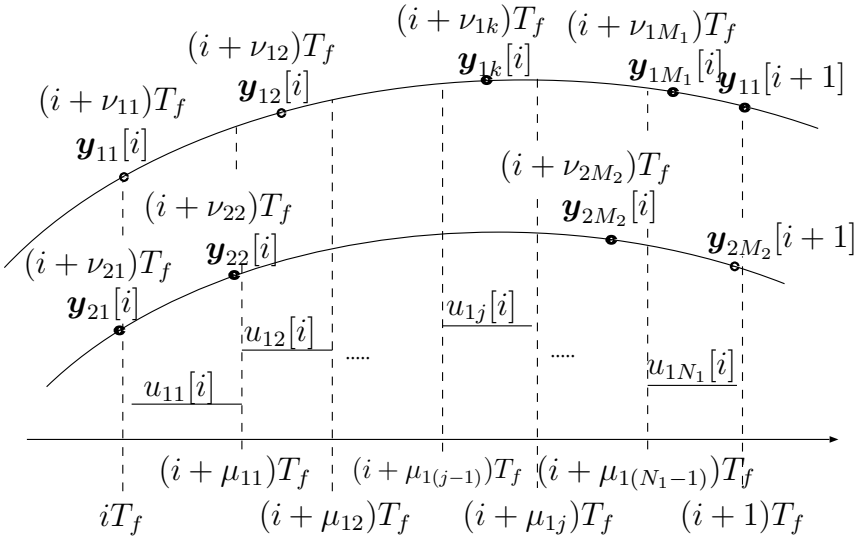

Figure 4.8: Multirate output control.

$\boldsymbol{e}_{cp}(\stackrel{\triangle}{=} \boldsymbol{x}_{cp} - \hat{\boldsymbol{x}}_{cp})$ becomes

$$\dot{\boldsymbol{e}}_{cp}(t) = \dot{\boldsymbol{x}}_{cp}(t) - \dot{\hat{\boldsymbol{x}}}_{cp}(t) = (\boldsymbol{A_{cp}} - \boldsymbol{K_{cp}}\boldsymbol{C_{cp}})\boldsymbol{e}_{cp}(t). \tag{4.30}$$

The sampled-data system for the frame period T_f is represented by

$$\boldsymbol{e}_{cp}((i+1)T_f) = e^{(\boldsymbol{A_{cp}} - \boldsymbol{K_{cp}}\boldsymbol{C_{cp}})T_f}\boldsymbol{e}_{cp}(iT_f). \tag{4.31}$$

In the proposed method, the multirate output control is employed, in which the qth plant output is detected M_q times during one frame period as shown in Fig. 4.8, and the discrete-time estimation errors ($\boldsymbol{e}_{dp}$) completely match the continuous-time estimation errors ($\boldsymbol{e}_{cp}$) at every frame period. This control scheme is a duality mechanism of the multirate input control. The selection of output multiplicities M_q is made with reference to the following

condition.

$$M_q \geq \rho_q \tag{4.32}$$

where $(\rho_1, ..., \rho_{p_p})$ is a set of generalized observability indices of $(\boldsymbol{A}_{cp}, \boldsymbol{C}_{cp})$ which are defined as follows.

Definition 4.1 *Generalized observability indices of* $(\boldsymbol{A}_{cp}, \boldsymbol{C}_{cp})$ *are defined as follows for* $\boldsymbol{A}_{cp} \in \boldsymbol{R}^{n_p \times n_p}$ *and* $\boldsymbol{C}_{cp} \in \boldsymbol{R}^{p_p \times n_p}$. *If* $(\boldsymbol{A}_{cp}, \boldsymbol{C}_{cp})$ *is an observable pair,* n_p *linearly independent vectors can be selected from*

$$\{\boldsymbol{c}_{c1}, .., \boldsymbol{c}_{cp_p}, \boldsymbol{c}_{c1}\boldsymbol{A}_{cp}, .., \boldsymbol{c}_{cp_p}\boldsymbol{A}_{cp}, .., \boldsymbol{c}_{cp_p}\boldsymbol{A}_{cp}^{n_p-1}\}$$

where $\boldsymbol{C}_{cp} = [\boldsymbol{c}_{c1}^T, .., \boldsymbol{c}_{cp_p}^T]^T$. *Letting* φ *be a set of these* n_p *vectors,* ρ_q *are defined by*

$$\rho_q = number\{k | \boldsymbol{c}_{cq}\boldsymbol{A}_{cp}^{k-1} \in \varphi\} \tag{4.33}$$

$$\sum_{q=1}^{p_p} \rho_q = n_p. \tag{4.34}$$

The discrete-time plant using multirate input and multirate output control is given by

$$\begin{aligned} \boldsymbol{x}_{dp}[i+1] &= \boldsymbol{A}\boldsymbol{x}_{dp}[i] + \boldsymbol{B}\boldsymbol{u}[i] && (4.35)\\ \boldsymbol{y}[i] &= \boldsymbol{C}\boldsymbol{x}[i] + \boldsymbol{D}\boldsymbol{u}[i], && (4.36) \end{aligned}$$

where the coefficient matrices $\boldsymbol{A}, \boldsymbol{B}, \boldsymbol{C}$, and $\boldsymbol{D}$ are calculated by (2.81), and $\boldsymbol{y}[i] \in \boldsymbol{R}^M (M \stackrel{\triangle}{=} M_1 + M_2 + ... + M_{p_p} \geq n_p)$ is the multirate output vector defined by

$$\boldsymbol{y}[i] = [y_{11}[i], \cdots, y_{1M_1}[i], y_{21}[i], \cdots, y_{pM_p}[i]]^T, \tag{4.37}$$

where y_{qk} is the qth plant output at $t = (i + \nu_{qk})T_f$ $(q = 1, 2, \cdots, p_p, k = 1, 2, \cdots, M_q)$.

Using the output $\boldsymbol{y}[i]$, let the discrete-time observer be

$$\hat{\boldsymbol{x}}_{dp}[i+1] = \boldsymbol{A}\hat{\boldsymbol{x}}_{dp}[i] + \boldsymbol{B}\boldsymbol{u}[i] + \boldsymbol{K}(\boldsymbol{y}[i] - (\boldsymbol{C}\hat{\boldsymbol{x}}[i] + \boldsymbol{D}\boldsymbol{u}[i])) \tag{4.38}$$

where the state of the discrete-time observer $\hat{\boldsymbol{x}}_{dp} \in \boldsymbol{R}^{n_p}$. The estimation error of the discrete-time state $\boldsymbol{e}_{dp} (\stackrel{\triangle}{=} \boldsymbol{x}_{dp} - \hat{\boldsymbol{x}}_{dp})$ is represented by

$$\begin{aligned} \boldsymbol{e}_{dp}[i+1] &= \boldsymbol{x}_{dp}[i+1] - \hat{\boldsymbol{x}}_{dp}[i+1] \\ &= (\boldsymbol{A} - \boldsymbol{K}\boldsymbol{C})\boldsymbol{e}_{dp}[i]. \end{aligned} \tag{4.39}$$

Comparing (4.31) and (4.39), if the following condition is satisfied, the estimation errors of the continuous-time states $(\boldsymbol{e}_{cp})$ completely match those of the discrete-time states $(\boldsymbol{e}_{dp})$ at every frame period.

$$e^{(\boldsymbol{A}_{cp} - \boldsymbol{K}_{cp}\boldsymbol{C}_{cp})T_f} = \boldsymbol{A} - \boldsymbol{K}\boldsymbol{C} \tag{4.40}$$

From (4.26), the necessary and sufficient condition for existence of $\boldsymbol{K}$ in (4.40) is given by

$$rank\boldsymbol{C} = rank \begin{bmatrix} \boldsymbol{C} \\ \boldsymbol{A} - e^{(\boldsymbol{A_{cp}} - \boldsymbol{K_{cp}}\boldsymbol{C_{cp}})T_f} \end{bmatrix}. \tag{4.41}$$

With regards to the matrix $\boldsymbol{C}$, the next theorem is proved in [72], if ρ_q is the generalized observability controllability index. For the case of the observability index, it is also proved in [10].

Theorem 4.1 *Let $(\boldsymbol{A}_{cp}, \boldsymbol{C}_{cp})$ be an observable pair. If the output multiplicities satisfy $M_q \geq \rho_q$ for $(q = 1, 2, .., p_p)$, for almost all $\nu_{qk}(k = 1, .., M_q)$ and almost all T, the matrix $\boldsymbol{C}$ has full column rank, i.e.*

$$rank\boldsymbol{C} = n_p. \tag{4.42}$$

Because of this theorem, the column rank $\boldsymbol{C}$ in (4.41) is full, thus, (4.41) is satisfied. As a result, the existence of $\boldsymbol{K}$ in (4.40) is assured. Solving (4.40), the parameters of the digital observer are given by

$$\boldsymbol{K} = (\boldsymbol{A} - e^{(\boldsymbol{A_{cp}} - \boldsymbol{K_{cp}}\boldsymbol{C_{cp}})T_f})\boldsymbol{C^{-}}. \tag{4.43}$$

The discretization method presented in this section is for full order observers only. However, this result was extended to minimum order observers in [72].

4.4 Controller Discretization with Sampling Restriction

In this section, hardware restrictions where the sampling period is relatively long ($T_u < T_y$) are considered, because this assumption is very common in motion control system as mentioned in section 1.1.2 and 3.2. For this system, a novel discretization method of an analogue controller is proposed using perfect state matching based on multirate input control. In the proposed scheme, the plant state of the digitally controlled system perfectly matches that of the ideal continuous-time system at M intersample points during T_y.

In the proposed methods of section 4.3, it was impossible to implement the internal model of disturbance because they do not consider the open-loop characteristics of the controller. On the other hand, in this section, the augmented system with disturbance is introduced to estimate and reject disturbance. By this approach, the obtained digital controller can have an internal model such as an integrator ($\frac{1}{z-1}$).

For simplification, the continuous-time system is assumed to be composed of a SISO plant and a one-degree-of-freedom controller with disturbance observer. The proposed methods, however, can be extended to more general cases in the same way as section 2.5.2 and 4.3.2.

For the restriction of $T_u < T_y$, the frame period T_f is defined as $T_f = T_y$ [1] , and the dynamics of the controller is described by T_f.

4.4.1 Design of Continuous-time Controller

In this section, the continuous-time controller is designed based on the regulator and the disturbance observer.

Consider the continuous-time plant model described by

$$\dot{\boldsymbol{x}}_p(t) = \boldsymbol{A}_{cp}\boldsymbol{x}_p(t) + \boldsymbol{b}_{cp}(u(t) - d(t)) \tag{4.44}$$

$$y(t) = \boldsymbol{c}_{cp}\boldsymbol{x}_p(t), \tag{4.45}$$

where $d(t)$ is the disturbance input. Let the disturbance model be

$$\dot{\boldsymbol{x}}_d(t) = \boldsymbol{A}_{cd}\boldsymbol{x}_d(t) \ , \ d(t) = \boldsymbol{c}_{cd}\boldsymbol{x}_d(t). \tag{4.46}$$

For example, the step type disturbance can be modeled by $\boldsymbol{A}_{cd} = 0, \boldsymbol{c}_{cd} = 1$. The continuous-time augmented system consisting of (4.44) and (4.46) is represented by

$$\dot{\boldsymbol{x}}(t) = \boldsymbol{A}_c\boldsymbol{x}(t) + \boldsymbol{b}_c u(t) \tag{4.47}$$

$$y(t) = \boldsymbol{c}_c\boldsymbol{x}(t), \tag{4.48}$$

$$\boldsymbol{A}_c \triangleq \begin{bmatrix} \boldsymbol{A}_{cp} & -\boldsymbol{b}_{cp}\boldsymbol{c}_{cd} \\ \boldsymbol{O} & \boldsymbol{A}_{cd} \end{bmatrix}, \boldsymbol{b}_c \triangleq \begin{bmatrix} \boldsymbol{b}_{cp} \\ \boldsymbol{0} \end{bmatrix}, \boldsymbol{x} \triangleq \begin{bmatrix} \boldsymbol{x}_p \\ \boldsymbol{x}_d \end{bmatrix},$$

$$\boldsymbol{c}_c \triangleq [\boldsymbol{c}_{cp}, \boldsymbol{0}].$$

For the plant (4.47), the continuous-time observer is designed using Gopinath's method as

$$\dot{\boldsymbol{v}}(t) = \hat{\boldsymbol{A}}_c\hat{\boldsymbol{v}}(t) + \hat{\boldsymbol{b}}_c y(t) + \hat{\boldsymbol{J}}_c\boldsymbol{u}(t) \tag{4.49}$$

$$\hat{\boldsymbol{x}}(t) = \hat{\boldsymbol{C}}_c\hat{\boldsymbol{v}}(t) + \hat{\boldsymbol{d}}_c y(t). \tag{4.50}$$

In order to regulate the plant state and reject the disturbance, the continuous-time regulator is designed by

$$u(t) = \boldsymbol{f}_{cp}\hat{\boldsymbol{x}}_p(t) + \boldsymbol{c}_{cd}\hat{\boldsymbol{x}}_d(t) = \boldsymbol{f}_c\hat{\boldsymbol{x}}(t), \tag{4.51}$$

$$\boldsymbol{f}_c \triangleq [\boldsymbol{f}_{cp}, \boldsymbol{c}_{cd}]. \tag{4.52}$$

Letting $\boldsymbol{e}_v$ be the estimation errors of the observer ($\boldsymbol{e}_v = \hat{\boldsymbol{v}} - \boldsymbol{v}$), the following equation is obtained.

$$\hat{\boldsymbol{x}}(t) = \boldsymbol{x}(t) + \hat{\boldsymbol{C}}\boldsymbol{e}_v(t). \tag{4.53}$$

From the above equations, the closed-loop system is represented by

$$\begin{bmatrix} \dot{\boldsymbol{x}}_p(t) \\ \dot{\boldsymbol{x}}_d(t) \\ \dot{\boldsymbol{e}}_v(t) \end{bmatrix} = \begin{bmatrix} \boldsymbol{A}_{Fcp} & \boldsymbol{O} & \boldsymbol{b}_{cp}\boldsymbol{f}_c\hat{\boldsymbol{C}}_c \\ \boldsymbol{O} & \boldsymbol{A}_d & \boldsymbol{O} \\ \boldsymbol{O} & \boldsymbol{O} & \hat{\boldsymbol{A}}_c \end{bmatrix} \begin{bmatrix} \boldsymbol{x}_p(t) \\ \boldsymbol{x}_d(t) \\ \boldsymbol{e}_v(t) \end{bmatrix}, \tag{4.54}$$

where $\boldsymbol{A}_{Fcp} \triangleq \boldsymbol{A}_{cp} + \boldsymbol{b}_{cp}\boldsymbol{f}_{cp}$. The transition of (4.54) from $t = iT_f$ to $t = (i + \nu_k)T_f$ is represented by

$$\begin{bmatrix} \boldsymbol{x}_p[i+\nu_k] \\ \boldsymbol{x}_d[i+\nu_k] \\ \boldsymbol{e}_v[i+1] \end{bmatrix} = \begin{bmatrix} e^{\boldsymbol{A}_{Fcp}\nu_k T_f} & \boldsymbol{O} & * \\ \boldsymbol{O} & e^{\boldsymbol{A}_d\nu_k T_f} & \boldsymbol{O} \\ \boldsymbol{O} & \boldsymbol{O} & e^{\hat{\boldsymbol{A}}_c T_f} \end{bmatrix} \begin{bmatrix} \boldsymbol{x}_p[i] \\ \boldsymbol{x}_d[i] \\ \boldsymbol{e}_v[i] \end{bmatrix}. \tag{4.55}$$

4.4.2 Discretization of the Controller by Multirate Input Control

In this section, the digital controller is obtained from the continuous-time controller designed in section 4.4.1 using multirate input control.

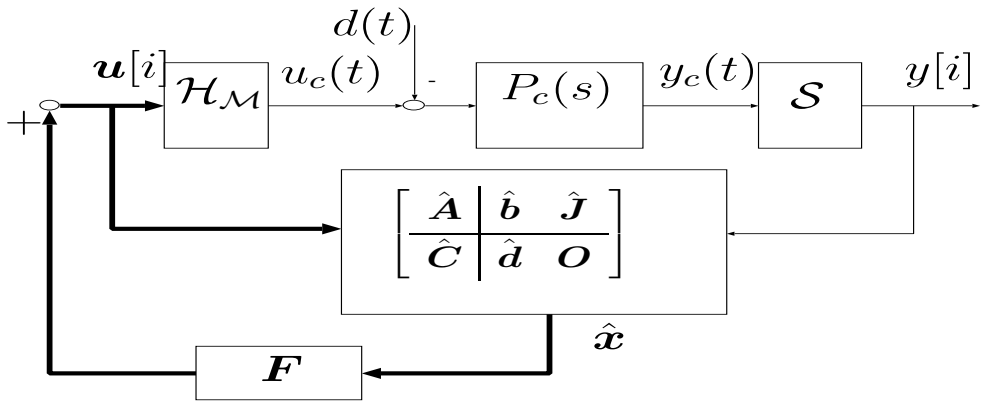

Figure 4.9: Multirate control with disturbance observer.

Discretizing (4.47) by multirate sampling control, the inter-sample plant state at $t = (i + \nu_k)T_f$ can be calculated from the kth row of (3.7) by

$$\boldsymbol{x}[i+\nu_k] = \tilde{\boldsymbol{A}}_k \boldsymbol{x}[i] + \tilde{\boldsymbol{B}}_k \boldsymbol{u}[i] \tag{4.56}$$

$$\tilde{\boldsymbol{A}}_k = \begin{bmatrix} \tilde{\boldsymbol{A}}_{pk} & \tilde{\boldsymbol{A}}_{pdk} \\ \boldsymbol{O} & \tilde{\boldsymbol{A}}_{dk} \end{bmatrix}, \tilde{\boldsymbol{B}}_k = \begin{bmatrix} \tilde{\boldsymbol{B}}_{pk} \\ \boldsymbol{O} \end{bmatrix}.$$

For the plant (4.47) discretized by (3.4), the discrete-time observer at the sampling points is obtained by

$$\hat{\boldsymbol{v}}[i+1] = \hat{\boldsymbol{A}}\hat{\boldsymbol{v}}[i] + \hat{\boldsymbol{b}}y[i] + \hat{\boldsymbol{J}}\boldsymbol{u}[i] \tag{4.57}$$

$$\hat{\boldsymbol{x}}[i] = \hat{\boldsymbol{C}}\hat{\boldsymbol{v}}[i] + \hat{\boldsymbol{d}}y[i]. \tag{4.58}$$

As shown in Fig. 4.9, let the feedback control law be

$$\boldsymbol{u}[i] = \boldsymbol{F}_p\hat{\boldsymbol{x}}_p[i] + \boldsymbol{F}_d\hat{\boldsymbol{x}}_d[i] = \boldsymbol{F}\hat{\boldsymbol{x}}[i], \tag{4.59}$$

where $\boldsymbol{F} \triangleq [\boldsymbol{F}_p, \boldsymbol{F}_d]$. From (4.56) $\sim$ (4.59), the closed-loop system is represented by

$$\begin{bmatrix} \boldsymbol{x}_p[i+\nu_k] \\ \boldsymbol{x}_d[i+\nu_k] \\ \boldsymbol{e}_v[i+1] \end{bmatrix} = \begin{bmatrix} \tilde{\boldsymbol{A}}_{pk} + \tilde{\boldsymbol{B}}_{pk}\boldsymbol{F}_p & \tilde{\boldsymbol{A}}_{pdk} + \tilde{\boldsymbol{B}}_{pk}\boldsymbol{F}_d & \tilde{\boldsymbol{B}}_{pk}\boldsymbol{F}\hat{\boldsymbol{C}} \\ \boldsymbol{O} & \tilde{\boldsymbol{A}}_{dk} & \boldsymbol{O} \\ \boldsymbol{O} & \boldsymbol{O} & \hat{\boldsymbol{A}} \end{bmatrix} \begin{bmatrix} \boldsymbol{x}_p[i] \\ \boldsymbol{x}_d[i] \\ \boldsymbol{e}_v[i] \end{bmatrix}. \tag{4.60}$$

Comparing (4.55) and (4.60), if the following conditions are satisfied, the plant state ($\boldsymbol{x}_p$) of the digitally controlled system completely matches that of the original continuous-time system at M inter-sample points on $t = (i + \nu_k)T_f$.

$$\tilde{\boldsymbol{A}}_{pk} + \tilde{\boldsymbol{B}}_{pk}\boldsymbol{F}_p = e^{\boldsymbol{A}_{Fcp}\nu_k T_f}, \tag{4.61}$$

$$\tilde{\boldsymbol{A}}_{pdk} + \tilde{\boldsymbol{B}}_{pk}\boldsymbol{F}_d = \boldsymbol{O}, \tag{4.62}$$

$$\boldsymbol{e}_v[i] = \boldsymbol{O}. \tag{4.63}$$

The simultaneous equations of (4.61) and (4.62) for all $k(=1,\cdots,M)$ become

$$\tilde{\boldsymbol{A}}_p + \tilde{\boldsymbol{B}}_p \boldsymbol{F}_p = \boldsymbol{E}, \quad \tilde{\boldsymbol{A}}_{pd} + \tilde{\boldsymbol{B}}_p \boldsymbol{F}_d = \boldsymbol{O}, \tag{4.64}$$

where $\tilde{\boldsymbol{A}}_p, \tilde{\boldsymbol{A}}_{pd}, \tilde{\boldsymbol{B}}_p$ and $\boldsymbol{E}$ are defined as

$$\begin{bmatrix} \tilde{\boldsymbol{A}}_{p1} \\ \vdots \\ \tilde{\boldsymbol{A}}_{pM} \end{bmatrix}, \begin{bmatrix} \tilde{\boldsymbol{A}}_{pd1} \\ \vdots \\ \tilde{\boldsymbol{A}}_{pdM} \end{bmatrix}, \begin{bmatrix} \tilde{\boldsymbol{B}}_{p1} \\ \vdots \\ \tilde{\boldsymbol{B}}_{pM} \end{bmatrix}, \begin{bmatrix} e^{\boldsymbol{A}_{Fcp}\nu_1 T_y} \\ \vdots \\ e^{\boldsymbol{A}_{Fcp}\nu_M T_y} \end{bmatrix}. \tag{4.65}$$

Because non-singularity of the matrix $\boldsymbol{B}_p$ is assured by theorem 2.3, $\boldsymbol{F}_p$ and $\boldsymbol{F}_d$ are obtained by

$$\boldsymbol{F}_p = \tilde{\boldsymbol{B}}_p^{-1}(\boldsymbol{E} - \tilde{\boldsymbol{A}}_{pd}), \quad \boldsymbol{F}_d = -\tilde{\boldsymbol{B}}_p^{-1}\tilde{\boldsymbol{A}}_{pd}. \tag{4.66}$$

In section 4.3.3, discretization of the observer was proposed based on multirate output control, where the plant output was detected more frequently. However, in this section, the discrete-time observer (4.57) is simply obtained, so that the eigenvalues of $\hat{\boldsymbol{A}}$ become identical to those of $e^{\hat{\boldsymbol{A}}_c T_f}$, because the plant is assumed to have a longer sampling period $(T_y > T_u)$.

Substituting (4.59) in (4.57), the feedback type controller is obtained by

$$\begin{bmatrix} \hat{\boldsymbol{v}}[i+1] \\ \boldsymbol{u}[i] \end{bmatrix} = \begin{bmatrix} \hat{\boldsymbol{A}} + \hat{\boldsymbol{J}}\boldsymbol{F}\hat{\boldsymbol{C}} & \hat{\boldsymbol{b}} + \hat{\boldsymbol{J}}\boldsymbol{F}\hat{\boldsymbol{d}} \\ \boldsymbol{F}\hat{\boldsymbol{C}} & \boldsymbol{F}\hat{\boldsymbol{d}} \end{bmatrix} \begin{bmatrix} \hat{\boldsymbol{v}}[i] \\ y[i] \end{bmatrix}. \tag{4.67}$$

4.4.3 Initial Value Compensation

In this section, the initial value of the controller (4.67) is considered in order to eliminate the estimation error of the observer and satisfy (4.63). From (4.58), if $\boldsymbol{x}[0]$ is known, the initial value of controller should be set to

$$\hat{\boldsymbol{C}}\hat{\boldsymbol{v}}[0] = \boldsymbol{x}[0] - \hat{\boldsymbol{d}}y[0]. \tag{4.68}$$

By this compensation, it is possible to prevent the overshoot of the step (or initial value) response because the plant state converges only affected by the mode of the regulator. Therefore, $\boldsymbol{f}_{cp}$ should be designed to assign the eigenvalues of $\boldsymbol{A}_{Fcp}$ to the small (or zero) overshoot region.

4.5 Summary

In this chapter, novel discretization methods both for controllers and observers were developed based on multirate input and multirate output control. One of the remarkable

advantages was that perfect state matching (PSM) control could be assured independent of the sampling period, in which the states of the sampled-data system became equal to those of the continuous-time system. As a result, stability of the discretized system was guaranteed.

Next, the proposed method was extended to systems with long sampling periods relative to the control input. This extension assured perfect state matching at M intersample points. Moreover, by introducing the augmented system, the obtained digital controllers have internal models of disturbance.

Part II

Applications

Chapter 5

Applications of Perfect Tracking Control

5.1 Abstract

In this chapter, the perfect tracking control proposed in chapter 2 is applied to several motion control systems. First, the position control system of servomotors in robot manipulators is considered as an example without special hardware restrictions ($T_u = T_y$). Combining the proposed feedforward controller with a H_∞ robust feedback controller, perfect tracking performance is achieved with robustness. Second, the proposed method is applied to the track-seeking control of hard disk drive as an example with time delay and long sampling period relative to the control input ($T_u < T_y$). For this system, it is shown that the proposed controller enables higher speed movement compared with the conventional single-rate controller. Simulations and experiments both of servomotor and hard disk drive are performed, and advantages of this approach are demonstrated.

5.2 High Performance Tracking Control for Servomotor of Robot Manipulator

In this section, the proposed perfect tracking control method is applied to the position control system of the servomotor in a two-link direct-drive robot manipulator.

5.2.1 Experimental Setup of Robot Manipulator

The configuration of experimental setup is shown in Fig. 5.1, and photographs are shown in Fig. 5.2. A personal computer (CPU: AMD-K6-2 300MHz) is used both for real-time

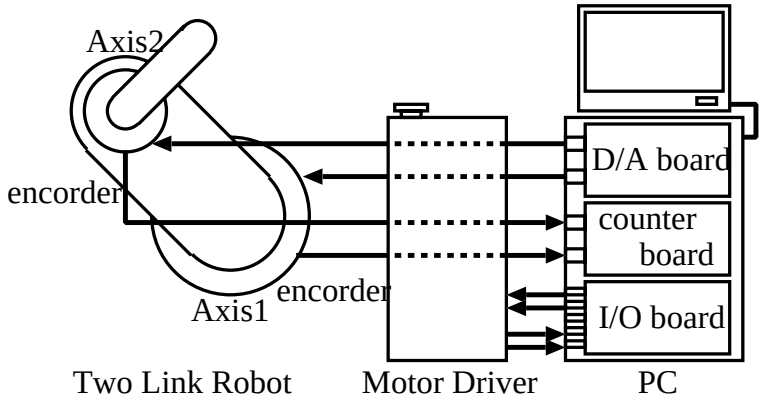

Figure 5.1: Configuration of experimental setup.

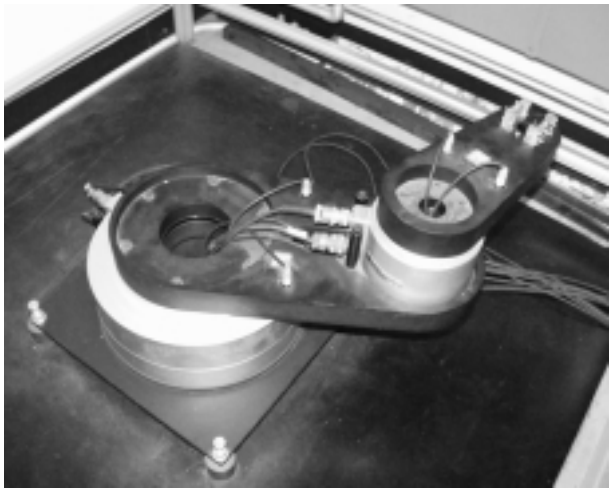

(a) Two-link direct drive robot.

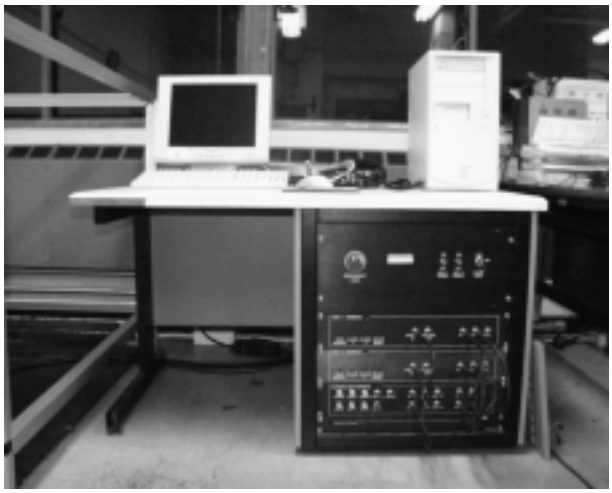

(b) Motor diver and control computer.

Figure 5.2: Photographs of experimental setup.

control of servomotors and development of software. In the PC, a D/A converter and a counter board are implemented to output the reference current and to input the motor angle. The servomotors are reluctance motors, where the current is controlled by the motor driver. The encoders generate 38 400 pulses per revolution. In order to realize real-time control, RTLinux is installed as the real-time operating system [98].

5.2.2 In Case without Hardware Restriction (Case 1: $T_y = T_u$)

First, the simplest example without hardware restrictions ($T_y = T_u$, case 1 in Fig. 2.9) is considered. The servomotor with current control is described by

$$P_c(s) = \frac{K}{Js^2}. \tag{5.1}$$

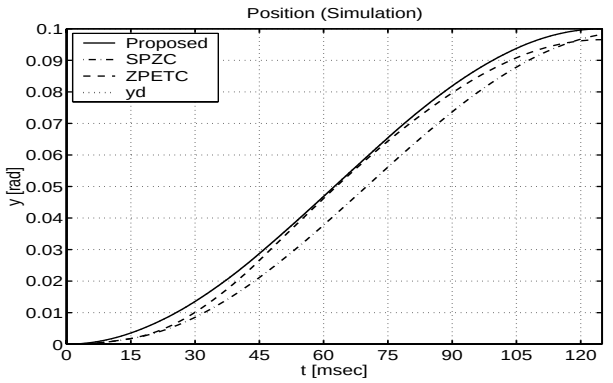

(a) Position

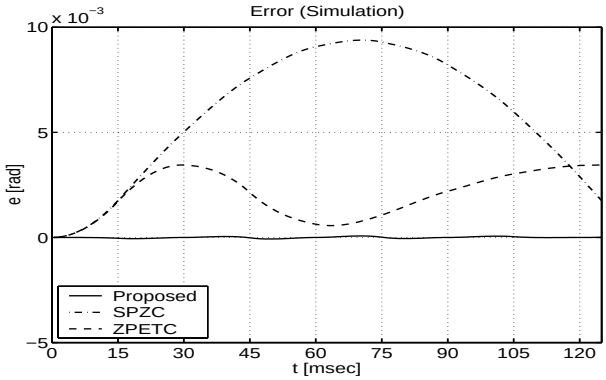

(b) Tracking error

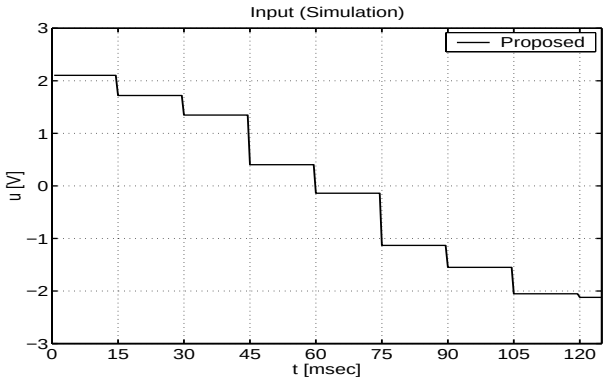

(c) Input

Figure 5.3: Simulation results ($T_y = T_u = 15$[ms])

The feedback controller $C_2[z]$ is a 3rd-order strictly proper system obtained from the continuous-time H_∞ mixed-sensitivity problem and Tustin transformation, which includes an integrator [75]. Calculating (2.20) and realizing the obtained $\boldsymbol{C}_1[z]$ and $\boldsymbol{C}_2[z]$ in minimum order, the controller $[\boldsymbol{C}_1, \boldsymbol{C}_2]$ becomes a 5th-order system.

Simulated and experimental results are shown in Fig. 5.3 and Fig. 5.4. The desired trajectory is a sinusoidal waveform represented by

$$\begin{aligned} \theta_d(iT_r) &= A(1 - \cos(\omega_{ref}\ iT_r)) \\ \omega_d(iT_r) &= A\omega_{ref} \sin(\omega_{ref}\ iT_r), \end{aligned} \tag{5.2}$$

where $\omega_{ref} = 2\pi \times 4$[rad/s]. In this system, both the input and output periods are $T_y = T_u = 15$[ms][1]. Because this plant is a 2nd-order system, the sampling period of the reference signal becomes $T_r = 30$[ms] ($N = 2$).

[1]In the experimental results (Fig. 5.4), the output signals are sampled at much shorter than 15 [ms] in order to display the intersample responses. The sampling period is set relatively long so as to make the comparison clear.

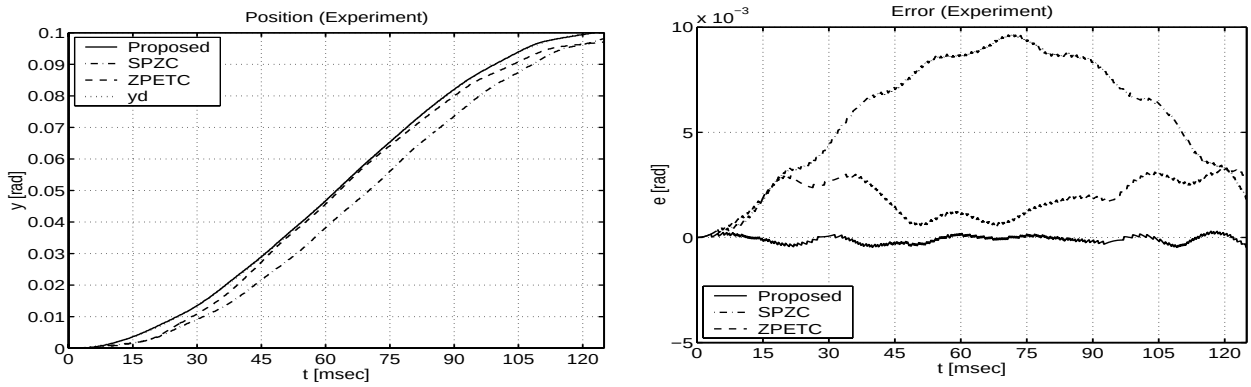

(a) Position

(b) Tracking error

Figure 5.4: Experimental results ($T_y = T_u = 15$[ms])

In the following simulations and experiments, the proposed method is compared with the SPZC and ZPETC proposed in [68], with the same T_y and T_u. The reference sampling period T_r of the proposed method is set twice as long as those of SPZC and ZPETC, because these methods are single-rate approaches and sampling periods are set to $T_y = T_u = T_r = 15$[ms]. However, the proposed controller utilizes the desired trajectories of both position and velocity, while SPZC and ZPETC use those of position only.

Fig. 5.3(a) and (b) show that the proposed method exhibits better performance than either SPZC or ZPETC. While the responses of SPZC and ZPETC include large tracking errors caused by the unstable zero, those of the proposed method have zero tracking error. The simulated time response of the control input is shown in Fig. 5.3(c), which indicates that the control input of the proposed method is smooth despite using multirate input control. Thus, we find that the proposed multirate feedforward method is very practical. Moreover, the experimental result also indicates that the proposed method has high tracking performance, as shown in Fig. 5.4. Fig. 5.3 and Fig. 5.4 also show that the intersample responses are very smooth, because not only position but also velocity follows the desired trajectories at every sampling point T_r.

The frequency responses from the desired trajectory $y_d[i]$ to the output $y[i]$ are shown in Fig. 5.5. Because the proposed method ensures perfect tracking control, the command response becomes 1 for all frequencies. In comparison, the gain of ZPETC decreases at high frequencies.

This example indicates that the proposed multirate feedforward controller has higher tracking performance than the single-rate controller even in the usual servo system ($T_y = T_u$) without special hardware restrictions.

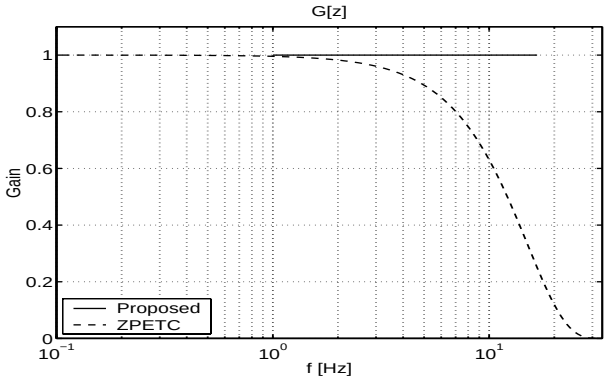

Figure 5.5: Frequency response $y[z]/y_d[z]$

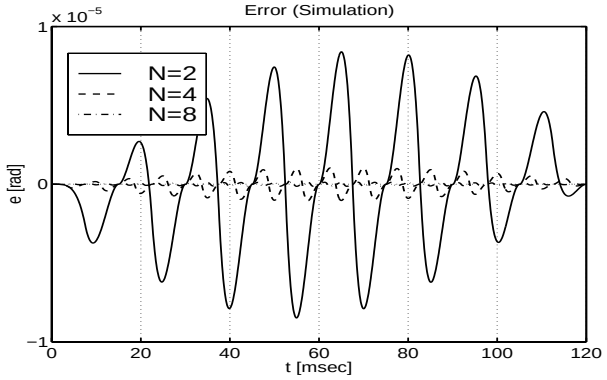

Figure 5.6: Simulation results ($T_y = 15$[ms], $T_u = T_y/N, T_r = 2T_u$).

5.2.3 In Case with Sampling Restriction (Case 2: $T_u = T_y/N$)

Next, it is assumed that the output sampling period is restricted to $T_y = 15$[ms] by the hardware, and the control input can be changed more frequently ($T_u = T_y/N$). In this case, perfect tracking control is guaranteed at L ($= N/n = N/2$) points during T_y. The single-rate feedback controller is designed with a 15[ms] period, and transformed by (2.38).

Fig. 5.6 shows the simulated tracking error of the proposed method for a 4 [Hz] sinusoidal desired trajectory. Compared with $N = 2$, the tracking performance is improved very much for large input multiplicities of $N = 4$ and 8, because perfect tracking control is ensured at L ($= N/2$) intersample points. This approach is applied to seeking control of hard disk drives in section 5.3.

5.2.4 Consideration of the intersample tracking error

As the proposed method assures perfect tracking control at every sampling point, in this section, the frequency response from the desired output to the tracking error is considered

including the intersample behavior.

When a sinusoidal desired output with angular frequency ϕ_0 is added to this sampled-data tracking control system, the intersample tracking error is composed of infinitely many sinusoidal components with angular frequencies

$$\phi_m \triangleq \phi_0 + m\omega_s \tag{5.3}$$

where $m = 0, \pm 1, \pm 2, \cdots$, and $\omega_s = \frac{2\pi}{T}$ [38]. Therefore, the classical theories in both continuous-time and discrete-time cannot be used to analyze the intersample behavior.

Analysis methods of the frequency response of sampled-data systems including intersample behavior are presented in [38] and [37]. These approaches have obtained the gain of the intersample response in infinite frequencies. However, in this section, the frequency response from sinusoidal desired trajectory with single frequency to intersample tracking error is considered because the frequency of the desired trajectory can be assumed to be below the Nyquist frequency. In practice, this concept is important in sampled-data control system [49].

Therefore, frequency responses of the error ratio of intersample tracking errors are numerically calculated. The error ratio of the sampled-data system is simply defined as

$$E_R^2(j\omega_{ref}) \triangleq \frac{\int_0^h e_y^2(t)dt}{\int_0^h y_d^2(t)dt} \tag{5.4}$$

where the tracking error $e_y(t) = y_d(t) - y(t)$. Although the above definition (5.4) is different from those given in [38] and [37], it is sometimes very useful in analyzing a sampled-data system [49].

In this simulation, $y(t)$, $y_d(t)$, and period h are the plant position, the desired position, and the period of the desired trajectory $2\pi/\omega_{ref}$, respectively. The integrals in (5.4) are numerically calculated for the very small period $\Delta t (\ll T, h)$.

Calculated results of the error ratio of (5.4) are shown in Fig. 5.7, which indicates that the tracking error of the proposed method is $100 \sim 1000$ times better than that of ZPETC and SPZC [68]. In other words, the tracing performance including intersample behavior is $100 \sim 1000$ times superior.

5.2.5 Comparison with the zero assignment method by multirate control

A significant feature of the proposed method is that the coefficient matrices of the state equation are directly assigned by multirate control (see (2.16)). Owing to this advantage, the proposed controller can be simply designed without considering the unstable zero problem.

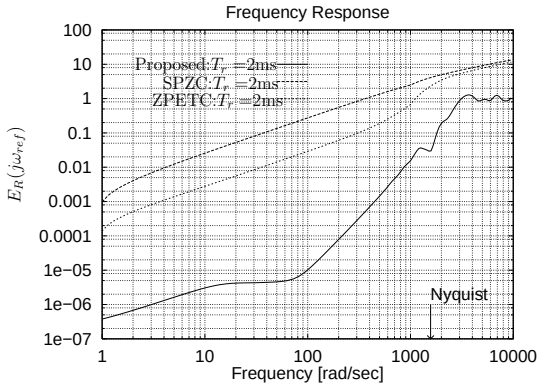

Figure 5.7: Frequency responses of the intersample tracking error.
(The error ratio (5.4) vs. frequency of the desired trajectory ω_{ref})

On the other hand, [3, 7, 8] had presented zero assignment methods by the multirate control. Historically, it was one of the most remarkable results of the multirate sampling control [1], as mentioned in section 1.1.1.

In this section, the zero assignment method of [3, 7] is applied to perfect tracking control, and compared with the proposed method. Next, the advantages of the proposed multirate feedforward control are demonstrated through simulations.

Zero assignment method by multirate control

In this section, the zero assignment method by multirate sampling presented in [3, 7] is reviewed.

For the discrete-time plant (2.7) discretized by multirate control, let the control law be

$$\boldsymbol{u}[i] = \boldsymbol{g}v[i] \ , \quad \boldsymbol{g} \stackrel{\triangle}{=} [g_1, \cdots, g_n]^T. \tag{5.5}$$

Substituting (5.5) for (2.7), the new discrete-time system is described by

$$\boldsymbol{x}[i+1] = \boldsymbol{A}\boldsymbol{x}[i] + \boldsymbol{B}\boldsymbol{g}v[i]. \tag{5.6}$$

The transfer function from the new input $v[i]$ to the output $y[i]$ is given by

$$\frac{y[i]}{v[i]} = \boldsymbol{c}_c[z\boldsymbol{I} - \boldsymbol{A}]^{-1}\boldsymbol{B}\boldsymbol{g} = \frac{\boldsymbol{c}_c adj(z\boldsymbol{I} - \boldsymbol{A})\boldsymbol{B}\boldsymbol{g}}{det(z\boldsymbol{I} - \boldsymbol{A})}. \tag{5.7}$$

Because the numerator polynomial of (5.7) becomes $(n-1)$th order for almost all T, all zeros of the new system (5.7) can be arbitrarily assigned by the parameter $\boldsymbol{g} \in \boldsymbol{R}^n$.

Next, consider the perfect tracking controller utilizing this method. First, the parameter $\boldsymbol{g}$ is chosen to match the system (5.7) with a model $M[z]$ which does not have unstable

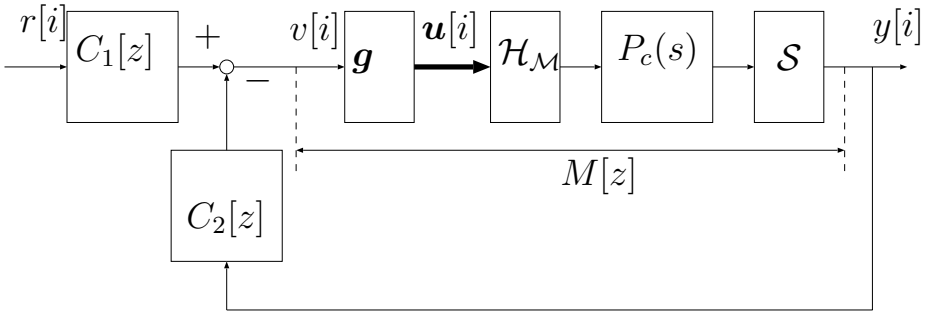

Figure 5.8: Perfect tracking system by the zero assignment method

zeros. Second, the feedback controller $C_2[z]$ is designed to stabilize the closed-loop system and to increase the robust performance. Third, let the feedforward controller $C_1[z]$ be

$$C_1[z] = \frac{1}{z^d G_{cl}[z]} = \frac{1 + M[z]C_2[z]}{z^d M[z]} \tag{5.8}$$

where $G_{cl}[z]$ is the closed-loop system composed of both $M[z]$ and $C_2[z]$, and d is the relative degree of $G_{cl}[z]$. Letting the reference be d-step ahead of the desired output, i.e. $r[i] = y_d[i+d]$, perfect tracking can be achieved. This control scheme is resented by Fig. 5.8.

Comparison by simulations

Consider the servomotor described by (5.1). The discrete-time plant discretized by the zero-order hold is given by

$$P[z] = \frac{T^2 K}{2J} \frac{z+1}{(z-1)^2}. \tag{5.9}$$

This discrete-time plant has an unstable zero at -1. Thus, utilizing multirate control (5.5), let the transfer function (5.7) match the following model $M[z]$ with a stable zero.

$$M[z] = \frac{T^2 K}{2J} \frac{z}{(z-1)^2} \tag{5.10}$$

From the above condition, the parameter $\boldsymbol{g}$ becomes

$$\boldsymbol{g} = [1.5, -0.5]^T. \tag{5.11}$$

The feedback controller $C_2[z]$ is obtained from the H_∞ mixed-sensitivity problem for $M[z]$, and the perfect tracking controller $C_1[z]$ is designed by (5.8).

The simulation results for a sinusoidal desired trajectory are shown in Fig. 5.9. While tracking error of the proposed method is almost zero, the zero assignment method has large tracking error in the intersample response as shown in Fig. 5.9(a). Moreover, Fig.

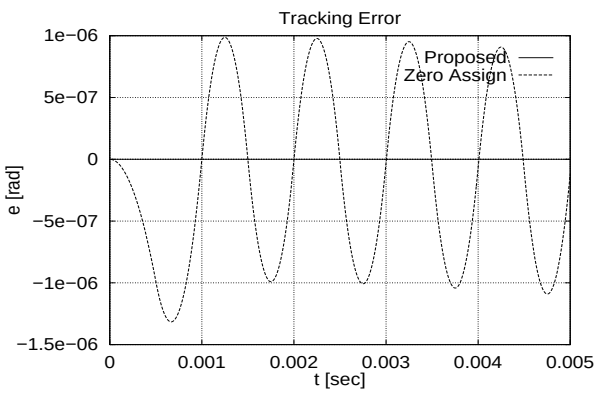

(a) Tracking errors

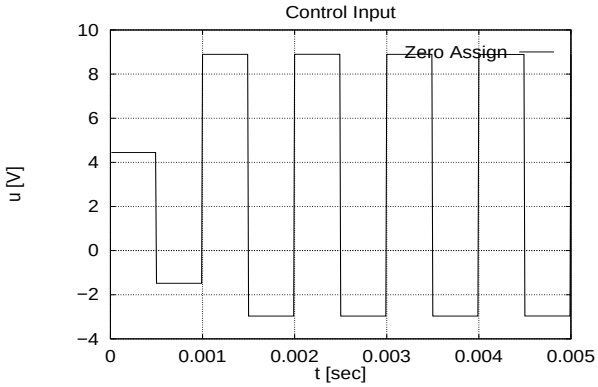

(b) Control input

Figure 5.9: Simulation results of the zero assignment method. ($T = 1$[ms])

5.9(b) indicates that the zero assignment method is not practical because its control input is highly oscillating. These problems of the zero assignment method have been indicated in [24]. According to [24], the zero assignment methods sometimes have the disadvantages of large overshoot and oscillation in the intersample points because the control input changes back and forth very quickly.

As a result, it is found that the perfect tracking controller realized by the zero assignment method [3, 7] has poorer tracking performance than the proposed method with regards to the intersample response. The reason is that the zero assignment method forces the zero to be arbitrarily assigned, and due to this, some stress may occur in the control loop, and the control input becomes oscillating.

On the other hand, the proposed method has no stress at any point of the control loop because all states of the plant are controlled to track the desired trajectory of the plant state. As a result, it can be said that the proposed multirate feedforward control is a significant and practical methodology for designing the multirate control system.

5.3 High Speed Seeking Control of Hard Disk Drive

5.3.1 Head-positioning System of Hard Disk Drive

In the head-positioning control of hard disk drives, the control strategy is divided into three modes: seeking mode, settling mode, and following mode. In the seeking mode, the head is moved to the desired track as fast as possible. Next, the head is settled to the track without overshoot in the settling mode. After that, the head needs to be positioned on the desired track while the information is read or written. In the following mode, the head is positioned precisely on the desired track under the vibrations generated by disk rotation and other disturbances.

In long-span seeking, where the seeking distance is comparatively long, high speed seeking is achieved by the mode-switching controller [99]. In the short-span seeking, however, single mode controllers based on two-degree-of-freedom control have advantages, because the mode-switching controller sometimes generates undesirable transient response [53, 54, 100, 101].

As shown in Fig. 5.10, in head-positioning control by the voice coil motor (VCM), the head position is detected by the servo signals embedded in the disks discretely. Therefore, the output sampling period T_y is decided by the number of these signals and the rotation frequency of the spindle motor. However, it is possible to set the control period T_u shorter than T_y because of the recent developments of computer technology. Thus, the controller can be regarded as a multirate control system having the hardware restriction of $T_u < T_y$.

In section 2.4, digital control systems having the hardware restriction of $T_u < T_y$ were assumed, which is defined as case 2 in Fig. 2.9(b), and a novel design method of the multirate feedforward controller was proposed. The proposed method achieved perfect tracking control (PTC) which has zero tracking error at M intersample points of T_y. Moreover, the proposed method was extended to systems with time delay in section 2.5.1. In HDD, multirate controllers have also demonstrated higher performance in both feedforward [54, 53] and feedback [50, 51, 55] characteristics. In this section, the proposed perfect tracking controller is applied to the track-seeking mode of HDD.

5.3.2 Modeling of the plant

The experimental setup is a 3.5-inch hard disk drive. Let the nominal model of this plant be

$$P_c(s) = \frac{K_f K_a}{M_p s^2} e^{-sT_d}. \tag{5.12}$$

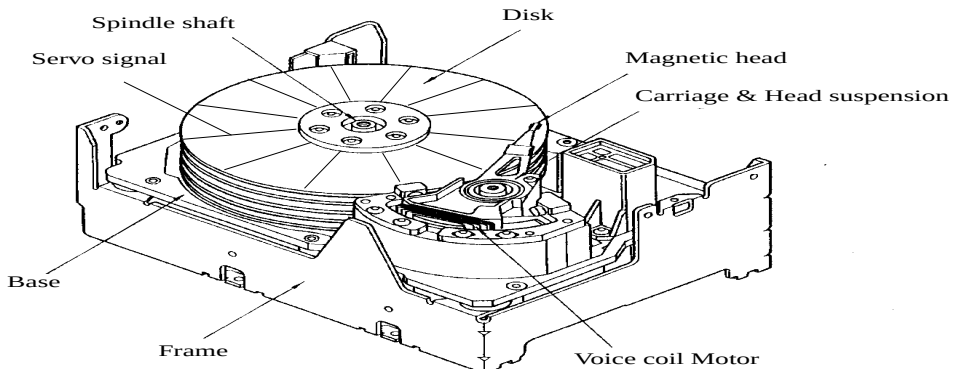

Figure 5.10: Hard disk drive.

Table 5.1: Parameters of 3.5-inch hard disk drive

Amplifier gain	K_a	1.996	A/V
Force constant	K_f	2.95	N/A
Mass	M_p	6.983	g
Track pitch	T_p	3.608	μm/trk
Sampling time	T_s	138.54	μsec
Calculation delay	T_{calc}	38	μsec
Equivalent delay	T_{equiv}	38.7	μsec
Input multiplicity	N	4	

The parameters of this plant are shown in Table 5.1. While servo signals are being detected at a constant period of about 138 [μs], the control input can be changed 4 times. Therefore, the proposed approach is applicable to this plant. In (5.12), the time delay $T_d = T_{calc} + T_{equiv}$ is considered, where T_{calc} is the calculation delay of the processor, and T_{equiv} is the equivalent delay of the current control and the notch filter for the second mechanical resonance mode. As shown in Fig. 5.11, the actual plant has the first mechanical resonance mode at around 2.7 [kHz] and the Nyquist frequency is at 3.6 [kHz]. In spite of these, the target seeking-time is set to 3 sampling periods (2.4 [kHz]) for one track seeking in the experiments.

Although only the rigid mode is included in the nominal model in this section, higher order models will be considered with the mechanical resonance mode in section 7.3.

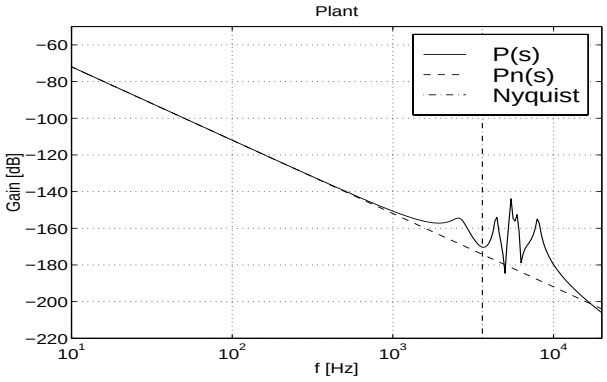

Figure 5.11: Frequency responses of plant.

5.3.3 Applications of perfect tracking controller to seeking mode

The perfect tracking controller is designed for input multiplicity $N = 4$. Because the plant is a second order system ($n = 2$), perfect tracking is assured $N/n = 2$ times during every sampling period. In the following simulations and experiments, the proposed method is compared with ZPETC proposed in [68]. The ZPETC is one of the most well-known and important feedforward controllers for control of mechanical systems. [53] and [100] applied it to hard disk drive control.

The control period T_u of ZPETC becomes four times as long as that of the proposed method because ZPETC is a single-rate controller[2] and the two methods are compared for the same sampling period T_y. The feedback controllers of the two methods are the same single-rate PI-Lead filter. Moreover, the desired trajectory (5.13) is selected, such that jerk (differential acceleration) is smooth in order not to excite the mechanical resonance mode.

$$y^*(s) = \frac{A_r}{s(\tau_r s + 1)^4} e^{-sT_d} \tag{5.13}$$

$$v^*(s) = \frac{A_r}{(\tau_r s + 1)^4} e^{-sT_d} \tag{5.14}$$

The parameters of these desired trajectories are shown in Table 5.2. In these experiments, the multirate feedforward input $\boldsymbol{u}_0[i]$ in Fig. 2.6 and Fig. 2.11 is obtained by off-line calculation in order to save processor resources. Therefore, the order of the feedforward controller and the desired trajectory are not related to the calculation time delay.

[2] [53, 102] attempted to extend ZPETC to multirate controllers.

Table 5.2: Parameters of the trajectories.

	A_r[trk]	$f_r(=1/2\pi\tau_r)$ [kHz]
Condition A	1	2.8
Condition B	6	1.7

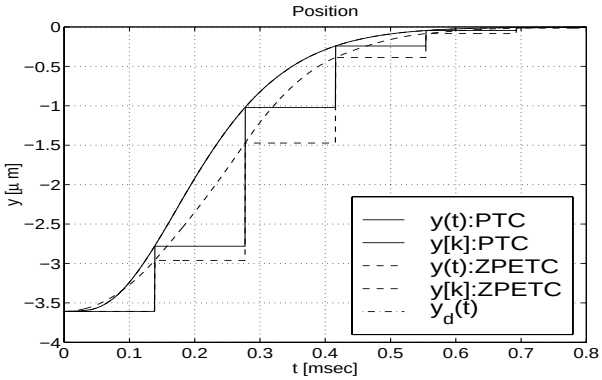

(a) Position

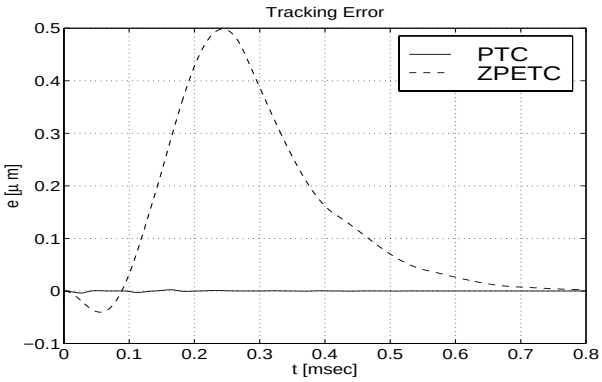

(b) Tracking error

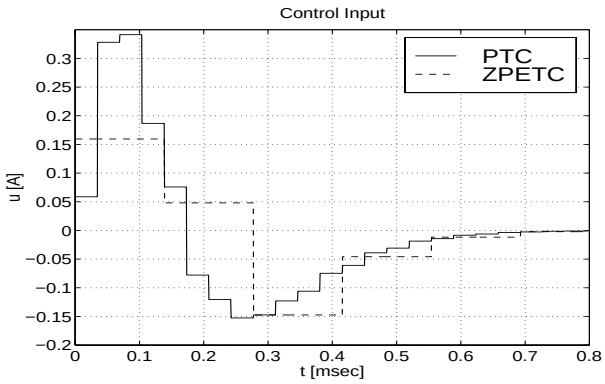

(c) Control input

Figure 5.12: Simulation results A (1trk).

Simulation results

Simulation results are shown in Fig. 5.12 and Fig. 5.13. The figures (a) and (b) show that the proposed method gives better performance than ZPETC. While the response of ZPETC has large tracking errors caused by the unstable zero, that of the proposed method has almost zero tracking error. Fig. (c) also indicates that the proposed multirate input is very smooth.

The frequency responses from the desired trajectory $y_d[i]$ to the output $y[i]$ are shown in Fig. 5.14. Because the proposed method (PTC) assures perfect tracking, the command

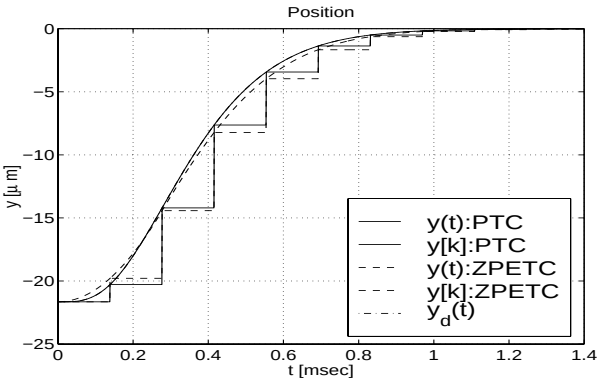

(a) Position

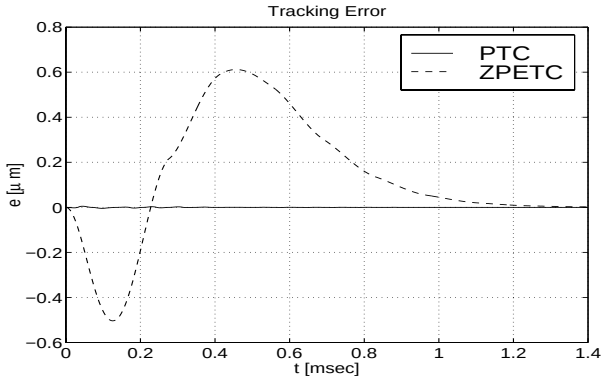

(b) Tracking error

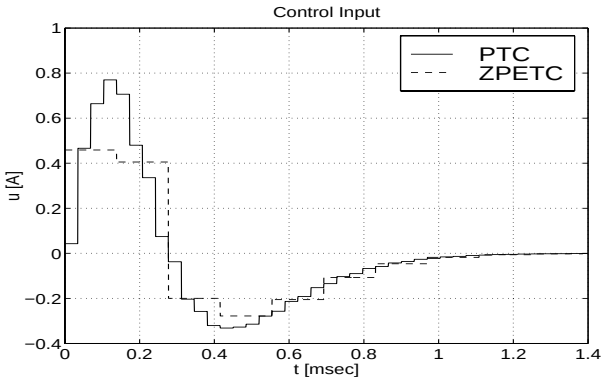

(c) Control input

Figure 5.13: Simulation results B (6trk).

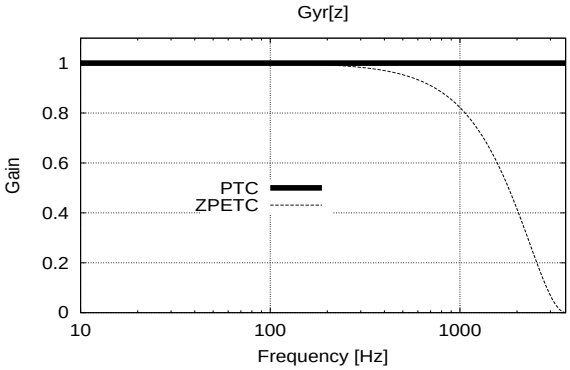

Figure 5.14: Frequency responses ($y[z]/y^*[z]$).

response becomes 1 at all frequencies. However, the gain of ZPETC decreases at high frequencies. The frequency of the short-span seeking is about 2 [kHz], therefore, the proposed method has advantages in high speed seeking control.

In the above simulations, the time delay was assumed to be zero ($T_d = 0$). Next,

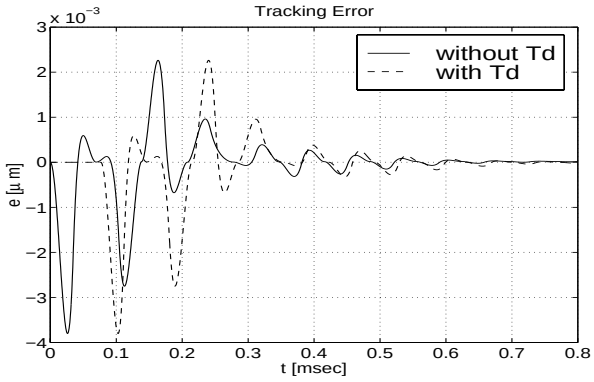

Figure 5.15: Simulation results with time delay (Condition A).

Fig. 5.15 shows the tracking errors including time delay $T_d = 76.7[\mu s]$, indicating that the tracking error becomes zero at $2(= M)$ intersample points without any loss of the tracking performance in spite of the existence of the time delay.

Experimental results

Experimental results are shown in Fig. 5.16 and Fig. 5.17. In figure (a), about 1,000 experimental data are overlaid. The figures (b) and (c) are the averages of the data, showing that the proposed method has high tracking performance. Although the actual plant has a mechanical resonance mode at around 2.7 [kHz], this mode is not suppressed by the notch filter in order to preserve the phase margin. In spite of that, the experiment under condition A (1 [trk]) adopts the wide bandwidth desired trajectory ($f_r = 2.8$ [kHz]) for high speed seeking. Therefore, Fig. 5.16(a)(b) have a overshoot of maximum height 0.4 [μm]. However, this overshoot is within the permissible range because the overshoot is small for HDD, compared to the track pitch of 3.6 [μm].

Because the position signal is detectable only at the sampling points, the difference between the proposed method and ZPETC is not clear in Fig. 5.16 and Fig. 5.17. Therefore, the proposed method is compared by using the average of the seeking-times measured in 2000 experiments. The seeking-time is defined as the time from the start of seeking to the point where the distance remaining falls under 0.4 [μm] and the overshoot is smaller than 0.4 [μm].

Table 5.3 shows the average seeking-times obtained in the experiments. The seeking-time of the proposed method (PTC) is much smaller than that of ZPETC and the conventional settling control [99]. In short-span seeking (1 [trk]), the seeking-time of the proposed method is 19 and 31 [%] shorter than that of ZPETC and the conventional method, respectively. In middle-span seeking (6 [trk]), the proposed method is 1 and 6

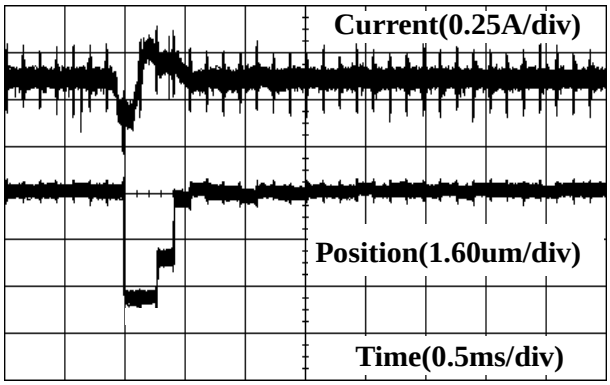

(a) 1000 times seeking

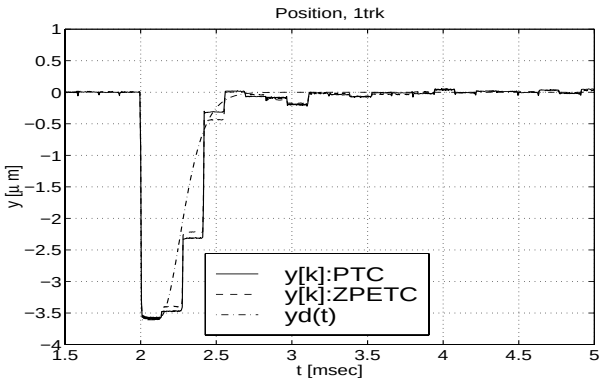

(b) Position (average)

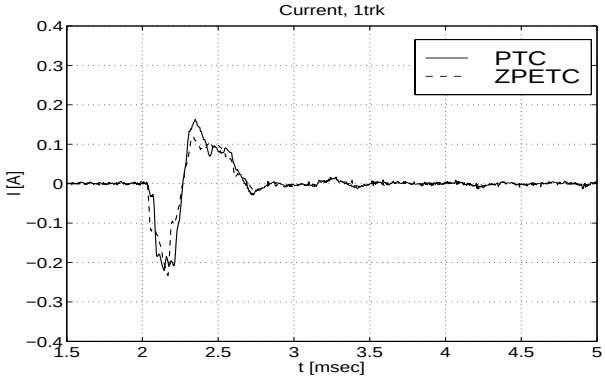

(c) Current (average)

Figure 5.16: Experimental results A (1trk).

Table 5.3: Experimental seeking-time.

	PTC [ms]	ZPETC [ms]	Conventional [ms]
A	0.4394	0.5226	0.5738
1trk	$(3.17T_s)$	$(3.77T_s)$	$(4.14T_s)$
B	1.200	1.325	1.933
6trk	$(8.66T_s)$	$(9.57T_s)$	$(14.0T_s)$

sampling periods faster respectively.

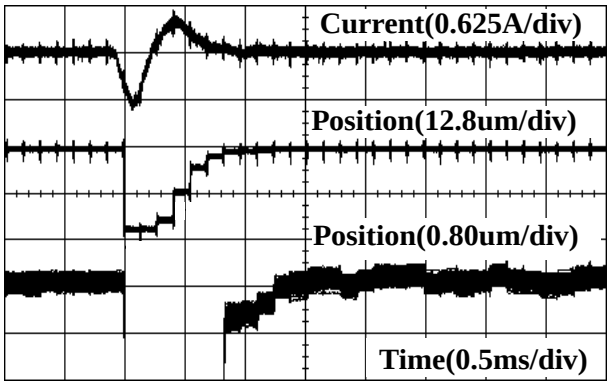

(a) 1000 times seeking

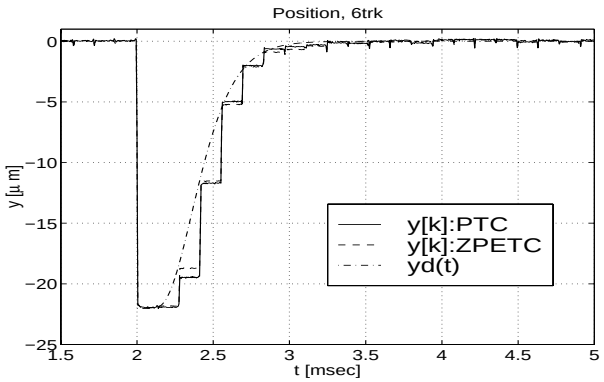

(b) Position (average)

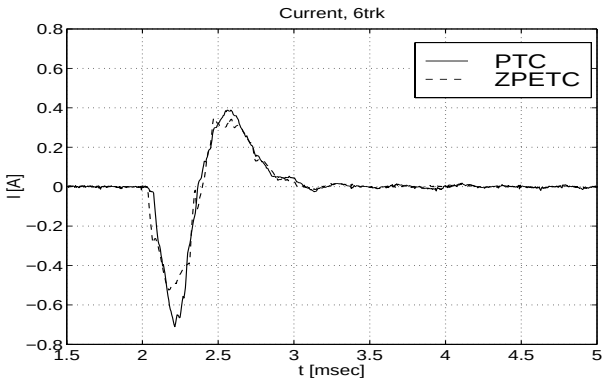

(c) Current (average)

Figure 5.17: Experimental results B (6trk).

5.4 Summary

In this chapter, the perfect tracking control developed in chapter 2 was applied to the motion control systems.

In section 5.2, two examples of position control using the servomotor of a robot manipulator were examined, and the advantages of the proposed method were demonstrated through simulations and experiments. The first example demonstrated that the proposed multirate controller had higher performance than the conventional single-rate controller, even in normal systems ($T_y = T_u$) without special hardware restrictions. The second example also indicated that the intersample response was improved by multirate feedforward control for systems with a long sampling period ($T_y > T_u$).

Next, in section 5.3, the proposed method was applied to the track-seeking mode of hard disk drives. The simulations and experiments demonstrated that the perfect tracking controller succeeded in achieving very fast seeking compared with the conventional

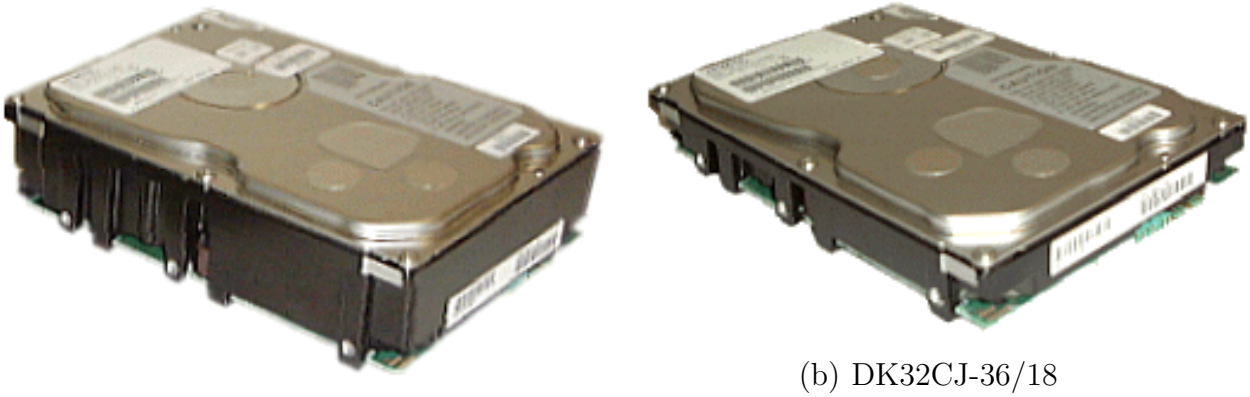

(a) DK31CJ-72

(b) DK32CJ-36/18

Figure 5.18: Products with perfect tracking controller.

methods. These experiments were performed in cooperation with Hitachi. After the experiments, Hitachi engineers have improved and implemented the proposed method in the latest drives shown in Fig. 5.18. According to the specifications of these products [103], the seeking time has improved very much compared with the products of other manufactures. The proposed method has partly contributed to the high data rate in these products.

Chapter 6

Applications of Perfect Disturbance Rejection

6.1 Abstract

In this chapter, the perfect disturbance rejection (PDR) control developed in chapter 3 is applied to motion control systems in which the sampling period of the sensor is shorter than the control period of the actuator. As examples, we look at the track-following mode of hard disk drives (HDD) and the visual servo system of robot manipulators. First, the perfect disturbance rejection controller is applied to the first-order disturbance mode of repeatable runout in HDD based on multirate feedback control. Second, the problem of the feedback approach is explained for higher disturbance modes, and the open-loop observer with switching function is implemented in order to overcome the problem. The intersample observer also compensates for the large delay generated by the hold and improves the stability margin of the closed-loop system. Finally, the proposed method is applied to visual servo systems by introducing the workspace controller and perspective transformation.

6.2 High Precision Following Control of HDD by PDR with Intersample Observer

6.2.1 Track Following Mode of Hard Disk Drive

In this section, the perfect disturbance rejection (PDR) control system proposed in chapter 3 is applied to the track-following mode of hard disk drives. The block diagram of the following mode is shown in Fig. 6.1. The disturbance $d_y(t)$ represents vibration of the

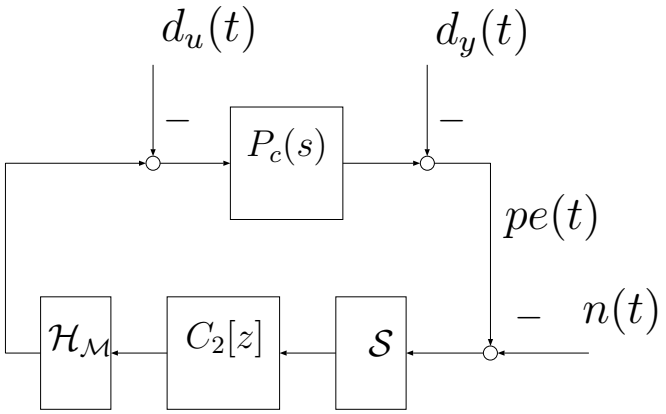

Figure 6.1: Following mode.

track generated by disk rotation, which is called track runout. The objective of this mode is to position the head on the desired track while information is being read or written and keeping the position error $pe(t)$ zero. $n(t)$ and $d_u(t)$ represent measurement noise and acceleration disturbance, respectively.

In the following mode, two kinds of disturbance should be considered: repeatable and non-repeatable runout. Repeatable runout (RRO) is synchronous with the disk rotation, and non-repeatable runout (NRRO) is asynchronous. There exist three approaches to reject RRO; (1) repetitive control, (2) feedback control based on the internal model principle, and (3) identification and feedforward control. In this section, the RRO is modeled by a sinusoidal disturbance, and it is perfectly rejected at M intersample points in the steady state. Therefore, the proposed approach of this section belongs to category (2).

6.2.2 Effects of perfect disturbance rejection and intersample observer

The controlled plant is the 3.5-inch hard disk drive used in section 5.3.2. The nominal plant is modeled by

$$P_c(s) = \frac{K_f K_a}{M_p s^2} e^{-sT_d}. \tag{6.1}$$

The parameters of this plant are shown in Table 5.1 of the previous chapter.

The disturbance models are considered as follows.

$$\text{(A)} : d(s) = \frac{1}{s(s^2 + \omega_R^2)}, \quad \text{(B)} : d(s) = \frac{1}{s} \tag{6.2}$$

The model (A) makes the sensitivity function $S(s)$ small at low frequencies and the rotation frequency of the disk $\omega_R (= 2\pi 120)$. The model (B) is introduced for comparison

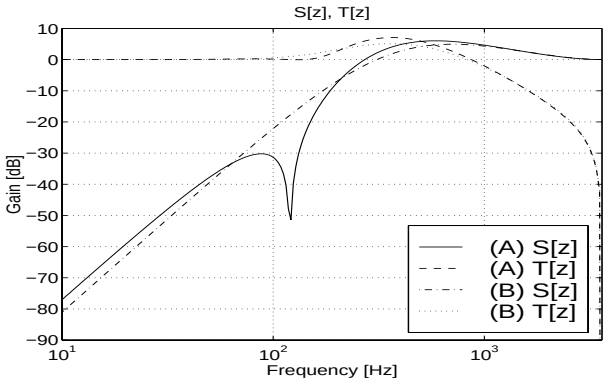

(a) $S[z], T[z] : N = 1$

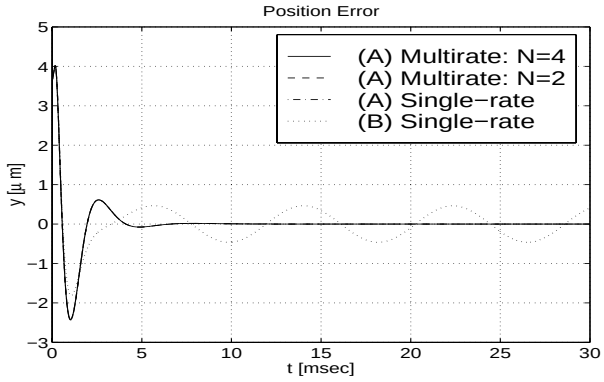

(b) Position error

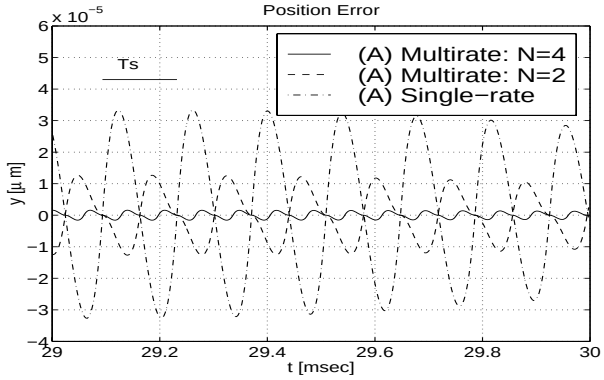

(c) Position error in steady state

Figure 6.2: Simulated results on the following mode.

with conventional PI-lead filters, because the controller consisting of state-feedback and disturbance observer for (B) becomes 2nd order with an integrator. In this section, only first order repeatable runout is considered as the disturbance model (A). However, high order runout is considered in section 6.3.

The perfect disturbance rejection controllers are designed with $N = 2, 4$. The proposed method is compared with the single-rate disturbance observer, in which the disturbance is modeled by $d[z] = Z[d(s)]$.

All poles of the regulator and observer are assigned to $\exp(-2\pi f_{cl} T_s)$ as shown in Table 6.1. These poles are selected to set the open-loop 0 dB cross-over to about 500[Hz]. Fig. 6.2(a) shows the sensitivity and complimentary sensitivity functions ($S[z]$ and $T[z]$) for model (A) and (B).

Effects of Perfect Disturbance Rejection Control

Fig. 6.2 shows the simulated results for a 120[Hz] sinusoidal runout added from $t = 0$, with amplitude 1 [trk] = 3.6[μm]. Although the transient position errors are large, the steady state position errors of the controller (A) become zero at the sampling points, because the feedback controller has the internal model of the RRO. However, Fig. 6.2(c) shows that the intersample responses have tracking error even in the steady state. It is shown that errors of the plant position and velocity become zero at every $T_s/M(= 2T_s/N)$ for the proposed controllers. Moreover, the intersample position errors of the proposed multirate methods are much smaller than that of the single-rate controller. Fig. 5.6 and Fig. 6.2(c) have very similar results indicating that the performance improves with increase of the input multiplicity both in the feedforward and the feedback characteristics.

Consideration of Time Delay in Perfect Disturbance Rejection Control

In the above simulations, the time delay is assumed to be zero ($T_d = 0$) for simplification. Next, the extended PDR with time delay is introduced, which was proposed in section 3.3.4. Fig. 6.3(a) shows the frequency response of the sensitivity and complementary sensitivity functions with time-delay[1]. Compared with the case of $T_d = 0$, the sensitivity worsens due to the time delay although the poles of both closed-loop systems are set to be identical. Thus, the convergence of the transient response for $T_d = 75$ [μs] becomes slower than that for $T_d = 0$, as shown Fig. 6.3(b). However, Fig. 6.3(c) shows that disturbance rejection performance in the steady state is maintained by the extended controller, and perfect disturbance rejection is achieved at $M(= N/2)$ intersample points.

Effects of Intersample Observer

The open loop characteristics are shown in Table 6.1 and Fig. 6.4. It is shown that the gain and phase margin are increased by the multirate feedback using the proposed intersample observer, in the same way as [50, 89]. However, this is the first attempt to reject RRO by multirate feedback control, thus, these results are significant in showing that the stability margin is recovered by multirate control for model (A). Moreover, in the proposed intersample observer, calculation resources can be saved because the feedback gain (3.33) is obtained by off-line calculation. The proposed scheme is applicable to various plants and types of disturbance because the proposed theory is very general.

[1]Some parameters such as T_s of Fig. 6.3 are set to be different from those of Fig. 6.2 in order to make Fig. 6.3(c) clear.

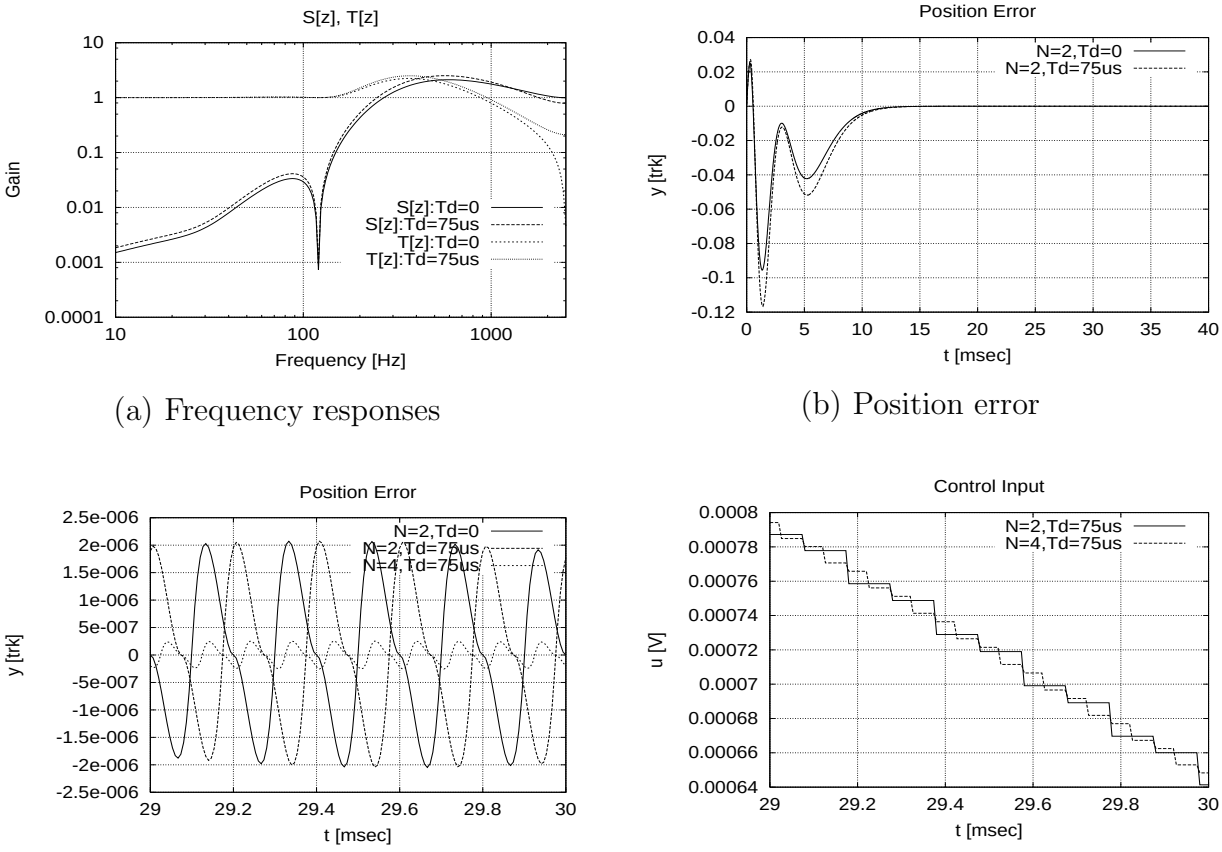

(a) Frequency responses

(b) Position error

(c) Position error (fine view)

(d) Control input (fine view)

Figure 6.3: Simulated results of PDR with time delay ($T_y = 200[\mu s], T_d = 75[\mu s]$)

Table 6.1: The open loop characteristics.

Disturbance Model	A	A	B	B
Input multiplicity N	1	4	1	4
Closed-loop poles f_{cl}	240	240	390	390
Gain margin [dB]	-6.93	-6.95	11.9	12.5
180 deg cross-over [Hz]	249	249	1573	1635
Phase margin [deg]	29.5	29.6	35.8	36.2
0 dB cross-over [Hz]	507	510	505	506

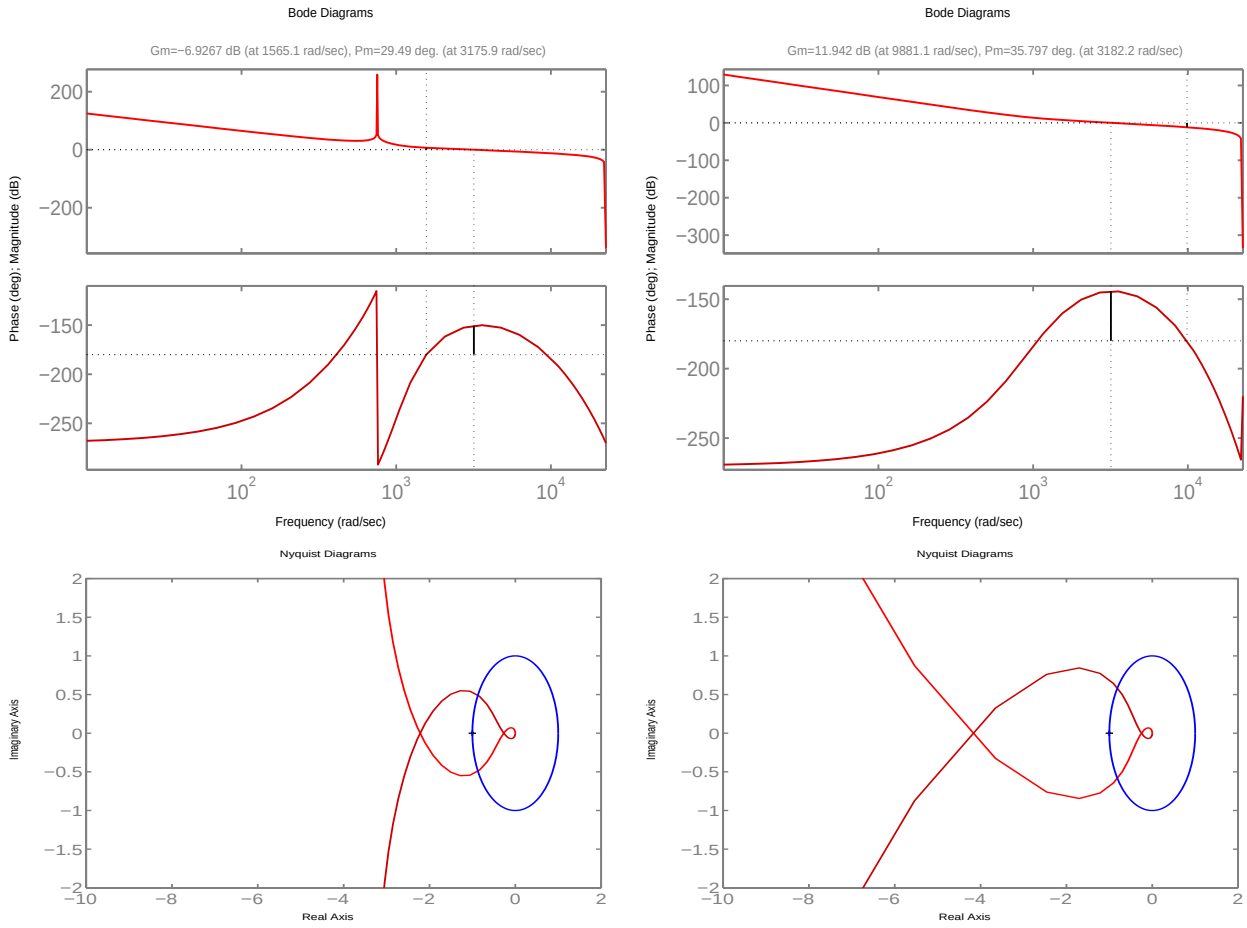

Model (A) Model (B)

Figure 6.4: Frequency responses of open loop characteristics ($N = 1$)

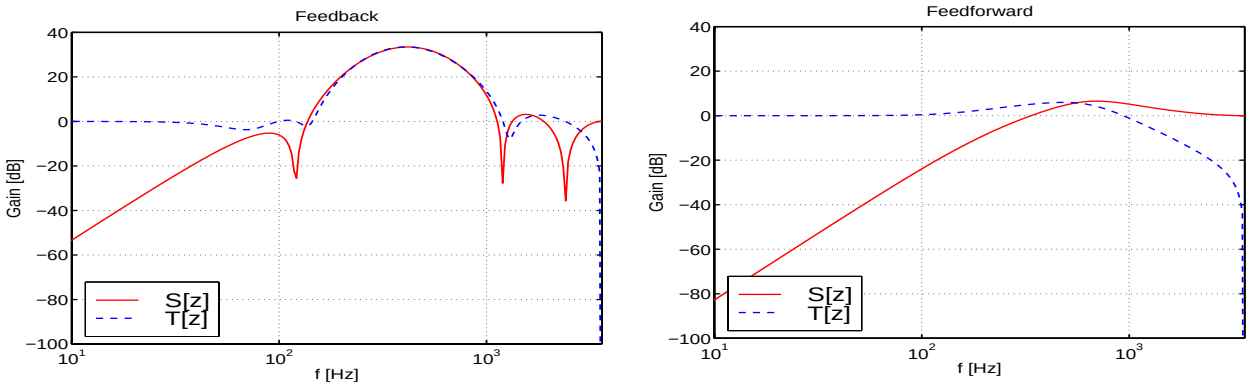

(a) Feedback

(b) Feedforward

Figure 6.5: Frequency responses $S[z], T[z]$.

6.3 High-order Periodic Disturbance Rejection Control for HDD

6.3.1 Feedforward and Feedback Repetitive Control

In this section, the multirate repetitive controllers proposed in section 3.4 are applied to the track-following mode of hard disk drives.

The nominal plant is modeled by

$$P_c(s) = \frac{K_f K_a}{M_p} \frac{1}{s^2}, \tag{6.3}$$

where the parameters of the plant are shown in Table 5.1. High order repeatable runout is considered at 1st, 10th, and 20th order[2], and modeled by

$$d(t) = \sum_{k=1,10,20} a_k \cos k\omega_0 t + b_k \sin k\omega_0 t, \tag{6.4}$$

where $\omega_0 = 2\pi 120$[rad/sec].

Fig. 6.5 shows the closed-loop characteristics both of the feedback (Fig. 3.2) and feedforward (Fig. 3.5) repetitive control systems. Fig. 6.5(a) indicates the disadvantages of the feedback repetitive controller, where the closed-loop characteristics worsens and it becomes difficult to assure stability robustness. On the other hand, in the proposed feedforward repetitive control (Fig. 3.5), the closed-loop characteristics depend only on $\boldsymbol{C}_2[z]$ which does not need to have the internal model of (6.4). Therefore, the feedback characteristics are better than those of the feedback approach as shown in Fig. 6.5(b).

[2]In practice, several large modes should be selected through experimental analysis.

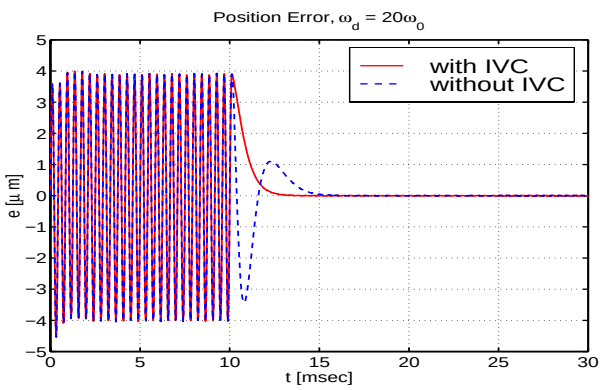

(a) Position error

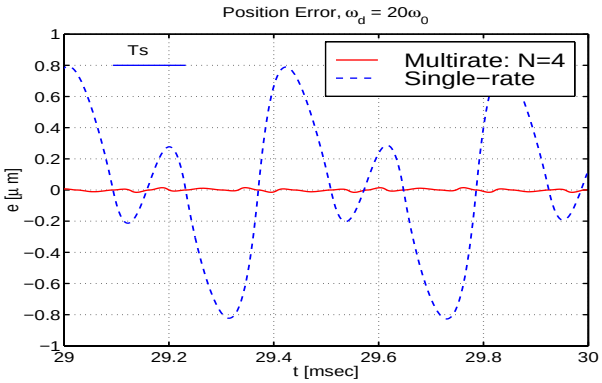

(b) Steady state

Figure 6.6: Feedforward repetitive control.
$d_y(t) = T_p \sin k\omega_0 t, T_p = 3.6\mu m, k = 20.$

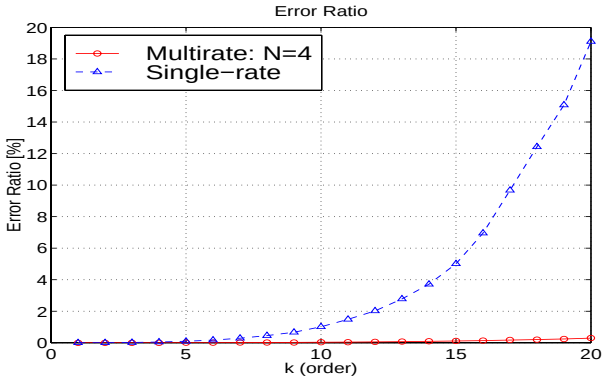

Figure 6.7: Error ratio $E_R(k)$.
(20th order corresponds to 2.4 [kHz].)

Fig. 6.6 shows the simulated results of the proposed repetitive feedforward control under the 20th order sinusoidal runout. The switch turns on only at $t_0 = 10$[ms]. As shown in Fig. 6.6(a), the position error converges quickly after the switching action. Moreover, it is shown that the proposed initial value compensation (IVC) can prevent the large overshoot. Fig. 6.6(b) shows that the intersample response of the conventional single-rate controller has large errors in the steady state. On the other hand, the errors of the plant position and velocity become zero at every $T_y/2$ with the proposed controllers[3]. Moreover, the intersample position error of the proposed multirate method is much smaller than that of the single-rate controller.

Fig. 6.7 shows analyzed results of the error ratio $E_R(k)$ for the disturbance order k.

[3]In the proposed method, perfect disturbance rejection is assured $M(= N/n_p = 4/2 = 2)$ times during T_y.

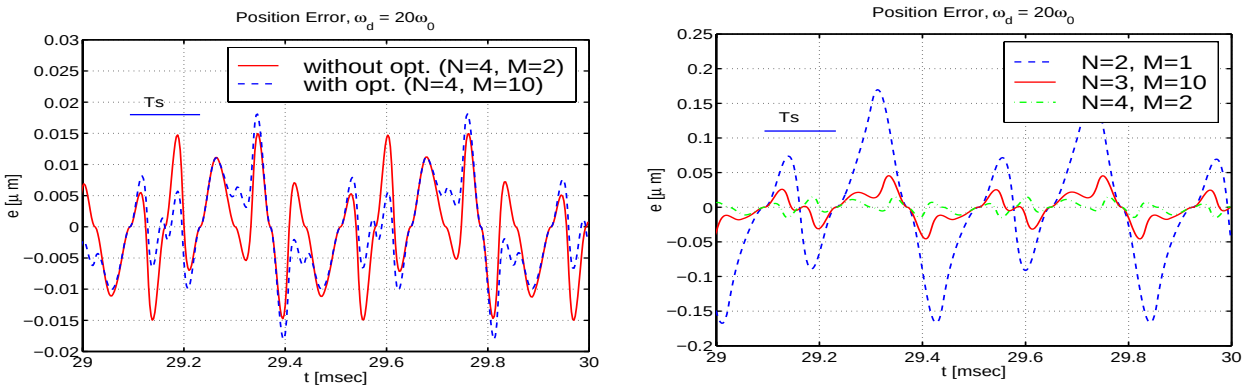

(a) with optimization

(b) $N = 2, 3, 4$

Figure 6.8: Optimized intersample response.

Considering the intersample response, the error ratio is calculated by

$$E_R^2(k) \triangleq \frac{\int_{t_s}^{t_s+kT_0} pe^2(t)dt}{\int_{t_s}^{t_s+kT_0} d_y^2(t)dt}, \tag{6.5}$$

where $d_y(t) = T_p \sin k\omega_0 t, T_0 = 2\pi/\omega_0$, and t_s is selected as 20[s] in order to evaluate the steady state. In the high frequency region close to the Nyquist frequency (3.6[kHz]), the disturbance rejection performance is much improved by the proposed multirate control, compared with the single-rate controller. Therefore, it is shown that the proposed method demonstrates effective performance for high-order disturbance.

6.3.2 Optimization of the Intersample Performance

In the above simulations (Fig. 6.5 $\sim$ 6.7), the state multiplicity is selected as $M = N/n(= 2)$ to reject the disturbance perfectly at M intersample points. In Fig. 6.8, however, the intersample performance is optimized by (3.51).

As shown in Fig. 6.8(a), the optimized intersample response of $M = 10$ is not much improved compared with the case without optimization of $M = 2$. Therefore, it can be said that the selection of $M = N/n$ proposed in section 3.4.1 is reasonable in the engineering sense because $\boldsymbol{F}_d$ of (3.26) is simpler than that of (3.51) and PDR is intuitively understandable. However, the optimization approach is valuable because it is applicable to the case where N/n is non-integer. As shown in Fig. 6.8(b), the intersample performance is improved with higher input multiplicity N.

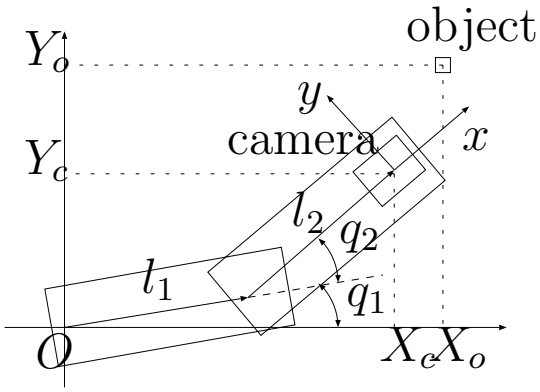

Figure 6.9: Two-link DD robot with camera.

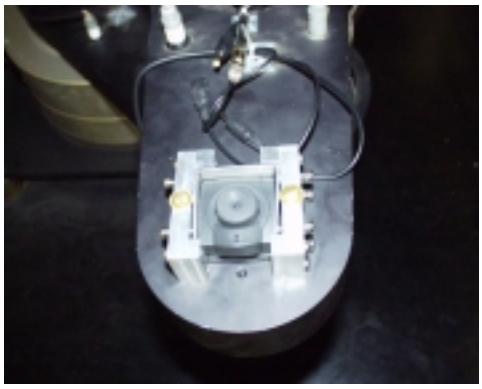

Figure 6.10: Photographs of robot with camera.

6.4 Visual Servoing of Robot Manipulator by Repetitive Disturbance Rejection Control

6.4.1 Sampling Restriction in Visual Servo System

In this section, the visual servo problem is considered [104, 105], in which the camera mounted on the robot manipulator tracks a moving object as shown in Fig. 6.9 and Fig. 6.10. Although the sampling period of the vision sensor such as a CCD camera is comparatively slow (over 33 [ms]), the control period of joint servo is fast (less than 1 [ms]). Therefore, multirate controllers have been developed and implemented in the visual servo system [56, 57, 58]. In this section, it is assumed that the motion of the object is periodic, and repetitive disturbance rejection control is applied based on the multirate feedback and feedforward approaches developed in section 3.4.

In order to focus on the dynamical problems of the multirate system, the kinematical problems of the visual servo system are assumed to be simple: the object movement is in

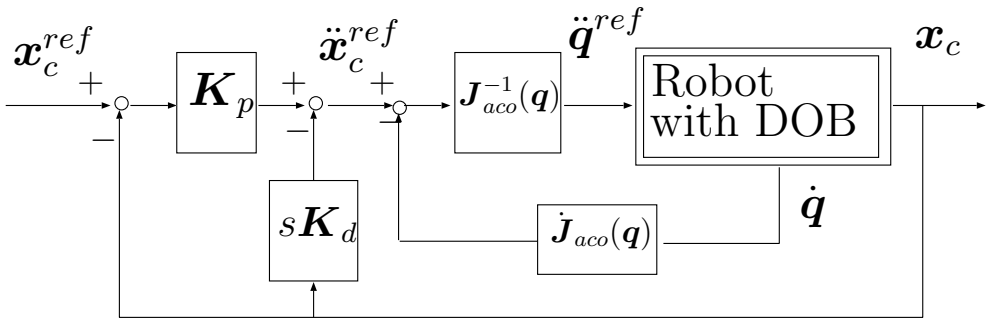

Figure 6.11: Workspace controller (inner-loop).

two-dimensional plane, and the depth information between the camera and the object z is known.

6.4.2 Modeling of Visual Servo System

First, the work space position controller is designed in order to control the camera position as shown in Fig. 6.11 [106]. Because this controller employs the robust disturbance observer (DOB) in the joint space, each joint axis is decoupled. Therefore, if the non-singularity of Jacobian $\boldsymbol{J}_{aco}$ is assured, the transfer function from the work space acceleration command $\ddot{\boldsymbol{x}}_c^{ref}$ to the work space position $\boldsymbol{x}_c(=[X_c, Y_c]^T)$ can be regarded as a double integrator system for the frequency region below the cut-off frequency [106]. Letting $\boldsymbol{x}_c^{ref}$ be the control input $\boldsymbol{u}$ of the outer visual servo system, the plant is modeled by the analog system (6.6) because the sampling period of the inner-loop is very short (1 [ms] in this experiment).

$$\boldsymbol{x}_c(s) = \boldsymbol{P}_c(s)\boldsymbol{u}(s), \quad \boldsymbol{P}_c(s) \stackrel{\triangle}{=} \frac{K_p}{s^2 + K_d s + K_p}\boldsymbol{I}_2 \tag{6.6}$$

In Fig. 6.11, the parameters of the position controller are set to $\boldsymbol{K}_p = diag\{100, 100\}$ and $\boldsymbol{K}_d = diag\{20, 20\}$.

Next, the perspective model of the camera is derived [107]. In Fig. 6.11, the object position (x, y) on the camera coordinate system is determined only by the relative position between the camera position $\boldsymbol{x}_c$ and object position $\boldsymbol{x}_o$. Therefore, the following model is obtained because (x, y) is mapped to the feature point $\boldsymbol{\xi}$ on the image plane, as shown in Fig. 6.12 [56].

$$\boldsymbol{\xi} = \frac{f}{z}\begin{bmatrix} x \\ y \end{bmatrix} = \frac{f}{z}\begin{bmatrix} \cos\theta & \sin\theta \\ -\sin\theta & \cos\theta \end{bmatrix}\begin{bmatrix} X_o - X_c \\ Y_o - Y_c \end{bmatrix} \tag{6.7}$$

Here f is the focus distance, z is the distance between the object and camera in the Z-axis direction, and $\theta \stackrel{\triangle}{=} q_1 + q_2$. Equation (6.7) is described by $\boldsymbol{\xi} = \iota(\theta)(\boldsymbol{x}_o - \boldsymbol{x}_c) = \iota(\theta)\boldsymbol{x}_e$.

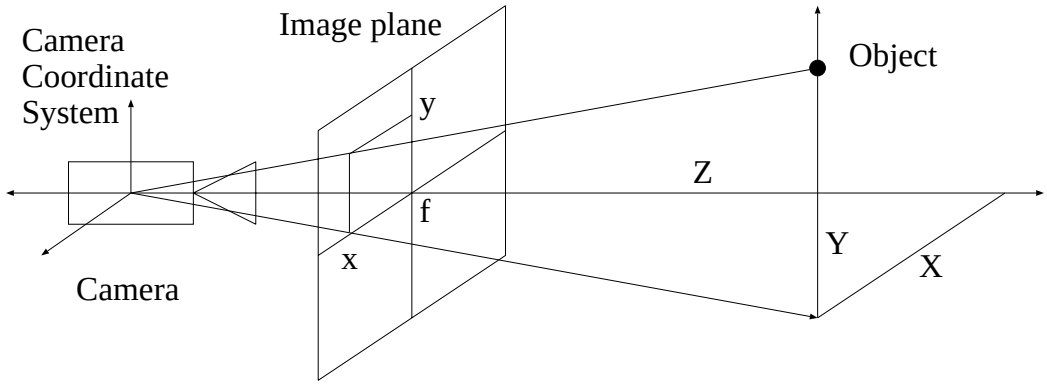

Figure 6.12: Perspective model

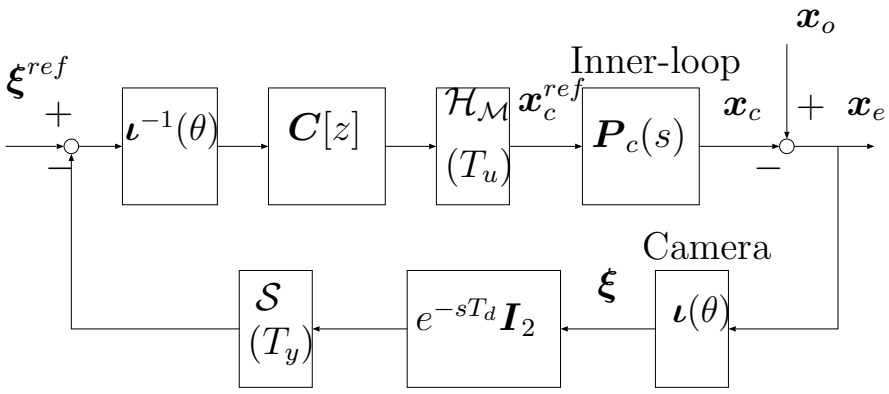

Figure 6.13: Visual servo system.

Fig. 6.13 shows the proposed control system. In this experiment, the desired feature $\boldsymbol{\xi}^{ref}$ is set to zero because the camera is controlled to be positioned just below the object. The movement of the object can be modeled as the output disturbance $\boldsymbol{x}_o$. Therefore, the proposed method can achieve high tracking performance because the periodic motion can be rejected by the proposed PDR. Moreover, the control system of Fig. 6.13 is linearized and diagonalized by the inverse transformation $\iota^{-1}(\theta)$ of (6.7)[4]. Thus, the controllers can be designed independently in the x and y axes. The sampling period of the image and the control period of the position command $\boldsymbol{x}_c^{ref}$ are set to $T_y = 100$ [ms] and $T_u = 25$ [ms], respectively. Because the input multiplicity is $N = 4$ and the order of plant (6.6) is $n = 2$, perfect disturbance rejection is assured at $2(= N/n)$ intersample points. T_d represents the time delay caused by image processing. Because this delay generates difficulty in control system, [108, 109, 110] have developed compensation methods for this delay, however, in this section, the time delay is assumed to be zero ($T_d = 0$) for simplification because the

[4]In case of the setup of Fig. 6.13, $\iota^{-1}(\theta)$ is easily obtained from the inverse matrix of (6.7). In general case, it can be calculated from the inverse Jacobian [105].

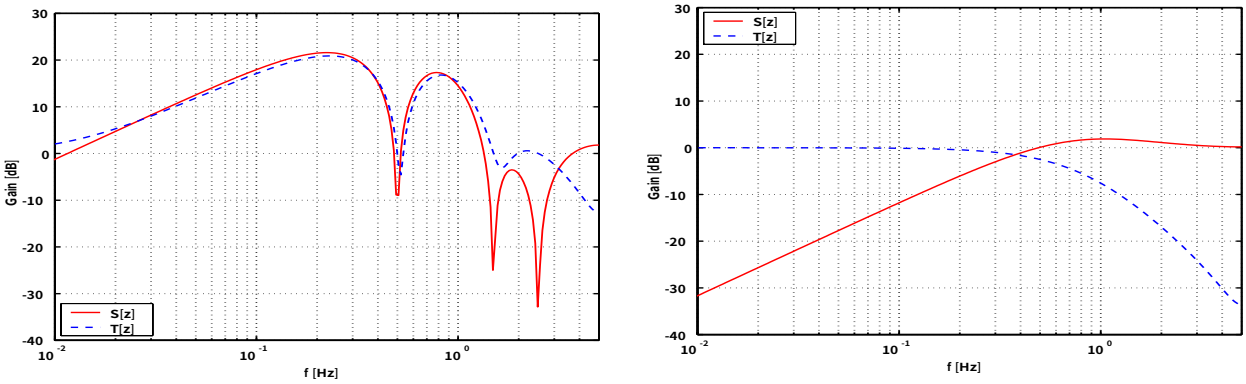

(a) Feedback

(b) Feedforward

Figure 6.14: Frequency responses $S[z], T[z]$.

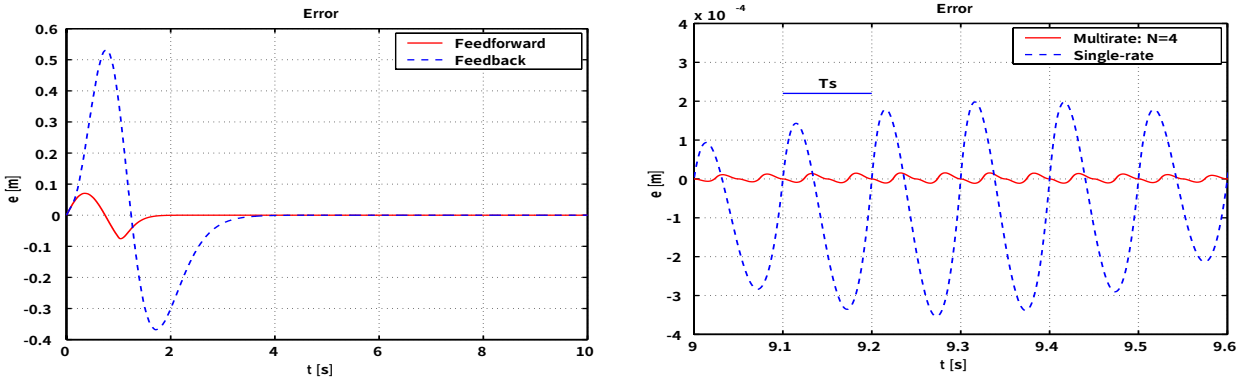

(a) Feedforward vs. Feedback

(b) Multirate vs. Single-rate

Figure 6.15: Position Error $X_o - X_c$ (simulation).

proposed perfect disturbance rejection control is applicable to systems with time delay, as demonstrated in section 6.2.2.

6.4.3 Simulation and experimental results

For the visual servo system, results parallel to those of the HDD in section 6.3 are obtained. In the experiments, the two-link direct drive robot mentioned in section 5.2 is utilized, and a personal computer is used both for joint servo control and image processing. The repetitive disturbance is modeled for k = 1st, 3rd, and 5th order. The period of the object's movement is $T_0 = 0.5$[s].

Fig. 6.14 shows the sensitivity and complementary sensitivity functions $S[z]$ and $T[z]$ both of the feedback (Fig. 3.2) and the feedforward (Fig. 3.5) control systems. Fig. 6.14(a)

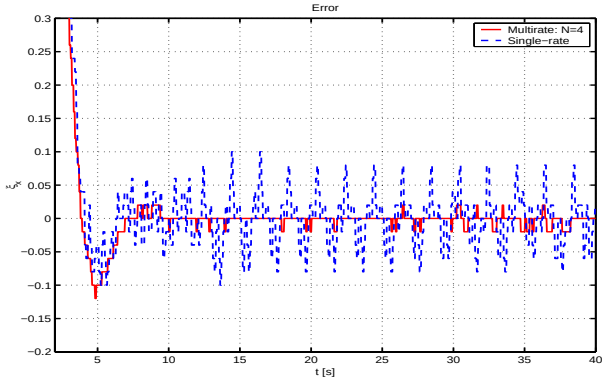

(a) Error in ξ_x

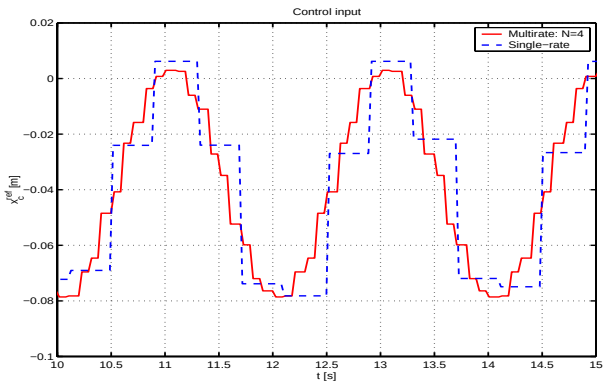

(b) Control input X_c^{ref}

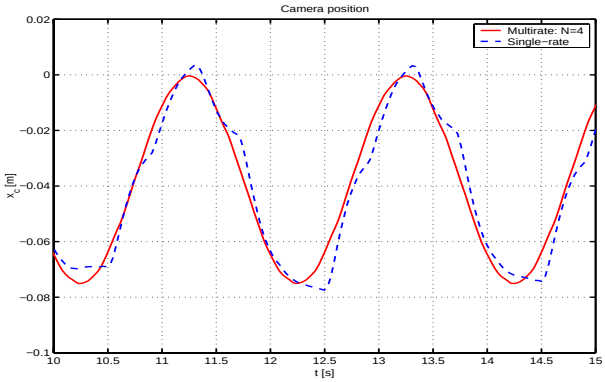

(c) Camera position X_c

Figure 6.16: Experimental results ($T_y = 400$ [ms], $N = 4$) .

indicates the disadvantages of the feedback repetitive controller, where the closed-loop characteristics worsen and it becomes difficult to assure stability robustness. On the other hand, in the proposed feedforward repetitive control (Fig. 3.5), the closed-loop characteristics depend only on $\boldsymbol{C}_2[z]$ which does not need to have the internal model of repetitive disturbance. Therefore, the feedback characteristics are better than those of the feedback approach for the visual servo system, just as they are for the HDD.

Fig. 6.15 shows the simulated results of position error $X_o - X_c$ for circular movement of the object. As shown in Fig. 6.15(a), the position error of the feedforward controller converges quickly after the switching action at $t_0 = 1.0$[s], while that of the feedback controller has large transient errors. In the steady state, the errors of the plant position and velocity become zero at every $T_y/2$ with the proposed controllers as shown in Fig. 6.15(b). The intersample position error of the proposed multirate method is much smaller than that of the single-rate controller.

The experimental results are shown in Fig. 6.16. In these experiments, the image is

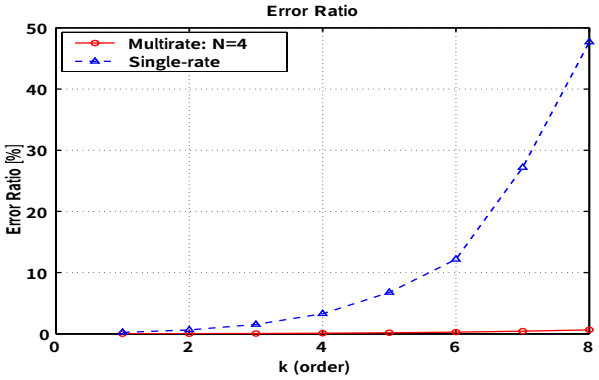

Figure 6.17: Error ratio $E_R(k)$.

detected at every 100 [ms]. In order to display the intersample response, the sampling period is set to $T_y = 400$ [ms] in the controller. Fig. 6.16(a) shows that the tracking error of the proposed multirate controller is much smaller than that of the single-rate controller. Moreover, as shown in Fig. 6.16(b) and (c), the camera position is very smooth because the multirate controller generates the intersample reference signal based on the disturbance model. Note that the amplitude and phase of the target movement are assumed to be unknown, and the information is estimated by the observer.

Fig. 6.17 shows analyzed results of the error ratio $E_R(k)$ for the disturbance order k. Considering the intersample response, the error ratio is calculated by

$$E_R^2(k) \triangleq \frac{\int_{t_0}^{t_0+kT_0}(X_o(t) - X_c(t))^2 dt}{\int_{t_0}^{t_0+kT_0} X_o^2(t) dt} \tag{6.8}$$

where $X_o(t) = \sin k\omega_0 t, \omega_0 = 2\pi/T_0$, and t_s is selected as 4 [s] in order to evaluate the steady state. In the high frequency region close to the Nyquist frequency, disturbance rejection performance is much improved by the proposed multirate control, compared with the single-rate controller. Therefore, it is shown that the proposed method demonstrates effective performance for high-order disturbance, just as for the case of HDD.

6.5 Summary

In this chapter, the perfect disturbance rejection (PDR) control developed in chapter 3 was applied to the track-following mode of hard disk drives (HDD) and visual servo systems of robot manipulators, having restrictions in the sampling mechanisms.

In section 6.2, the first order repeatable runout (RRO) of HDD was considered as a disturbance model, and it was perfectly rejected at M intersample points. Next, it was shown that in the steady-state performance is preserved even if the plant contains time

delay. Finally, the intersample observer was implemented, and analysis of the frequency response proved the recovery of the stability margin.

Second, in section 6.3, high order RRO was taken into account, and feedback and feedforward multirate control were compared. The advantage of the feedforward approach is demonstrated by the frequency response of the closed-loop system. Moreover, by the use of the optimization of intersample response, it was shown that the proposed PDR gave practical and reasonable results.

Third, in section 6.4, the proposed method is applied to the visual servo system of robot manipulators. By using the workspace controller with the robust joint servo system and the inverse transformation of nonlinear perspective transformation, the system becomes a linear system and applicable to the proposed theory.

Chapter 7

Applications of Perfect State Matching

7.1 Abstract

In this chapter, the perfect state matching (PSM) control developed in chapter 4 is applied to motion control systems based on multirate sampling control. First, the position control system for a dc servomotor with disturbance observer is utilized as an example without hardware restriction in the sampling scheme. Simulations and experiments are performed, and the advantages of this approach are demonstrated. Because the proposed method assures the response matching independent of sampling period, it enables to bring out the maximum performance of a control system.

Second, vibration suppression control is proposed based on multirate input control for a system in which the Nyquist frequency is relatively closed to the mechanical resonance mode and the sampling period is longer than the control period. For a two-mass system model of hard disk drive, simulations demonstrate the possibility of controlling the critical resonance mode.

7.2 Discretization of a Position Controller for Servomotor with Disturbance Observer

7.2.1 Discretization of Controller

In this section, the proposed discretization method is applied to the position control system for a dc servomotor with disturbance observer as shown in Fig. 7.1 based on the perfect state matching control.

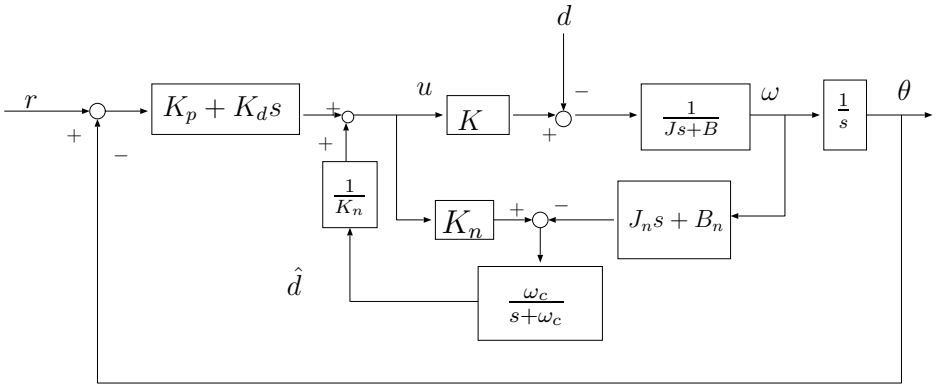

Figure 7.1: The position control with the disturbance observer.

In the experiments, DSP(NEC: μPD77230, 32-b floating point) is used, and the 1/100 gear ratio dc servomotor is driven by a 10-kHz switching frequency MOSFET chopper. The pulse counter generates 1 000 pulses per revolution on the motor shaft (it becomes 100 000 pulse/revolution on the geared shaft), and the speed is detected by a tachometer through a 12-b A/D converter [111].

In the design of the continuous-time controller, assuming that the disturbance torque d is a step function, the plant is represented by

$$\dot{\boldsymbol{x}}_{cp}(t) = \boldsymbol{A}_{cp}\boldsymbol{x}_{cp}(t) + \boldsymbol{b}_{cp}u_{cp}(t) \tag{7.1}$$

$$\boldsymbol{A}_{cp} = \begin{bmatrix} 0 & 1 & 0 \\ 0 & -\frac{B}{J} & -\frac{1}{J} \\ 0 & 0 & 0 \end{bmatrix}, \boldsymbol{b}_{cp} = \begin{bmatrix} 0 \\ \frac{K}{J} \\ 0 \end{bmatrix}, \boldsymbol{x}_{cp} = \begin{bmatrix} \theta \\ \omega \\ d \end{bmatrix}$$

where θ is angular position, ω is angular velocity, and u_{cp} is the dc voltage of the motor terminal. Assuming the command input r to be a step function, the continuous-time control law is given by

$$\begin{aligned} u_{cp} &= K_p(r-\theta) - K_d\omega + \tfrac{1}{K_n}\hat{d} \\ &= \boldsymbol{f}_{cp}\hat{\boldsymbol{x}}_{cp} + g_{cp}r \end{aligned} \tag{7.2}$$

where $\boldsymbol{f}_{cp} = [-K_p, -K_d, \frac{1}{K_n}], g_{cp} = K_p, \hat{\boldsymbol{x}}_{cp} = [\theta, \omega, \hat{d}]^T$. As shown in Fig. 7.1, the continuous-time disturbance observer is also given by

$$\begin{aligned} \dot{\hat{v}}_c(t) &= \hat{A}_c\hat{v}_c(t) + \hat{B}_c\omega(t) + \hat{J}_c u_{cp}(t) \\ \hat{d}(t) &= \hat{v}_c(t) + l_c\,\omega(t) \end{aligned} \tag{7.3}$$

where $\hat{A}_c = -\omega_c, \hat{B}_c = -B_n\omega_c + J_n\omega_c^2, \hat{J}_c = K_n\omega_c$, and ω_c is the cut-off frequency of the low pass filter.

The nominal values of the plant constants are $J_n = 0.0730$ [kg·m^2] , $B_n = 3.26$ [kg·m^2/s], $K_n = 0.388$ [N·m/V]. The continuous-time control parameters are $K_p = 8.91, K_d = -4.99, \omega_c = 300$ [rad/s].

First, the control law (7.2) is discretized. Although $(\boldsymbol{A}_{cp}, \boldsymbol{B}_{cp})$ in (7.1) is not controllable, the conditions in (4.27) are satisfied for input multiplicity $N_1 = 2$. From (4.28), the discretized control laws for $T = 0.4[ms], \mu_{11} = 0.5$ are obtained, as follows.

$$\begin{bmatrix} \boldsymbol{u}_{11}[i] \\ \boldsymbol{u}_{12}[i] \end{bmatrix} = \begin{bmatrix} -33.4 & 3.38 & 2.57 \\ -33.6 & 3.34 & 2.57 \end{bmatrix} \begin{bmatrix} \theta[i] \\ \omega[i] \\ \hat{d}[i] \end{bmatrix} + \begin{bmatrix} 33.4 \\ 33.6 \end{bmatrix} \boldsymbol{r}[i]$$

Second, the disturbance observer in (7.3) is redesigned in the same way as in section 4.3.3 [72]. For $T = 0.4$ [ms], $\mu_{11} = 0.5$, the discrete-time observer is obtained by

$$\begin{aligned} \hat{v}_d[i+1] &= \hat{A}_d \hat{v}_d[i] + \hat{B}_d \omega[i] + \hat{J}_{11} u_{11}[i] + \hat{J}_{12} u_{12}[i] \\ \hat{d}[i] &= \hat{v}_d[i] + l_d\, \omega[i] \end{aligned} \tag{7.4}$$

where $l_d = -20.8, \hat{A}_d = 0.887, \hat{B}_d = 1.99, \hat{J}_{11} = 2.12 \times 10^{-2}, \hat{J}_{12} = 2.21 \times 10^{-2}$.

7.2.2 Simulations and Experiments

Because the proposed method utilizes the multirate input control with $N = 2$, the output sampling period T is twice as long as the input sampling period T_u. In the following simulations and experiments, the proposed method is compared with the Tustin (bilinear) transformation with the same input sampling period in order to make the calculation costs of two systems equal for fair comparison. Therefore, the output sampling period of the proposed method is twice as long as that of the Tustin transformation.

Simulated and experimental results are shown in Fig. 7.2 and Fig. 7.3. For the very short sampling period (0.2 [ms]), we find that the Tustin transformation and the proposed transformation have almost the same time response. However, for the long sampling period (8 [ms]), as shown in Fig. 7.2 and Fig. 7.3(b), the proposed method gives better performance than the Tustin transformation. While the responses of Tustin transformation are unstable, those of the proposed method are stable, and exactly match the continuous-time responses.

The simulated time responses of the control input are shown in Fig. 7.2(c), which indicates that the control input of the proposed method is smooth despite using multirate control.

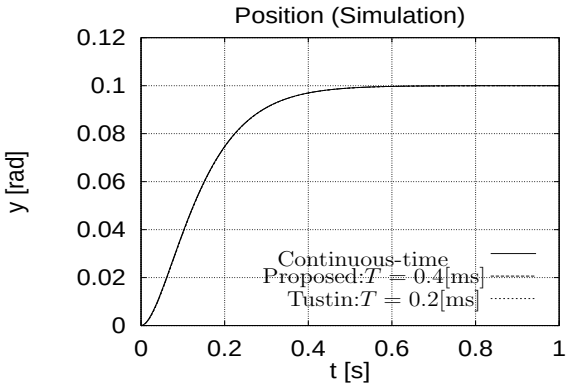

(a) Position responses ($T_u = 0.2[ms]$).

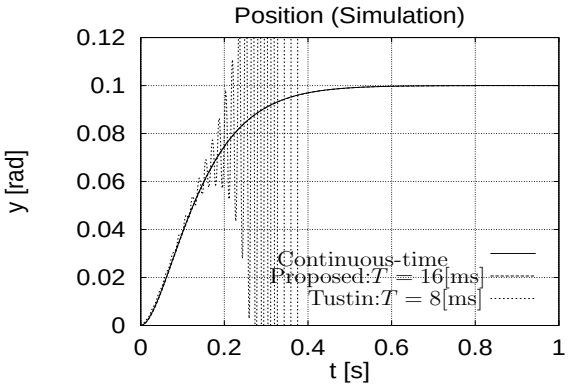

(b) Position responses ($T_u = 8[ms]$).

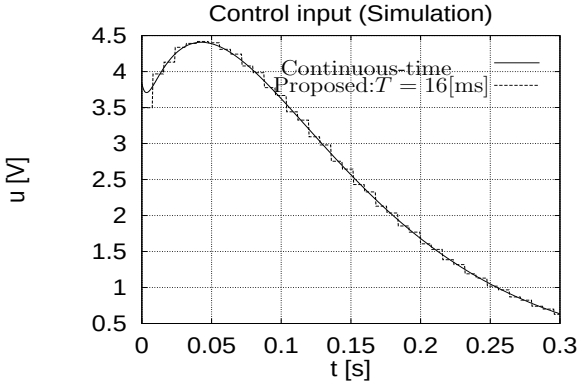

(c) Control input responses($T_u = 8[ms]$).

Figure 7.2: Simulation results.

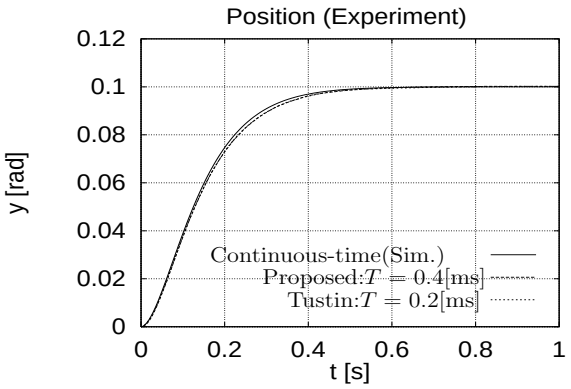

(a) Position responses ($T_u = 0.2[ms]$).

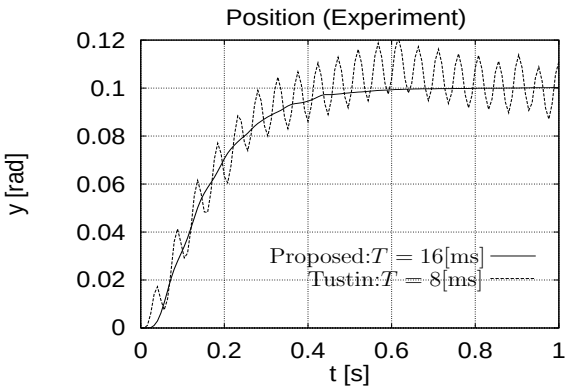

(b) Position responses ($T_u = 8[ms]$).

Figure 7.3: Experiment results.

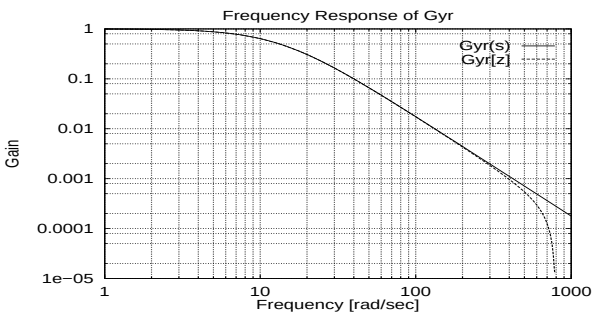

(a) Command responses (G_{yr}).

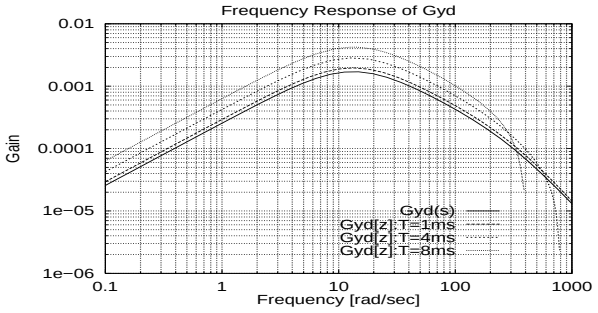

(b) Disturbance responses (G_{yd}).

Figure 7.4: Frequency responses.

7.2.3 Frequency Responses of the Closed-loop Systems

The frequency responses from the command input (r) to the plant state (θ) are shown in Fig. 7.4(a). In the wide frequency band below the Nyquist frequency, the discrete-time response obtained by the proposed method ($G_{yr}[z]$) matches the continuous-time response ($G_{yr}(s)$). That is guaranteed by (4.15), (4.22), (4.24) and (4.25).

The frequency responses from the disturbance torque (d) to the plant state (θ) are also shown in Fig. 7.4(b), which indicates that the longer the sampling period is, the poorer the disturbance rejection performance is. Therefore, Fig. 7.4(b) shows the practical limitations of the sampling period for the proposed method.

7.2.4 Disturbance Responses

The simulation results of the time responses for step function type disturbances (5 [N $\cdot$ m], t $>$ 1 [s]) are shown in Fig. 7.5. For the short sampling period (0.4 [ms]), the discretized system has almost the same performance as the continuous-time system. However, as mentioned above (Fig. 7.4(b)), the disturbance rejection performance becomes poor for the large sampling period (16 [ms]).

The time responses of the disturbance estimation errors are shown in Fig. 7.5(b). The estimation error of the discrete-time observer obtained by the proposed method completely matches that of the continuous-time observer at every sampling period. Fig. 7.5(b) also assures that there is no offset between the command input (r) and the plant state (θ).

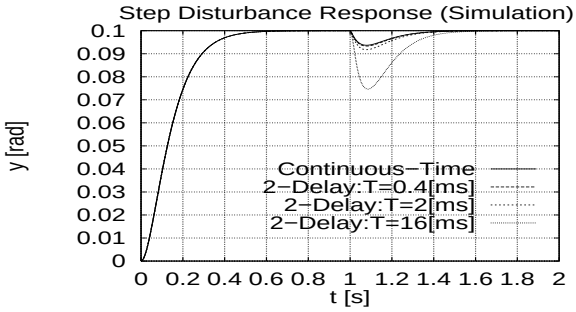

(a) Position responses.

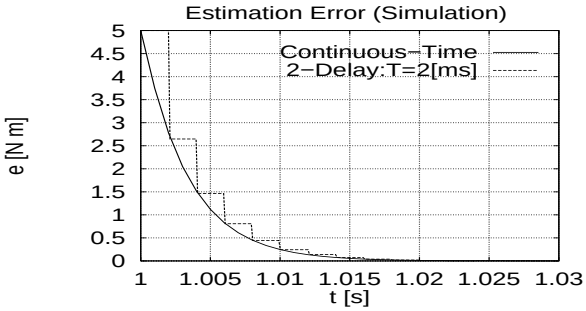

(b) Estimation errors of disturbance.

Figure 7.5: Responses under step type disturbance(simulation).

7.3 Vibration Suppression Control in Semi-Nyquist Frequency Region for HDD

7.3.1 Vibration Suppression Control with Sampling Restriction

Vibration suppression control is an important problem in motion control systems of steel rolling mill, flexible arm, large-scale space structure, hard disk drive, etc. Thus, a lot of controllers have been developed for two or multi-mass systems [112, 113, 114, 115].

However, if the resonance mode is relatively closed to the Nyquist frequency, it is very difficult to suppress this mode because conventional single-rate controllers do not have enough performance in the semi-Nyquist frequency region. In this section, a novel vibration suppression controller is proposed for this critical mode by introducing multirate input control. The proposed methods are further applied to the head-positioning system of hard disk drives.

Vibration suppression controllers have been proposed with various different approaches in the continuous-time system [112]. To implement them in digital control systems, the designed analog controllers are discretized by the Tustin transformation or other methods. Because these transformations are based only on the open-loop characteristics of the controller, the closed-loop has poor performance or becomes unstable when the resonance mode is close to the Nyquist frequency.

On the other hand, in section 4.3, a novel discretization method of controllers was proposed based on the perfect state matching (PSM) control with multirate sampling control, in which the closed-loop characteristics were taken into account. Moreover, in section 4.4, it was extended to systems with relatively long sampling periods. In this section, the proposed method is applied to the vibration suppression control system where the resonance mode is in the semi-Nyquist frequency region. The advantages of the proposed method are that 1) the controller is discretized based on the closed-loop characteristics, and 2) the plant state of the digitally controlled system completely matches that of the original continuous-time system at M inter-sample points during T_y.

7.3.2 Modeling of the plant with mechanical resonance mode

In this section, the proposed vibration suppression controllers are applied to the settling and following modes of the 3.5-inch hard disk drive used in section 5.3.2. Taking account of the mechanical resonance mode, let the nominal model of this plant be

$$P_c(s) = \frac{K_f K_a}{M_p} \frac{1}{s^2} \frac{\omega_{1n}^2}{s^2 + 2\zeta_{1n}\omega_{1n}s + \omega_{1n}^2}. \tag{7.5}$$

Table 7.1: Parameters of the 3.5-inch hard disk drive including mechanical resonance mode.

Amplifier gain	K_a	1.996	A/V
Force constant	K_f	2.95	N/A
Mass	M_p	6.983	g
Track pitch	T_p	3.608	μm/trk
Sampling time	T_s	138.54	μsec
Input multiplicity	N	4	
Mechanical resonance	ω_{1n}	$2\pi \times 2.7 \times 10^3$	rad/sec
Damping	ζ_{1n}	0.1	

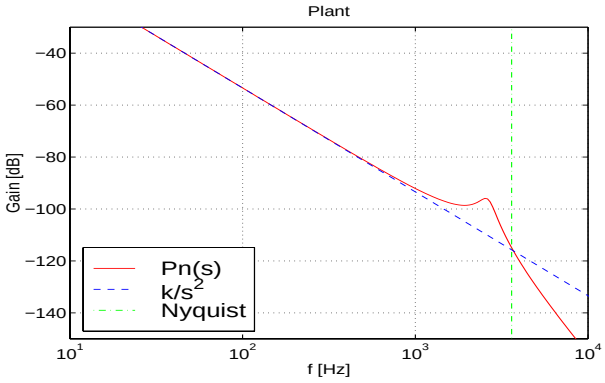

Figure 7.6: Frequency responses of plant.

The parameters of this plant are shown in Table 7.1. This model is obtained from the frequency response of Fig. 5.11 in the experimental analysis. As shown in Fig. 7.6, the actual plant has the first mechanical resonance mode at around 2.7 [kHz], and its variation range is ± 500 [Hz]. The Nyquist frequency (3.6 [kHz]) is close to this resonance mode. Therefore, it is very difficult to suppress the vibration with the conventional single-rate controller.

7.3.3 Vibration Suppression Control Based on Multirate Input Control

The continuous-time controller is designed by the regulator and disturbance observer, in which the disturbance is modeled by the step type function $d(s) = 1/s$, the poles of the regulator are set to $(s+\omega_c)^4$, and those of the observer are set to $(s+\omega_c)^2(s^2+2\zeta_1\omega_{1n}s+\omega_{1n}^2)$. As shown in Fig. 7.7, this controller has notch characteristics at the resonance frequency. The parameter ω_c is tuned such that the bandwidth of the closed-loop system

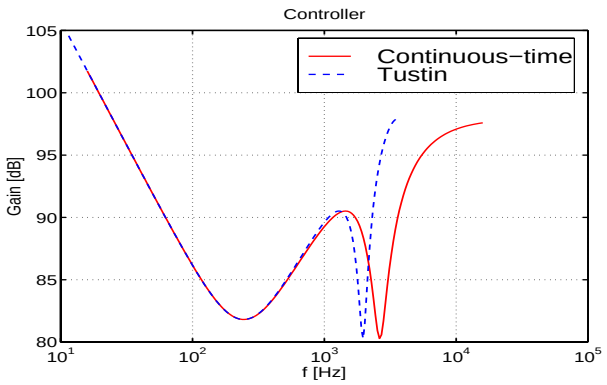

(a) Gain

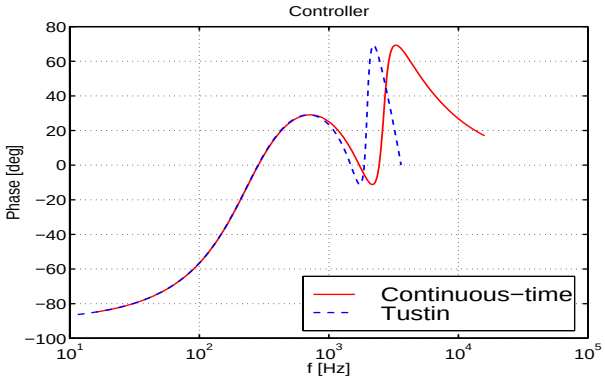

(b) Phase

Figure 7.7: Frequency responses of controller.

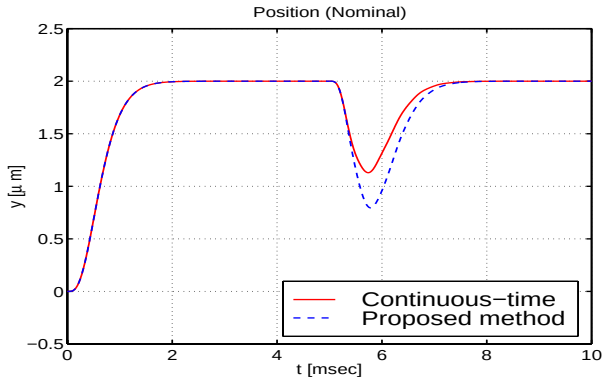

(a) Proposed controller

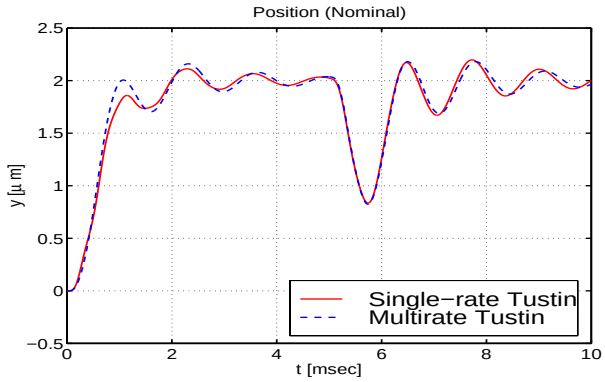

(b) Tustin transformations

Figure 7.8: Step and disturbance responses ($\omega_1 = \omega_{1n}$).

is set as high as possible, and the $\pm$ 1 [kHz] resonance variation is stabilized. Fig. 7.7 also shows that the Tustin transformation has large approximation error because the resonance mode is close to the Nyquist frequency.

Simulated results are shown in Fig. 7.8, which indicate that the proposed method has better performance than the Tustin transformations. In Fig. 7.8(b), the "Multirate Tustin" method consists of the digital controller discretized by Tustin transformation with T_y/N and the interpolator which has an up-sampler and a zero-order-hold [116]. While the responses of the Tustin transformations are oscillating, those of the proposed method have no vibration and show a step response identical to the ideal continuous-time system.

Fig. 7.9 shows the sensitivity and complementary sensitivity functions ($S[z]$ and $T[z]$) of the closed loop systems. As shown in Fig. 7.9(b), the proposed method retains the

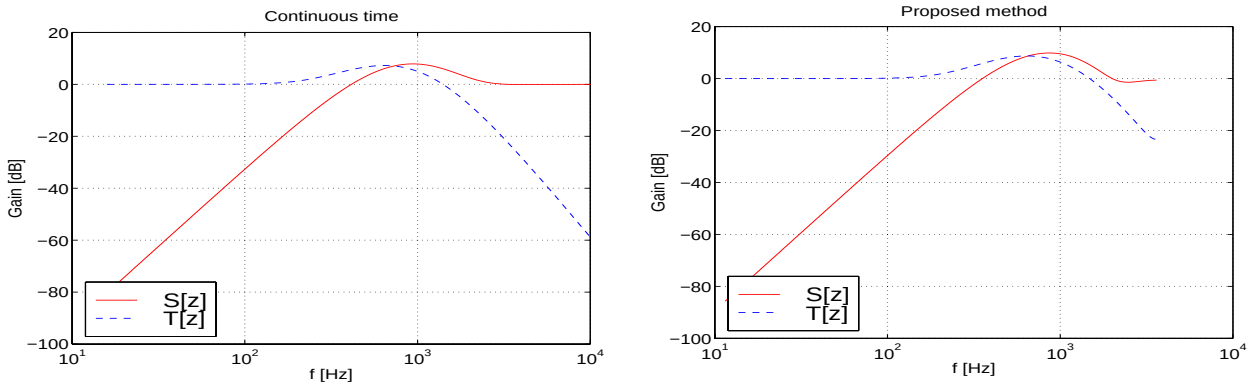

(a) Continuous-time

(b) Proposed controller

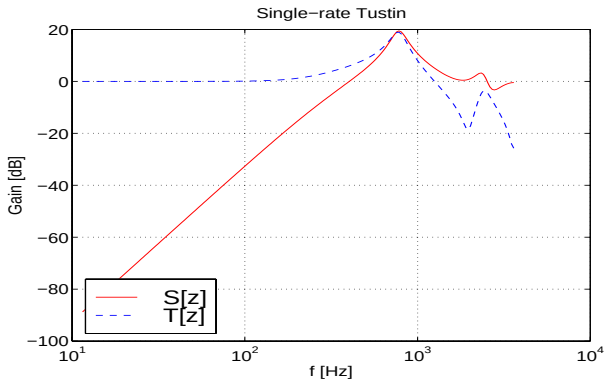

(c) Single-rate Tustin

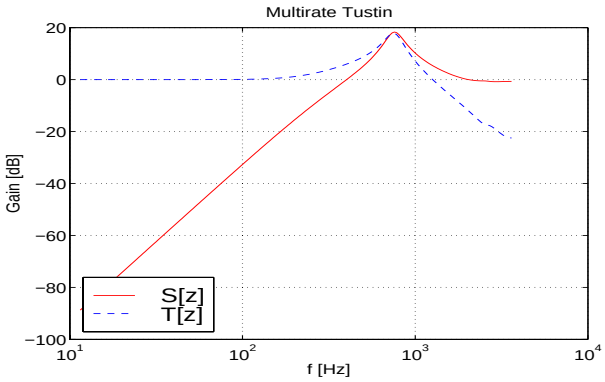

(d) Multirate Tustin

Figure 7.9: Frequency responses ($S[z]$ and $T[z]$).

ideal characteristics of the original continuous-time controller (Fig. 7.9(a)) because the proposed method is based on the closed-loop system. On the other hand, in conventional Tustin transformations (Fig. 7.9 (c) and (d)), the closed-systems are quite different from the original analog system, because those controllers are discretized based only on the open-loop characteristics.

Fig. 7.10 shows the responses for the case where the frequency of the mechanical resonance mode fluctuates 500 [Hz], indicating that the proposed method has high robustness. Because the frequency response of the closed-loop system is well preserved as shown in Fig. 7.9, the high robustness of the original analogue system is maintained in the obtained discrete-time system.

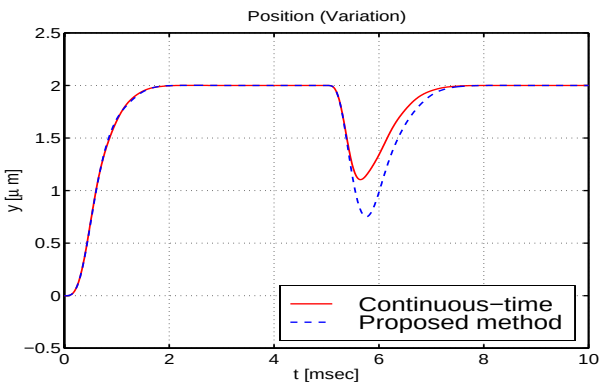

(a) Proposed controller

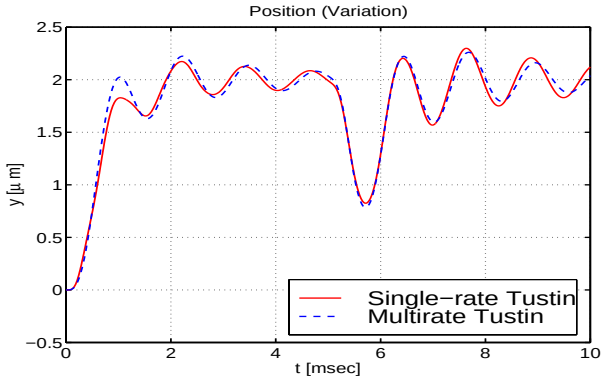

(b) Tustin transformations

Figure 7.10: Step and disturbance under parameter variation ($\omega_1 = \omega_{1n} - 500[Hz]$).

7.4 Summary

In this chapter, the novel discretization method of continuous-time controllers developed in chapter 4 was applied to motion control systems based on the perfect state matching (PSM) control with multirate sampling control.

In section 7.2, position control using a dc servomotor was selected as an example, and simulations and experiments were performed. The results indicated that the proposed method had better performance than the Tustin transformed digital controller. The disturbance rejection performances were considered in both the time and frequency domains.

Next, in section 7.3, a novel vibration suppression controller was developed for the 2-mass system of hard disk drives, in which the mechanical resonance mode is relatively close to the Nyquist frequency. Simulation results show the possibility of controlling this critical mode by multirate input control.

In order to obtain a high performance control system, the control bandwidth has to be set as wide as possible. However, in conventional methods such as the Tustin transformation, it is impossible to broaden the bandwidth too much, because the closed-loop system becomes unstable. On the other hand, the proposed method allows us to try the limits of the given hardware.

In this dissertation, perfect state matching is proposed for the controller discretization problem. However, it is applicable not only to the discretization but also to the model matching problem. By using PSM, the plant state can be controlled to match desirable continuous-time systems in both the feedforward and feedback characteristics. Thus, it can be said that the PSM is one of the fundamental schemes for multirate sampling control

together with PTC and PDR.

Chapter 8

Conclusion

In this dissertation, a general framework of multirate sampling control was constructed, and was developed into practical methodology by applying it to various motion control systems. In the first part, three fundamental control schemes were developed theoretically. They were 1) perfect tracking control (PTC) by multirate feedforward control, 2) perfect disturbance rejection (PDR) control by multirate feedback control, and 3) perfect state matching (PSM) control by multirate sampling control. In the second part, the proposed schemes were applied to practical motion control systems such as servomotors of robot manipulators, hard disk drives, two-mass systems, and visual servo systems. These applications demonstrated that the proposed methods were very effective in the practical motion control systems even when there were severe specifications.

This work can be classified by the hardware restrictions in the sampling scheme and according to the feedforward and feedback approaches, as shown in Table 8.1. While previous theoretical research dealt mainly with the case without sampling restrictions ($T_u = T_y$) as mentioned in chapter 1, this dissertation considered the cases with and without the restrictions in both feedforward and feedback schemes. Particularly, systems with relatively long sampling period were given emphasis because many motion control systems are in this category.

The details of this framework are summarized in Table 8.1.

For the multirate feedforward approach, a novel perfect tracking control (PTC) method was proposed in chapter 5. First, this theory was constructed for the case without hardware restrictions ($T_u = T_y$) in section 2.3. Second, it was extended to the cases with unequal sampling periods ($T_u < T_y$ and $T_u > T_y$) in section 2.4. Third, time delay and multivariable systems were handled in section 2.5. Moreover, it was shown that the structure of the proposed perfect tracking controller was very simple and clear.

The perfect tracking control was applied to motion control systems in chapter 5. As

an example without hardware restrictions ($T_u = T_y$), position control system using the servomotor of a robot manipulator was examined in section 5.2, and the advantages of the proposed method were demonstrated through simulations and experiments. Next, in section 5.3, the proposed method was applied to the track-seeking mode of hard disk drives, as an example with time delay and long sampling period relative to the control period ($T_u < T_y$).

In the multirate feedback approach, systems with long sampling period were dealt with in chapter 3, because the feedback characteristics such as disturbance rejection performance and stability robustness are never improved by multirate control for the case without hardware restrictions [12, 23]. For these systems, perfect disturbance rejection (PDR) control was developed in section 3.3, which cancels the effects of disturbance of the plant state at M intersample points in the steady state. Next, the intersample observer was proposed, which increased the stability margin by estimation and compensation of the intersample response. The proposed method was further extended to systems with time delay. In section 3.4, two multirate repetitive controllers were proposed, which were 1) feedback approach based on internal model principle and 2) feedforward disturbance rejection approach based on the open-loop estimation and switching function. By using the latter approach, it became possible to reject high-order periodic disturbance without sacrifice of the closed-loop characteristics.

The perfect disturbance rejection (PDR) controller was applied to the track-following mode of hard disk drives (HDD) and the visual servo systems of robot manipulators in chapter 6. In section 6.2, the first order repeatable runout (RRO) of HDD was rejected by PDR. The intersample observer was implemented, and analysis of the frequency response proved the recovery of the stability margin. In section 6.3, high-order RRO was taken into account, and it was rejected by both feedback and feedforward multirate control. The advantage of the feedforward approach was demonstrated by the frequency response of the closed-loop system. Next, in section 6.4, simulations and experiments showed that PDR had high performance in the visual servo system of robot manipulators.

In section 4.3, novel discretization methods for both controller and observer were developed based on perfect state matching (PSM) control. This method was applicable to both feedforward and feedback controllers. In section 4.4, PSM was extended to the system with relatively long sampling period ($T_u < T_y$). The remarkable advantages of the PSM were 1) the proposed method was based on the closed-loop system and 2) the transient responses were preserved independent of the sampling period. As a result, the stability of the discretized system was assured.

Perfect state matching (PSM) control was applied to motion control systems in chapter

7. In section 7.2, position control using a dc servomotor was selected as an example, and simulations and experiments were performed, the results of which indicated that the proposed method had better performance than the Tustin transformed digital controller. Next, in section 7.3, a novel vibration suppression controller was developed for hard disk drives, in which the mechanical resonance mode was relatively close to the Nyquist frequency.

In the application part of this dissertation, the proposed methods were not applied to systems with hardware restriction of short sampling period ($T_u > T_y$). There may be no appropriate applications at the laboratory level, however, this category includes large scale systems such as chemical plants and steel mills. For these systems, it is possible to improve plant state estimation by using multirate output control, which can be extended from the results of section 4.3.3.

As a conclusion, this dissertation succeeded in constructing a general and integrated framework of multirate sampling control. While the theoretical novelty is important, the engineering significance is immeasurable, since the proposed methods proved to be practical methods which make full use of computer performance. In the application examples, the performance of the proposed method was superior to that of the conventional method. Moreover, the proposed method has already been implemented in commercial products. These facts show that this dissertation is a major breakthrough in control engineering and has broken down the wall which conventional technology could not overcome.

Restriction	case 1 ($T_u > T_y$)	case 2 ($T_u = T_y$)	case 3 ($T_u < T_y$)
Applications	Large scale system	Usual system, Servomotor	HDD, Visual servo system
Feedforward	• Perfect tracking control (section 2.4)	• Controller discretization (section 4.3,7.2) • Perfect tracking control (section 2.3, 5.2)	• Inter-sample perfect tracking control (section 2.4, 5.3) • Feedforward repetitive disturbance rejection (section 3.4, 6.3)
Feedback	• Improvement of Estimation (Extension of section 4.3.3)	• Controller and observer discretization (section 4.3,7.2)	• Perfect disturbance rejection (section 3.3, 6.2) • Intersample observer (section 3.3, 6.2) • Feedback repetitive disturbance rejection (section 3.4, 6.3) • Controller discretization (section 4.4) • Vibration suppression in semi-Nyquist frequency region (section 7.3)

Table 8.1: General framework of multirate sampling control for digital motion control

Appendix A

Proof of (2.14)

In this section, it is shown that (2.14) equals (2.13). It has already been proved for the case of one-degree-of-freedom [76]. It is now extended to two-degree-of-freedom.

Let the right and left coprime factorizations of $\boldsymbol{P}[z]$ be

$$\boldsymbol{P}[z] = \boldsymbol{N}\boldsymbol{M}^{-1} = \tilde{\boldsymbol{M}}^{-1}\tilde{\boldsymbol{N}}. \tag{A.1}$$

All internally stabilizing controllers $\boldsymbol{C}_1$ and $\boldsymbol{C}_2$ can be parameterized as in [74]

$$\boldsymbol{C}_1 = (\tilde{\boldsymbol{X}} - \boldsymbol{Q}\tilde{\boldsymbol{N}})^{-1}\boldsymbol{K}, \tag{A.2}$$

$$\begin{aligned}\boldsymbol{C}_2 &= (\tilde{\boldsymbol{X}} - \boldsymbol{Q}\tilde{\boldsymbol{N}})^{-1}(\tilde{\boldsymbol{Y}} - \boldsymbol{Q}\tilde{\boldsymbol{M}}) \\ &= (\boldsymbol{Y} - \boldsymbol{M}\boldsymbol{Q})(\boldsymbol{X} - \boldsymbol{N}\boldsymbol{Q})^{-1},\end{aligned} \tag{A.3}$$

where $\boldsymbol{X}, \boldsymbol{Y}, \tilde{\boldsymbol{X}}, \tilde{\boldsymbol{Y}} \in \boldsymbol{RH}_\infty$ satisfy the following Bezout identity.

$$\begin{bmatrix} \tilde{\boldsymbol{X}} & -\tilde{\boldsymbol{Y}} \\ -\tilde{\boldsymbol{N}} & \tilde{\boldsymbol{M}} \end{bmatrix} \begin{bmatrix} \boldsymbol{M} & \boldsymbol{Y} \\ \boldsymbol{N} & \boldsymbol{X} \end{bmatrix} = \boldsymbol{I} \tag{A.4}$$

Here, the following theorem is proved in [76].

Theorem A.1 *Suppose* $\boldsymbol{P}[z] = \boldsymbol{C}(z\boldsymbol{I} - \boldsymbol{A})^{-1}\boldsymbol{B} + \boldsymbol{D}$ *where* $(\boldsymbol{A}, \boldsymbol{B})$ *is stabilizable and* $(\boldsymbol{C}, \boldsymbol{A})$ *is detectable. Select* $\boldsymbol{F}$ *and* $\boldsymbol{K}$ *such that* $\boldsymbol{A}_F \triangleq \boldsymbol{A} + \boldsymbol{B}\boldsymbol{F}$ *and* $\boldsymbol{A}_H \triangleq \boldsymbol{A} + \boldsymbol{H}\boldsymbol{C}$ *are stable. The parameters satisfying (A.1) and (A.4) are represented by*

$$\boldsymbol{M}[z] = \left[\begin{array}{c|c} \boldsymbol{A}_F & \boldsymbol{B} \\ \hline \boldsymbol{F} & \boldsymbol{I} \end{array}\right], \quad \boldsymbol{N}[z] = \left[\begin{array}{c|c} \boldsymbol{A}_F & \boldsymbol{B} \\ \hline \boldsymbol{C} + \boldsymbol{D}\boldsymbol{F} & \boldsymbol{D} \end{array}\right]$$

$$\tilde{\boldsymbol{X}}[z] = \left[\begin{array}{c|c} \boldsymbol{A}_H & -\boldsymbol{B} - \boldsymbol{H}\boldsymbol{D} \\ \hline \boldsymbol{F} & \boldsymbol{I} \end{array}\right], \quad \tilde{\boldsymbol{Y}}[z] = \left[\begin{array}{c|c} \boldsymbol{A}_H & -\boldsymbol{H} \\ \hline \boldsymbol{F} & \boldsymbol{O} \end{array}\right]$$

$$\tilde{\boldsymbol{M}}[z] = \left[\begin{array}{c|c} \boldsymbol{A}_H & \boldsymbol{H} \\ \hline \boldsymbol{C} & \boldsymbol{I} \end{array}\right], \quad \tilde{\boldsymbol{N}}[z] = \left[\begin{array}{c|c} \boldsymbol{A}_H & \boldsymbol{B} + \boldsymbol{H}\boldsymbol{D} \\ \hline \boldsymbol{C} & \boldsymbol{D} \end{array}\right]$$

$$\boldsymbol{X}[z] = \left[\begin{array}{c|c} \boldsymbol{A}_F & -\boldsymbol{H} \\ \hline \boldsymbol{C}+\boldsymbol{DF} & \boldsymbol{I} \end{array}\right], \ \boldsymbol{Y}[z] = \left[\begin{array}{c|c} \boldsymbol{A}_F & \boldsymbol{H} \\ \hline -\boldsymbol{F} & \boldsymbol{O} \end{array}\right].$$

From the above parameterization, it is shown that (2.14) equals (2.13). In Fig. 2.5, consider the state observer described by

$$\begin{aligned} \hat{\boldsymbol{x}}[i+1] &= \boldsymbol{A}_H\hat{\boldsymbol{x}}[i] - \boldsymbol{H}\boldsymbol{y}[i] + (\boldsymbol{B}+\boldsymbol{HD})\boldsymbol{u}[i] \\ \hat{\boldsymbol{y}} &= \boldsymbol{C}\hat{\boldsymbol{x}}[i] + \boldsymbol{D}\boldsymbol{u}[i], \end{aligned} \tag{A.5}$$

where $\hat{\boldsymbol{x}}$ is the estimated plant state. Equation (A.5) can be represented by the following transfer functions.

$$\begin{aligned} \hat{\boldsymbol{x}} &= -(z\boldsymbol{I}-\boldsymbol{A}_H)^{-1}\boldsymbol{H}\boldsymbol{y} + (z\boldsymbol{I}-\boldsymbol{A}_H)^{-1}(\boldsymbol{B}+\boldsymbol{HD})\boldsymbol{u}, \\ \hat{\boldsymbol{y}} &= -\boldsymbol{C}(z\boldsymbol{I}-\boldsymbol{A}_H)^{-1}\boldsymbol{H}\boldsymbol{y} \\ &\quad +\{\boldsymbol{C}(z\boldsymbol{I}-\boldsymbol{A}_H)^{-1}(\boldsymbol{B}+\boldsymbol{HD})+\boldsymbol{D}\}\boldsymbol{u} \\ &= (\boldsymbol{I}-\tilde{\boldsymbol{M}})\boldsymbol{y} + \tilde{\boldsymbol{N}}\boldsymbol{u} \end{aligned} \tag{A.6}$$

The error of the estimated output is obtained as

$$\boldsymbol{e}_y = \hat{\boldsymbol{y}} - \boldsymbol{y} = -\tilde{\boldsymbol{M}}\boldsymbol{y} + \tilde{\boldsymbol{N}}\boldsymbol{u}. \tag{A.7}$$

From the above equations, (2.14) is transformed into (2.13) as follows.

$$\begin{aligned} \boldsymbol{u} &= \boldsymbol{F}\hat{\boldsymbol{x}} + \boldsymbol{Q}\boldsymbol{e}_y + \boldsymbol{K}\boldsymbol{r} \\ &= -\boldsymbol{F}(z\boldsymbol{I}-\boldsymbol{A}_H)^{-1}\boldsymbol{H}\boldsymbol{y} + \boldsymbol{F}(z\boldsymbol{I}-\boldsymbol{A}_H)^{-1}(\boldsymbol{B}+\boldsymbol{HD})\boldsymbol{u} \\ &\quad +\boldsymbol{Q}\boldsymbol{e}_y + \boldsymbol{K}\boldsymbol{r} \\ &= \tilde{\boldsymbol{Y}}\boldsymbol{y} + (\boldsymbol{I}-\tilde{\boldsymbol{X}})\boldsymbol{u} + \boldsymbol{Q}(-\tilde{\boldsymbol{M}}\boldsymbol{y} + \tilde{\boldsymbol{N}}\boldsymbol{u}) + \boldsymbol{K}\boldsymbol{r} \end{aligned} \tag{A.8}$$

$$(\tilde{\boldsymbol{X}} - \boldsymbol{Q}\tilde{\boldsymbol{N}})\boldsymbol{u} = (\tilde{\boldsymbol{Y}} - \boldsymbol{Q}\tilde{\boldsymbol{M}})\boldsymbol{y} + \boldsymbol{K}\boldsymbol{r} \tag{A.9}$$

$$\begin{aligned} \boldsymbol{u} &= (\tilde{\boldsymbol{X}} - \boldsymbol{Q}\tilde{\boldsymbol{N}})^{-1}(\tilde{\boldsymbol{Y}} - \boldsymbol{Q}\tilde{\boldsymbol{M}})\boldsymbol{y} \\ &\quad +(\tilde{\boldsymbol{X}} - \boldsymbol{Q}\tilde{\boldsymbol{N}})^{-1}\boldsymbol{K}\boldsymbol{r} \qquad \text{(A.10)} \\ &= \boldsymbol{C}_1\boldsymbol{r} + \boldsymbol{C}_2\boldsymbol{y} \qquad \text{(A.11)} \end{aligned}$$

Appendix B

Derivation of (2.20)

From (A.2), the derivation of (2.20) is as follows [74].

$$\begin{aligned} \boldsymbol{C}_1 &= (\tilde{\boldsymbol{X}} - \boldsymbol{Q}\tilde{\boldsymbol{N}})^{-1}\boldsymbol{K} \\ &= (\tilde{\boldsymbol{X}} - \boldsymbol{Q}\tilde{\boldsymbol{N}})^{-1}\{(\tilde{\boldsymbol{X}} - \boldsymbol{Q}\tilde{\boldsymbol{N}})\boldsymbol{M} - (\tilde{\boldsymbol{Y}} - \boldsymbol{Q}\tilde{\boldsymbol{M}})\boldsymbol{N}\}\boldsymbol{K} \end{aligned} \tag{B.1}$$

Since the following equations are satisfied from the Bezout identity (A.4),

$$\tilde{\boldsymbol{X}}\boldsymbol{M} - \tilde{\boldsymbol{Y}}\boldsymbol{N} = \boldsymbol{I}, \quad \tilde{\boldsymbol{M}}\boldsymbol{N} = \tilde{\boldsymbol{N}}\boldsymbol{M} \tag{B.2}$$

(B.1) is rewritten as

$$\begin{aligned} \boldsymbol{C}_1 &= \{\boldsymbol{M} - (\tilde{\boldsymbol{X}} - \boldsymbol{Q}\tilde{\boldsymbol{N}})^{-1}(\tilde{\boldsymbol{Y}} - \boldsymbol{Q}\tilde{\boldsymbol{M}})\boldsymbol{N}\}\boldsymbol{K} \\ &= (\boldsymbol{M} - \boldsymbol{C}_2\boldsymbol{N})\boldsymbol{K}. \end{aligned} \tag{B.3}$$

Appendix C

Proof of (3.51)

In this section, the optimum solution of (3.50) is obtained by the Lagrange's undetermined multiplier method.

Defining $\tilde{\boldsymbol{A}}_{pd} = \begin{bmatrix} \boldsymbol{A}_X \\ \boldsymbol{A}_Y \end{bmatrix}$, the problem of (3.50) can be rewritten as

$$\min_{\boldsymbol{F}_d} \left\| \begin{bmatrix} \boldsymbol{A}_X \\ \boldsymbol{A}_Y \end{bmatrix} + \begin{bmatrix} \boldsymbol{X} \\ \boldsymbol{Y} \end{bmatrix} \boldsymbol{F}_d \right\| \quad \text{s. t.} \quad \boldsymbol{A}_Y + \boldsymbol{Y}\boldsymbol{F}_d = \boldsymbol{O}. \tag{C.1}$$

If the Frobenius norm is adopted, this problem can be formulated by

$$\min_{\boldsymbol{F}_d} \|\boldsymbol{E}\|_F, \ \boldsymbol{E} = \boldsymbol{A}_X + \boldsymbol{X}\boldsymbol{F}_d, \ \text{s. t.} \ \boldsymbol{A}_Y + \boldsymbol{Y}\boldsymbol{F}_d = \boldsymbol{0} \tag{C.2}$$

Decomposing each row as $\boldsymbol{A}_X = [\boldsymbol{a}_{x1}, \cdots, \boldsymbol{a}_{xn_p}], \boldsymbol{A}_Y = [\boldsymbol{a}_{y1}, \cdots, \boldsymbol{a}_{yn_p}], \boldsymbol{E} = [\boldsymbol{e}_1, \cdots, \boldsymbol{e}_{n_p}]$, and $\boldsymbol{F}_d = [\boldsymbol{f}_1, \cdots, \boldsymbol{f}_{n_p}]$, (C.2) is rewritten as

$$\min_{\boldsymbol{F}_d} \|\boldsymbol{e}_i\|_2, \ \boldsymbol{e}_i = \boldsymbol{a}_{xi} + \boldsymbol{X}\boldsymbol{f}_i, \ \text{s. t.} \ \boldsymbol{a}_{yi} + \boldsymbol{Y}\boldsymbol{f}_i = \boldsymbol{0}, \ \text{for} \ i = 1, \cdots, n_p, \tag{C.3}$$

because $\|\boldsymbol{E}\|_F^2 = \sum_{i=1}^{n_p} \|\boldsymbol{e}_i\|_2^2$.

The problem of (C.3) can be solved by the Lagrange's undetermined multiplier method. The Lagrange function is defined by

$$\begin{aligned} g &= \boldsymbol{e}_i^T \boldsymbol{e}_i + \boldsymbol{\lambda}^T (\boldsymbol{a}_{yi} + \boldsymbol{Y}\boldsymbol{f}_i) \\ &= (\boldsymbol{a}_{xi} + \boldsymbol{X}\boldsymbol{f}_i)^T (\boldsymbol{a}_{xi} + \boldsymbol{X}\boldsymbol{f}_i) + \boldsymbol{\lambda}^T (\boldsymbol{a}_{yi} + \boldsymbol{Y}\boldsymbol{f}_i) \\ &= \boldsymbol{a}_{xi}^T \boldsymbol{a}_{xi} + \boldsymbol{a}_{xi}^T \boldsymbol{X}\boldsymbol{f}_i + \boldsymbol{f}_i^T \boldsymbol{X}^T \boldsymbol{a}_{xi} + \boldsymbol{f}_i^T \boldsymbol{X}^T \boldsymbol{X}\boldsymbol{f}_i + \boldsymbol{\lambda}^T \boldsymbol{a}_{yi} + \boldsymbol{\lambda}^T \boldsymbol{Y}\boldsymbol{f}_i. \end{aligned} \tag{C.4}$$

The solution of (C.3) is obtained from (C.5) and (C.6).

$$\begin{aligned} \frac{\partial \boldsymbol{g}}{\partial \boldsymbol{f}_i} &= (\boldsymbol{a}_{xi}^T \boldsymbol{X})^T + \boldsymbol{X}^T \boldsymbol{a}_{xi} + 2\boldsymbol{X}^T \boldsymbol{X}\boldsymbol{f}_i + (\boldsymbol{\lambda}^T \boldsymbol{Y})^T \\ &= 2\boldsymbol{X}^T \boldsymbol{a}_{xi} + 2\boldsymbol{X}^T \boldsymbol{X}\boldsymbol{f}_i + \boldsymbol{Y}^T \boldsymbol{\lambda} = \boldsymbol{0}, \end{aligned} \tag{C.5}$$

$$\frac{\partial \boldsymbol{g}}{\partial \boldsymbol{\lambda}} = \boldsymbol{a}_{yi} + \boldsymbol{Y}\boldsymbol{f}_i = \boldsymbol{0} \tag{C.6}$$

(C.5) is rewritten as

$$\boldsymbol{f}_i = -\boldsymbol{Z}\boldsymbol{X}^T\boldsymbol{a}_{xi} - \boldsymbol{Z}\boldsymbol{Y}^T\boldsymbol{\lambda}/2, \tag{C.7}$$

where $\boldsymbol{Z} = (\boldsymbol{X}^T\boldsymbol{X})^{-1}$. Substituting (C.6) for (C.7), it becomes

$$\boldsymbol{a}_{yi} - \boldsymbol{Y}\boldsymbol{Z}\boldsymbol{X}^T\boldsymbol{a}_{xi} - \boldsymbol{Y}\boldsymbol{Z}\boldsymbol{Y}^T\boldsymbol{\lambda}/2 = \boldsymbol{0}. \tag{C.8}$$

Thus, the undetermined multiplier λ is obtained by

$$\boldsymbol{\lambda} = 2(\boldsymbol{Y}\boldsymbol{Z}\boldsymbol{Y}^T)^{-1}(\boldsymbol{a}_{yi} - \boldsymbol{Y}\boldsymbol{Z}\boldsymbol{X}^T\boldsymbol{a}_{xi}). \tag{C.9}$$

Substituting (C.7) for (C.9), the solution of (C.3) is given by

$$\begin{aligned} \boldsymbol{f}_i &= -\boldsymbol{Z}\boldsymbol{X}^T\boldsymbol{a}_{xi} - \boldsymbol{Z}\boldsymbol{Y}^T(\boldsymbol{Y}\boldsymbol{Z}\boldsymbol{Y}^T)^{-1}(\boldsymbol{a}_{yi} - \boldsymbol{Y}\boldsymbol{Z}\boldsymbol{X}^T\boldsymbol{a}_{xi}) \\ &= (\boldsymbol{Z}\boldsymbol{Y}^T(\boldsymbol{Y}\boldsymbol{Z}\boldsymbol{Y}^T)^{-1}\boldsymbol{Y}\boldsymbol{Z}\boldsymbol{X}^T - \boldsymbol{Z}\boldsymbol{X}^T)\boldsymbol{a}_{xi} - \boldsymbol{Z}\boldsymbol{Y}^T(\boldsymbol{Y}\boldsymbol{Z}\boldsymbol{Y}^T)^{-1}\boldsymbol{a}_{yi}. \end{aligned} \tag{C.10}$$

Finally, (3.51) is proved by considering all $i(= 1, \cdots, n_p)$ as

$$\begin{aligned} \boldsymbol{F}_d &= (\boldsymbol{Z}\boldsymbol{Y}^T(\boldsymbol{Y}\boldsymbol{Z}\boldsymbol{Y}^T)^{-1}\boldsymbol{Y}\boldsymbol{Z}\boldsymbol{X}^T - \boldsymbol{Z}\boldsymbol{X}^T)\boldsymbol{A}_X - \boldsymbol{Z}\boldsymbol{Y}^T(\boldsymbol{Y}\boldsymbol{Z}\boldsymbol{Y}^T)^{-1}\boldsymbol{A}_Y \\ &= \boldsymbol{Z}[\boldsymbol{Y}^T(\boldsymbol{Y}\boldsymbol{Z}\boldsymbol{Y}^T)^{-1}\boldsymbol{Y}\boldsymbol{Z}\boldsymbol{X}^T - \boldsymbol{X}^T, -\boldsymbol{Y}^T(\boldsymbol{Y}\boldsymbol{Z}\boldsymbol{Y}^T)^{-1}]\tilde{\boldsymbol{A}}_{pd}. \end{aligned} \tag{C.11}$$

Bibliography

[1] M. Araki, "Recent developments in digital control theory," in *12th IFAC World Congress*, vol. 9, pp. 251–260, July 1993.

[2] A. B. Chammas and L. T. Leondes, "On the design of linear time invariant systems by periodic output feedback," *Int. J. Contr.*, vol. 27, no. 6, pp. 885–894, 1978.

[3] P. T. Kabamba, "Control of linear systems using generalized sampled-data hold functions," *IEEE Trans. Automat. Contr.*, vol. 32, no. 9, pp. 772–783, 1987.

[4] A. B. Chammas and L. T. Leondes, "Pole assignment by piecewise constant feedback," *Int. J. Contr.*, vol. 29, no. 1, pp. 31–38, 1979.

[5] T. Kaczorek, "Pole placement for linear discrete-time systems by periodic output feedbacks," *Syst. Cont. Lett.*, vol. 6, no. 4, pp. 267–269, 1985.

[6] M. Araki and T. Hagiwara, "Pole assignment by multirate-data output feedback," *Int. J. Control*, vol. 44, no. 6, pp. 1661–1673, 1986.

[7] K. L. Moore, S. P. Bhattacharyya, and M. Dahleh, "Arbitrary pole and zero assignment with N-delay input control using stable controllers," in *Conf. Decision Contr.*, pp. 1253–1258, 1989.

[8] T. Mita, Y. Chida, Y. Kazu, and H. Numasato, "Two-delay robust digital control and its applications – avoiding the problem on unstable limiting zeros," *IEEE Trans. Automat. Contr.*, vol. 35, no. 8, pp. 962–970, 1990.

[9] K. J. Åström, P. Hangander, and J. Sternby, "Zeros of sampled system," *Automatica*, vol. 20, no. 1, pp. 31–38, 1984.

[10] T. Hagiwara and M. Araki, "Design of a state state feedback controller based on the multirate sampling of plant output," *IEEE Trans. Automat. Contr.*, vol. 33, no. 9, pp. 812–819, 1988.

[11] T. Hagiwara and M. Araki, "Time-varying digital controllers," *J. SICE*, vol. 27, no. 12, pp. 1071–1077, 1988. (in Japanese).

[12] P. P. Khargonekar, K. Poolla, and A. Tannenbaum, "Robust control of linear time-invariant plants using periodic compensation," *IEEE Trans. Automat. Contr.*, vol. 30, no. 11, pp. 1088–1096, 1985.

[13] K. Z. Liu and T. Mita, "Design of an optimal series compensatory based on darma model," *Systems and Control Letters*, vol. 8, no. 5, pp. 417–423, 1987.

[14] T. Mita, B. C. Pang, and K. Z. Liu, "Design of optimal strongly stable digital control systems and applications to output feedback control of mechanical systems," *Int. J. Control*, vol. 45, no. 6, pp. 2071–2082, 1987.

[15] P. T. Kabamba and C. Yang, "Simultaneous controller design for linear time-invariant systems," *IEEE Trans. Automat. Contr.*, vol. 36, no. 1, pp. 106–111, 1991.

[16] M. E. Sezer and D. D. Siljak, "Decentralized multirate control," *IEEE Trans. Automat. Contr.*, vol. 35, no. 1, pp. 60–65, 1990.

[17] R. Ortega and G. Kreisselmeier, "Discrete-time model reference adaptive control for continuous-time systems using generalized sampled-data hold functions," *IEEE Trans. Automat. Contr.*, vol. 35, no. 3, pp. 334–338, 1990.

[18] Y. Miyasato, "Adaptive control by periodic time-varying feedback," *Trans. SICE*, vol. 17, no. 11, pp. 1244–1250, 1988. (in Japanese).

[19] B. A. Francis and T. T. Georgiou, "Stability theory for linear time-invariant plants with periodic digital controllers," *IEEE Trans. Automat. Contr.*, vol. 33, no. 9, pp. 820–832, 1988.

[20] D. G. Meyer, "A parameterization of stabilizing controllers for multirate sampled-data systems," *IEEE Trans. Automat. Contr.*, vol. 35, no. 2, pp. 233–236, 1990.

[21] R. Ravi, P. P. Khargonekar, K. D. Minto, and C. N. Nett, "Controller parameterization for time-varying multirate plants," *IEEE Trans. Automat. Contr.*, vol. 35, no. 11, pp. 1259–1262, 1990.

[22] J. W. Grizzle and P. V. Kokotovic, "Feedback linearization of sampled-data systems," *IEEE Trans. Automat. Contr.*, vol. 33, no. 9, pp. 857–859, 1988.

[23] J. S. Shamma and M. A. Dahleh, "Time-varying versus time-invariant compensation for rejection of persistent bounded disturbances and robust stabilization," *IEEE Trans. Automat. Contr.*, vol. 36, no. 7, pp. 838–847, 1991.

[24] K. L. Moore, S. P. Bhattacharyya, and M. Dahleh, "Capabilities and limitations of multirate control schemes," *Automatica*, vol. 29, no. 4, pp. 941–951, 1993.

[25] M. Er and B. D. O. Anderson, "Performance study of multirate output controllers under noise disturbances," *Int. J. Control*, vol. 56, no. 3, pp. 531–545, 1992.

[26] S. Hara, Y. Yamamoto, and H. Fujioka, "Modern and classical analysis / synthesis methods in sampled-data control – a brief overview with numerical examples –," in *Conf. Decision Contr.*, pp. 1251–1256, 1996.

[27] T. Chen and B. Francis, *Optimal Sampled-Data Control Systems*. Springer, 1995.

[28] T. Chen and B. A. Francis, "On the L_2-induced norm of a sampled-data system," *Systems and Control Letters*, vol. 15, pp. 211–219, 1990.

[29] T. Chen and B. A. Francis, "H_2-optimal sampled-data control," *IEEE Trans. Automat. Contr.*, vol. 36, no. 1, pp. 50–58, 1991.

[30] B. Bamieh and J. B. Peason, "The H_2 problem for sampled-data systems," *Systems and control letters*, vol. 19, pp. 1–12, 1992.

[31] P. T. Kabamba and S. Hara, "Worst-case analysis and design of sampled-data control systems," *IEEE Trans. Automat. Contr.*, vol. 38, no. 9, pp. 1337–1357, 1993.

[32] B. A. Bamieh and J. B. Pearson, "A general framework for linear periodic systems with applications to H_∞ sampled-data control," *IEEE Trans. Automat. Contr.*, vol. 37, no. 4, pp. 418–435, 1992.

[33] Y. Hayakawa, S. Hara, and Y. Yamamoto, "H_∞ type problem for sampled-data control systems – a solution via minimum energy characterization," *IEEE Trans. Automat. Contr.*, vol. 39, no. 11, pp. 2278–2284, 1994.

[34] H. T. Toivonen, "Sampled-data control of continuous-time systems with an H_∞ optimality criterion," *Automatica*, vol. 28, pp. 45–54, 1992.

[35] Y. Yamamoto, "New approach to sampled-data systems; a function space method," in *Conf. Decision Contr.*, pp. 1882–1887, 1990.

[36] Y. Yamamoto, "A function space approach to sampled-data systems and tracking problems," *IEEE Trans. Automat. Contr.*, vol. 39, no. 4, pp. 703–713, 1994.

[37] Y. Yamamoto and P. P. Khargonekar, "Frequency response of sampled-data systems," *IEEE Trans. Automat. Contr.*, vol. 41, no. 2, pp. 166–176, 1996.

[38] M. Araki, Y. Ito, and T. Hagiwara, "Frequency response of sampled-data systems," *Automatica*, vol. 32, no. 4, pp. 483–497, 1996.

[39] Y. Yamamoto, A. G. Madievski, and B. D. O. Anderson, "Computation and convergence of frequency response via fast sampling for sampled-data control systems," in *Conf. Decision Contr.*, pp. 2157–2162, 1997.

[40] J. P. Keller and B. D. O. Anderson, "A new approach to the discretization of continuous-time controllers," *IEEE Trans. Automat. Contr.*, vol. 37, no. 2, pp. 214–223, 1992.

[41] P. G. Voulgaris and B. Bamieh, "Optimal H_∞ and H_2 control of hybrid multirate systems," *Systems and control letters*, vol. 20, pp. 249–261, 1993.

[42] T. Chen and L. Qiu, "H_∞ design of general multirate sampled-data control systems," *Automatica*, vol. 30, no. 7, pp. 1139–1152, 1994.

[43] L. Qiu and T. Chen, "H_2-optimal design of multirate sampled-data systems," *IEEE Trans. Automat. Contr.*, vol. 39, no. 2, pp. 2506–2511, 1994.

[44] S. Nakagawa, Y. Hamada, Y. Hata, and T. Yamaguchi, "Design of track settling control system to reduce the residual vibration during track seek of magnetic disk drives," in *IEE of Japan Technical Meeting Record*, no. IIC-00-57, pp. 47–52, 2000. (in Japanese).

[45] G. Dullerud and K. Glover, "Robust stabilization of sampled-data systems to structured lti perturbations," *IEEE Trans. Automat. Contr.*, vol. 38, no. 10, pp. 1497–1508, 1993.

[46] T. Kimura, H. Fujioka, K. Tokai, and T. Takamori, "Sampled-data H_∞ control for a pneumatic cylinder system," in *Conf. Decision Contr.*, pp. 759–760, 1996.

[47] M. Hirata, T. Atsumi, and K. Nonami, "High performance digital servo design for HDD by using sampled-data H_∞ control theory," in *IEEE Int. Workshop Advanced Motion Control*, pp. 86–91, March 2000.

[48] J. Ishikawa, "A study on multirate sampled-data control for hard disk drives," in *IEE of Japan Technical Meeting Record*, no. IIC-00-55, pp. 31–38, 2000. (in Japanese).

[49] H. Fujioka and Y. Kuwano, "A design heuristic of sampled-data systems taking," in *SICE Symposium on Dynamical System Theory*, pp. 1251–1256, 1996. (in Japanese).

[50] W.-W. Chiang, "Multirate state-space digital controller for sector servo systems," in *Conf. Decision Contr.*, pp. 1902–1907, 1990.

[51] A. M. Phillips and M. Tomizuka, "Multirate estimation and control under time-varying data sampling with application to information storage devices," in *Amer. Control Conf.*, pp. 4151–4155, 1995.

[52] P. A. Weaver and R. M. Ehrlich, "The use of multirate notch filters in embedded-servo disk drives," in *Amer. Control Conf.*, pp. 4156–4160, June 1995.

[53] M. Kobayashi, T. Yamaguchi, I. Oshimi, Y. Soyama, Y. Hara, and H. Hirai, "Multirate zero phase error feedforward control for magnetic disk drives," in *JSME, IIP '98*, pp. 21–22, August 1998. (in Japanese).

[54] S. Takakura, "Design of the tracking system using N-Delay two-degree-of-freedom control and its application to hard disk drives," in *IEEE Conf. Control Applications*, pp. 170–175, August 1999.

[55] T. Hara and M. Tomizuka, "Performance enhancement of multi-rate controller for hard disk drives," *IEEE Trans. Magnetics*, vol. 35, no. 2, pp. 898–903, 1999.

[56] K. Hashimoto and H. Kimura, "Visual servoing with nonlinear observer," *IEEE Int. Conf. Robotics and Automation*, pp. 484–489, 1995.

[57] M. Nemani, T. C. Tsao, and S. Hutchinson, "Multi-rate analysis and design of visual feedback digital servo-control system," *ASME, J. Dynam. Syst., Measur., and Contr.*, vol. 116, pp. 44–55, March 1994.

[58] J. T. Feeddma and O. R. Mitchell, "Vision guided servoing with feature-based trajectory generation," *IEEE Trans. Robotics and Automation*, vol. 5, no. 5, pp. 691–700, 1989.

[59] Y. Hori, T. Umeno, T. Uchida, and Y. Konno, "An instantaneous speed observer for high performance control of dc servomotor using DSP and low precision shaft encoder," in *4th European Conf. on Power Electronics*, vol. 3, pp. 647–652, 1991.

[60] The Japan Society of Precision Engineering, *Present and Future Technology of Ultraprecision Positioning.* Fuji Technosystem, 2000. (in Japanese).

[61] T. Chen and B. A. Francis, "Design of multirate filter banks by H_∞ optimization," *IEEE Trans. Signal Processing*, vol. 43, pp. 2822–2830, 1995.

[62] Y. Yamamoto, H. Fujioka, and P. P. Khargonekar, "Signal reconstruction via sampled-data control with multirate filter banks," in *Conf. Decision Contr.*, pp. 3395–3400, 1997.

[63] S. Urikura and A. Nagata, "Ripple-free deadbeat control for sampled-data systems," *IEEE Trans. Automat. Contr.*, vol. 32, no. 6, pp. 474–482, 1987.

[64] I. D. Landau and M. Tomizuka, *Theory and practice of adaptive control systems.* Ohmsha, 1981. (in Japanese).

[65] Y. Hori and K. Ohnishi, *Applied control engineering.* Maruzen, 1988. (in Japanese).

[66] K. Ohnishi, M. Shibata, and T. Murakami, "Motion control for advanced mechatronics," *IEEE/ASME Trans. Mechatronics*, vol. 1, no. 1, pp. 56–67, 1996.

[67] T. Umeno, T. Kaneko, and Y. Hori, "Robust servosystem design with two degrees of freedom and its application to novel motion control of robot manipulators," *IEEE Trans. Industrial Electronics*, vol. 40, no. 5, pp. 473–485, 1993.

[68] M. Tomizuka, "Zero phase error tracking algorithm for digital control," *ASME, J. Dynam. Syst., Measur., and Contr.*, vol. 109, pp. 65–68, March 1987.

[69] B. Haack and M. Tomizuka, "The effect of adding zeros to feedforward controllers," *ASME, J. Dynam. Syst., Measur., and Contr.*, vol. 113, pp. 6–10, March 1991.

[70] D. Torfs, J. D. Schutter, and J. Swevers, "Extended bandwidth zero phase error tracking control of nonminimal phase systems," *ASME, J. Dynam. Syst., Measur., and Contr.*, vol. 114, pp. 347–351, September 1992.

[71] E. Gross, M. Tomizuka, and W. Messner, "Cancellation of discrete time unstable zeros by feedforward control," *ASME, J. Dynam. Syst., Measur., and Contr.*, vol. 116, pp. 33–38, March 1994.

[72] H. Fujimoto and A. Kawamura, "New digital redesign method in use of N-Delay control," *Trans. IEE of Japan*, vol. 117-D, no. 5, pp. 645–654, 1997. (in Japanese).

[73] T. Mita, S. Hara, and R. Kondo, *Introduction to Digital Control*. CORONA Publishing Co., LTD., 1988. (in Japanese).

[74] T. Sugie and T. Yoshikawa, "General solution of robust tracking problem in two-degree-of-freedom control systems," *IEEE Trans. Automat. Contr.*, vol. 31, no. 6, pp. 552–554, 1986.

[75] T. Mita, M. Hirata, and S. B. Villas, "H_∞ servo controller design for plants having poles on the $j\omega$ axis," in *Conf. Decision Contr.*, pp. 2568–2573, 1995.

[76] K. Zhou, J. Doyle, and K. Glover, *Robust and Optimal Control*. Prentice-Hall, Inc, 1996.

[77] Y. Zhao and H. Kimura, "Two-degrees-of-freedom dead-beat control system with robustness," *Int. J. Control*, vol. 48, no. 1, pp. 303–315, 1988.

[78] H. Fujimoto and A. Kawamura, "Perfect tracking digital motion control based on two-degree-of-freedom multirate feedforward control," in *IEEE Int. Workshop Advanced Motion Control*, pp. 322–327, June 1998.

[79] H. Fujimoto, Y. Hori, T. Yamaguchi, and S. Nakagawa, "Proposal of perfect tracking and perfect disturbance rejection control by multirate sampling and applications to hard disk drive control," in *Conf. Decision Contr.*, pp. 5277–5282, 1999.

[80] H. Fujimoto, Y. Hori, T. Yamaguchi, and S. Nakagawa, "Proposal of seeking control of hard disk drives based on perfect tracking control using multirate feedforward control," in *IEEE Int. Workshop Advanced Motion Control*, pp. 74–79, March 2000.

[81] H. Fujimoto and Y. Hori, "Visual servoing based on multirate sampling control," in *IEEE Int. Conf. Robotics and Automation*, 2001. (to be presented).

[82] G. F. Franklin and J. D. Powell, *Digital Control of Dynamic Systems*. Addison-Wesley Publishing Company, 1980.

[83] H. Fujimoto, A. Kawamura, and M. Tomizuka, "Proposal of generalized digital redesign method in use of N-delay control," in *Amer. Control Conf.*, pp. 3290–3294, June 1997.

[84] H. Fujimoto, A. Kawamura, and M. Tomizuka, "Generalized digital redesign method for linear feedback system based on N-delay control," *IEEE/ASME Trans. Mechatronics*, vol. 4, no. 2, pp. 101–109, 1999.

[85] P. Lancaster and M. Tismenetsky, *The Theory of Matrices.* Academic Press, Inc., 1985.

[86] T. Inoue and M. Nakano, "High accuracy control of a proton synchrotron magnet power supply," in *8th IFAC World Congress*, vol. XX, pp. 216–221, 1983.

[87] S. Hara, Y. Yamamoto, T. Omata, and M. Nakano, "Repetitive control system – a new-type servo system," *IEEE Trans. Automat. Contr.*, vol. 33, pp. 659–668, 1988.

[88] C. Kempf, W. Messner, M. Tomizuka, and R. Horowitz, "Comparison of four discrete-time repetitive algorithms," *IEEE Contr. Syst. Mag.*, vol. 13, no. 5, pp. 48–54, 1993.

[89] F. Suzuki and Y. Hori, "Improvement of stability margin with instantaneous speed observer," in *IEE of Japan, JIASC 1999*, vol. 3, pp. 503–506, August 1999. (in Japanese).

[90] C. Smith, K. Takeuchi, and M. Tomizuka, "Cost effective repetitive controllers for data storage devices," in *14th IFAC World Congress*, vol. B, pp. 407–412, July 1999.

[91] *Digital Control Systems.* Holt Rinehart and Winston Inc., 1980.

[92] B. C. Kuo and D. W. Peterson, "Optimal discretization of continuous-data control system," *Automatica*, vol. 9, pp. 125–129, 1973.

[93] L. S. Shieh, J. L. Zhang, and S. Ganesan, "Pseudo-continuous-time quadratic regulators with pole in a specific region," *IEE Proc. Pt. D*, vol. 137, no. 5, pp. 297–301, 1990.

[94] R.A.Yackel, B.C.Kuo, and G.Singh, "Digital redesign of continuous systems by matching of states at multiple sampling periods," *Automatica*, vol. 10, no. 1, pp. 105–111, 1974.

[95] L. S. Shieh, X. M. Zhao, and J. L. Zhang, "Locally optimal-digital redesign of continuous-time systems," *IEEE Trans. on Ind. Elec.*, vol. 36, no. 4, pp. 511–515, 1989.

[96] K. S. Rattan, "Digitalization of continuous control systems," *IEEE Trans. Automat. Contr.*, vol. 29, no. 3, pp. 282–285, 1984.

[97] K. S. Rattan, "Compensating for computational delay in digital equivalent of continuous control systems," *IEEE Trans. Automat. Contr.*, vol. 34, no. 8, pp. 895–899, 1989.

[98] "RTLinux.org home page." http://www.rtlinux.org/.

[99] T. Yamaguchi, H. Numasato, and H. Hirai, "A mode-switching control for motion control and its application to disk drives: Design of optimal mode-switching conditions," *IEEE/ASME Trans. Mechatronics*, vol. 3, no. 3, pp. 202–209, 1998.

[100] L. Yi and M. Tomizuka, "Two-degree-of-freedom control with robust feedback control for hard disk servo systems," *IEEE/ASME Trans. Mechatronics*, vol. 4, no. 1, pp. 17–24, 1999.

[101] J. Ishikawa, Y. Yanagita, Y. Hattori, and M. Hashimoto, "Head positioning control for law sampling rate systems based on two degree-of-freedom control," *IEEE Trans. Magnetics*, vol. 32, no. 3, pp. 1787–1792, 1996.

[102] Y. Gu and M. Tomizuka, "High performance tracking control system under measurement constraints by multirate control," in *14th IFAC World Congress*, vol. C, pp. 67–71, July 1999.

[103] "Introduction of DK31CJ-72 and DK32CJ-36/18 (home page of Hitachi Ltd.)." http://www.hitachi.co.jp/Prod/comp/storage/dk35/e-dk31c_32c/index.html.

[104] L. E. Weiss, A. C. Sanderson, and C. P. Newman, "Dynamic sensor based control of robots with visual feedback," *IEEE J. Robotics and Automation*, vol. 3, no. 5, pp. 404–417, 1987.

[105] S. Hutchinson, G. D. Hager, and P. I. Corke, "A tutorial on visual servo control," *IEEE Trans. Robotics and Automation*, vol. 12, no. 5, pp. 3745–3750, 1996.

[106] T. Murakami and K. Ohnishi, "A study of stability and workspace decoupling control based on robust control in multi-degrees-of-freedom robot," *Trans. IEE of Japan*, vol. 113-D, no. 5, pp. 639–646, 1993. (in Japanese).

[107] K. Hashimoto, T. Ebine, and H. Kimura, "Visual servoing with hand-eye manipulator – optimal control approach," *IEEE Trans. Robotics and Automation*, vol. 12, no. 5, pp. 766–774, 1996.

[108] M. Nakadokoro, S. Komada, and T. Hori, "Stereo visual servo of robot manipulators by estimated image feature without 3D reconstruction," in *IEE of Japan, JIASC '99*, vol. 1, pp. 451–454, August 1999. (in Japanese).

[109] Y. Iwasaki, T. Murakami, and K. Ohnishi, "An approach of visual servoing control considering compensation of time delay," in *IEE of Japan Technical Meeting Record*, no. IIC-97-23, pp. 91–95, Feb 1997. (in Japanese).

[110] S. Okazaki, H. Fujimoto, and Y. Hori, "Proposition of a robust controller for visual feedback system with long dead time," in *IEE of Japan Technical Meeting Record*, no. IIC-00-18, pp. 103–108, 2000. (in Japanese).

[111] A. Kawamura, K. Miura, and T. Ishizwawa, "Observer based sliding mode CP control of two axis scara robot," in *Proc. IEEE Int. Workshop Adv. Motion Contr.*, pp. 197–202, March 1990.

[112] N. Matsui and Y. Hori, "Advanced technologies in motor control," *Trans. IEE of Japan*, vol. 113, no. 10, pp. 1122–1137, 1993. (in Japanese).

[113] Y. Hori, H. Iseki, and K. Sugiura, "Basic consideration of vibration suppression and disturbance rejection control of multi-inertia system using SFLAC (state feedback and load acceleration control)," *IEEE Trans. Industrial Applications*, vol. 30, no. 4, pp. 889–896, 1994.

[114] K. Sugiura and Y. Hori, "Vibration suppression in 2- and 3-mass system based on the feedback of imperfect derivative of estimated torsional torque," *IEEE Trans. Industrial Electronics*, vol. 43, no. 1, pp. 56–65, 1996.

[115] Y. Hori, H. Sawada, and Y. Chun, "Slow resonance ratio control for vibration suppression and disturbance rejection in torsional system," *IEEE Trans. Industrial Electronics*, vol. 46, no. 1, pp. 162–168, 1999.

[116] Y. Gu, M. Tomizuka, and J. Tornero, "Digital redesign of continuous time controller by multirate sampling and high order holds," in *Conf. Decision Contr.*, pp. 3422–3427, 1999.

List of Publications

Journals

1. Hiroshi Fujimoto and Atsuo Kawamura "New Digital Redesign Method in use of N-Delay Control", *Trans. IEE of Japan*, vol. 117-D, no. 5, pp. 645 – 654, 1997.(in Japanese)

2. Hiroshi Fujimoto, Atsuo Kawamura, and Yoichi Hori, "Proposal of Advanced Perfect Tracking Control Based on Generalized Multirate Sampling Control and Comparison with Zero Assignment Method", *Annual Report of Engineering Research Institute, School of Engineering, University of Tokyo*, Vol. 57, pp. 207 – 214, 1998.(in Japanese)

3. Hiroshi Fujimoto, Atsuo Kawamura, and Masayoshi Tomizuka, "Generalized Digital Redesign Method for Linear Feedback System Based on N-Delay Control", *IEEE/ASME Trans. Mechatronics*, Vol. 4, No. 2, pp. 101 – 109, 1999.

4. Hiroshi Fujimoto and Yoichi Hori, "Proposal of Inter-Sampling Perfect Tracking and Perfect Disturbance Rejection Controllers in use of Multirate Sampling Control – Extensions to Systems with delay and Applications to the HDD Control – , *Annual Report of Engineering Research Institute, School of Engineering, University of Tokyo*, Vol. 58, 1999.(in Japanese)

5. Hiroshi Fujimoto, Yoichi Hori, and Atsuo Kawamura, "Perfect Tracking Control Method Based on Multirate Feedforward Control", *Trans. SICE*, vol. 36, no. 9, pp. 766–772, 2000.(in Japanese)

6. Hiroshi Fujimoto, Yoichi Hori, Takashi Yamaguchi, and Shinsuke Nakagawa, "Seeking Control of Hard Disk Drives by Perfect Tracking using Multirate Sampling Control", *Trans. IEE of Japan*, vol. 120-D, no. 10, pp. 1157–1164, 2000.(in Japanese)

7. Hiroshi Fujimoto, Yoichi Hori, and Takashi Yamaguchi, "Motion Control Based on Multirate Feedforward Control – Application to Seeking Control of Hard Disk Drive –", *Journal of SICE*, vol. 39, no. 10, pp. 639–642, 2000.(in Japanese)

8. Hiroshi Fujimoto, Yoichi Hori, and Atsuo Kawamura, "Perfect Tracking Control based on Multirate Feedforward Control with Generalized Sampling Periods", *IEEE Trans. Industrial Electronics*, Vol. 48, No. 3, 2001. (to be published)

International conference

1. Hiroshi Fujimoto, Atsuo Kawamura, and Masayoshi Tomizuka, "Proposal of Generalized Digital Redesign Method in use of N-Delay Control", in *Proc. 1997 American Control Conference (ACC97)*, pp. 3290 – 3294, Albuquerque, 1997.

2. Hiroshi Fujimoto and Atsuo Kawamura, "New Digital Redesign Method by N-Delay Control and its Application", in *Proc. Power Conversion Conference (PCC97)*, pp. 525 – 530, Nagaoka, 1997.

3. Hiroshi Fujimoto and Atsuo Kawamura, "Generalized Digital Redesign Method by N-Delay Control and its Application to Motion Control", in *Proc. IEEE Power Electronics Specialists Conference (PESC98)*, pp. 1835 – 1841, Fukuoka, 1998.

4. Hiroshi Fujimoto and Atsuo Kawamura, "Perfect Tracking Digital Control in use of Two-Degree-of-Freedom Multirate Feedforward Control for Mechatronics", in *Proc. TITech COE/Super Mechano-Systems Workshop '98*, pp. 85 – 93, Tokyo, 1998.

5. Hiroshi Fujimoto and Atsuo Kawamura, "Perfect Tracking Digital Motion Control Based on Two-Degree-of-Freedom Multirate Feedforward Control", in *Proc. International Workshop on Advanced Motion Control (AMC98)*, pp. 322 – 327, Coimbra, 1998.

6. Hiroshi Fujimoto, Yoichi Hori, and Atsuo Kawamura, "High Performance Perfect Tracking Control Based on Multirate Feedforward / Feedback Controllers with Generalized Sampling Periods", in *Proc. 1999 IFAC World Congress*, vol. C, pp. 61 – 66, Beijing, 1999.

7. Hiroshi Fujimoto, Yoichi Hori, Takashi Yamaguchi, and Shinsuke Nakagawa, "Advanced Control of Hard Disk Drive by Perfect Tracking and Perfect Disturbance Rejection Control in use of Multirate Sampling Control", in *Proc. 4th The Univ.*

of Tokyo – Seoul Nat. Univ. Joint Seminar on Electrical Engineering, pp. 35 – 40, Seoul, 1999.

8. Hiroshi Fujimoto, Yoichi Hori, Takashi Yamaguchi, and Shinsuke Nakagawa, "Proposal of Perfect Tracking and Perfect Disturbance Rejection Control by Multirate Sampling and Applications to Hard Disk Drive Control", in *Proc. 38th IEEE Conference on Decision and Control (CDC99)*, pp. 5277 – 5282, Phoenix, 1999.

9. Hiroshi Fujimoto, Yoichi Hori, Takashi Yamaguchi, and Shinsuke Nakagawa, "Proposal of Seeking Control of Hard Disk Drives based on Perfect Tracking Control using Multirate Feedforward Control" in *Proc. International Workshop on Advanced Motion Control (AMC2000)*, pp. 74 – 79, Nagoya, 2000.

10. Hiroshi Fujimoto, Yoichi Hori, and Atsuo Kawamura, "Structure of Perfect Tracking Controller based on Generalized Sampling Periods", in *Proc. International Power Electronics Conference (IPEC2000)*, vol. 1, pp. 337 – 342, Tokyo, 2000. (*3)

11. Hiroshi Fujimoto and Yoichi Hori, "Vibration Suppression and Disturbance Rejection Control in Semi-Nyquist Frequency Region Based on a Novel Multirate Sampling Control with Initial Value Compensation", in *Proc. International Conference and Exhibition on Power Electronics and Motion Control (PEMC2000)*, vol. 6, pp. 190–196, Kosice (Slovakia), 2000.

12. Hiroshi Fujimoto and Yoichi Hori, "Vibration Suppression and Optimal Repetitive Disturbance Rejection Control in Semi-Nyquist Frequency Region using Multirate Sampling Control", in *Proc. 39th IEEE Conference on Decision and Control (CDC2000)*, pp. 3745–3750, Sydney, 2000.

13. Hiroshi Fujimoto and Yoichi Hori, "Visual Servoing Based on Multirate Sampling Control", in *Proc. Int. Conf. Robotics and Automation (ICRA2001)*, Seoul, 2001.(to be presented)

Domestic conference

1. Hiroshi Fujimoto and Atsuo Kawamura "Proposal of Digital Redesign by N_l-Delay Control", *1996 National Convention Record I.E.E Japan*, No. 685, pp. 3.234 – 3.235, 1996.(in Japanese)

2. Hiroshi Fujimoto and Atsuo Kawamura “Proposal of Digital Redesign in use of N-Delay Control and its Application”, *IEE of Japan Technical Meeting Record*, IIC-96-13, pp. 31 – 40, 1996.(in Japanese)

3. Hiroshi Fujimoto and Atsuo Kawamura “New Digital Redesign Method in use of N-Delay Control”, *1996 National Convention Record I.E.E Japan – Industry Application Society –*, No. 154, pp. 51 – 56, 1996.(in Japanese), (*1)

4. Hiroshi Fujimoto and Atsuo Kawamura “Digital Redesign Method in use of N-Delay Control”, *1997 National Convention Record I.E.E Japan*, pp. S.15-25 – S.15-28, 1997.(in Japanese)

5. Hiroshi Fujimoto and Atsuo Kawamura “Perfect Tracking Control Based on Multirate Sampling Control”, *IEE of Japan Technical Meeting Record*, IIC-97-16, pp. 47 – 54, 1997.(in Japanese)

6. Hiroshi Fujimoto and Atsuo Kawamura “Proposal of Perfect Tracking Control Based on Multirate Input Sampling Control”, *1997 National Convention Record I.E.E Japan*, No. 979, pp. 4-314 – 4-315, 1997.(in Japanese)

7. Hiroshi Fujimoto and Atsuo Kawamura “Proposal of Robust Perfect Tracking States Control by Multirate Feedforward Control”, *1998 National Convention Record I.E.E Japan*, No. 875, pp. 4-265 – 4-266, 1998.(in Japanese)

8. Hiroshi Fujimoto, Atsuo Kawamura, and Yoichi Hori “Advanced Perfect Tracking Control Based on Multirate Feedforward / Feedback Controllers”, *1998 National Convention Record I.E.E Japan – Industry Application Society –*, Vol.2, pp 166-169, 1998.(in Japanese)

9. Hiroshi Fujimoto, Yoichi Hori, and Atsuo Kawamura “Improvement of Feedback Characteristics for Perfect Tracking Control in use of Multirate Two-degree-of-freedom Control” – Proposal of Perfect Disturbance Rejection Control and Applications to HDD control – *IEE of Japan Technical Meeting Record*, IIC-99-2, pp. 7 – 14, 1999.(in Japanese), (*2)

10. Hiroshi Fujimoto, Yoichi Hori, Takashi Yamaguchi, and Shinsuke Nakagawa, “Seeking Control of Hard Disk Drives by Perfect Tracking using Multirate Sampling Control”, *1999 National Convention Record I.E.E Japan – Industry Application Society –*, Vol.3, pp. 535 – 540, 1999.(in Japanese)

11. Hiroshi Fujimoto and Yoichi Hori, "Proposal of Vibration Suppression and Disturbance Rejection Control in Semi-Nyquist Frequency Region Based on Multirate Sampling Control" *IEE of Japan Technical Meeting Record*, IIC-00-23, pp. 133 – 136, 2000.

12. Hiroshi Fujimoto and Yoichi Hori, "Proposal of Vibration Suppression Control in Semi-Nyquist Frequency Region and High-Order Repetitive Disturbance Rejection Control Based on Multirate Sampling Control – Optimization of Inter-sample Disturbance Rejection Performance –" *IEE of Japan Technical Meeting Record*, IIC-00-56, pp. 39 – 46, 2000.

13. Hiroshi Fujimoto and Yoichi Hori, " Proposal of Repetitive Disturbance Rejection Control using Multirate Sampling Control and Application to Visual Servo System", *2000 National Convention Record I.E.E Japan – Industry Application Society –*, Vol. 1, pp. 766–772, 2000.(in Japanese)

14. Hiroshi Fujimoto and Yoichi Hori, "Vibration Suppression and Periodic Disturbance Rejection Control Based on Multirate Sampling Control", *Dynamical System Theory Symposium*, pp. 225–230, 2000.(in Japanese)

Coauthor paper

1. Shuntaro Okazaki, Hiroshi Fujimoto, and Yoichi Hori, "Proposition of a robust controller for visual feedback system with long dead time" *IEE of Japan Technical Meeting Record*, IIC-00-18, pp. 103 – 108, 2000.

2. Kunihiko Saruta, Hiroshi Fujimoto, and Yoichi Hori, "Visual servoing system with feature prediction using motion observer" *IEE of Japan Technical Meeting Record*, IIC-01-13, 2001.(in Japanese, to be presented)

Coauthor book

1. Hiroshi Fujimoto, In "Motor technology practical handbook (Edited by D. Ebihara, Y. Hori, and H. Doumeki)",
   Chapter 2-8: "Digital redesign",
   Chapter 2-10: "Perfect tracking control based on multirate sampling control",
   The Nikkan Kogyo Shinbun, Ltd., 2001.(in Japanese, to be published)

Awards

1. Hiroshi Fujimoto, "Excellent Paper Presentation Award" for paper (*1), in *National Convention, IEE of Japan, Industry Application Society*, August, 1996.

2. Hiroshi Fujimoto, "Inose Academic Encouragement Award", July, 1997.

3. Hiroshi Fujimoto, "Excellent Paper Presentation Award" for paper (*2), in *IEE of Japan Technical Meeting*, January, 1999.

4. Hiroshi Fujimoto, "Student Encouragement Award " for paper (*3), in *International Power Electronics Conference*, January, 2000.